Doctoral Dissertation

Studies on the Factors Determining Molecular Structures of 1,2-Dihaloethenes, 1,2-Dihalodiazenes and Analgesic Peptide Derivatives.

Takashi Yamamoto

August 29, 2008

Submitted to
The Department of Chemistry,
School of Science,
The University of Tokyo, Japan

Thesis Committee:

Professor Shuji Tomoda (Supervisor)
Professor Takayuki Kawashima (Co-supervisor)
Professor Kazuo Tachibana (Co-supervisor)
Professor Kaoru Yamauchi (Co-supervisor)
Professor Hayato Tsuji (Co-supervisor)

Studies on the Factors Determining Molecular Structures of 1,2-Dihaloethenes, 1,2-Dihalodiazenes and Analgesic Peptide Derivatives.

ABSTRACT

The interaction of a drug on its targeting receptor has been described using the "key and lock" concept in which the molecular structure of a drug plays a critical role. The chemical definition of molecular structure is the three-dimensional arrangement of the atoms and chemical bonds which constitute a molecule. In this thesis, the discussions were made on the determining factors of a molecular structure for simple molecules (1,2-dihaloethenes and 1,2-dihalodiazenes) and for rather large bioactive peptide, using the theoretical chemistry with orbital-orbital interaction and the structural biochemistry with the NMR experiments.

In the first half of this thesis, the factors determining the thermodynamically stable molecular structure are discussed on the 1,2-dihaloethene (XHC=CHX, X = F, Cl or Br) and 1,2-dihalodiazene systems (XN=NX, X = F, Cl or Br). The "*cis*-effect" is the puzzling phenomenon, in which the *cis*-isomer is thermodynamically more or equally stable compared to the corresponding *trans*-isomer in some molecules with a double bond. In order to clarify the predominant factor of the *cis*-effects in the 1,2-dihaloethene and 1,2-dihalodiazene systems, the energetic effects of intra-molecular hyperconjugations and steric repulsion in each molecular system were theoretically estimated using the natural bond orbital (NBO) theory. Although 1,2-dihaloethenes and 1,2-dihalodiazenes were the electronic isosteres, the dominant factor of their *cis*-effects was completely opposite by each system. In 1,2-dihaloethene systems, the LP effect (halogen lone pair delocalization into the antibonding orbitals of C=C bond) was the dominant factor of the *cis*-effect. Meanwhile, the *cis*-effect in the 1,2-

dihalodiazene systems originates mainly in the antiperiplanar interactions (AP effect) rather than the LP effect. Moreover, the greater AP effect in the 1,2-dihalodiazene systems makes the N′–X′ bond easier to cleave (longer N–X bond length) and the energetic level of N–Br bonding orbital in 1,2-dibromodiazenes was found higher than that of the nitrogen lone pair, indicating the significant instability of this molecule. The importance of these discussions is quantitative elucidation of the dominance of hyperconjugative mechanisms, especially lone-pair-related hyperconjugations, over the steric effects on the electronic and energetic view of a simple and general molecular structure, such as 1,2-dihaloethene and 1,2-dihalodiazene systems, to determine their thermodynamically stable molecular structures. This quantum-chemical concept regarding the orbital-orbital interactions could be a guide to new aspect of modern organic chemistry to understand diverse molecular phenomena. Since many bioactive ligands have a double bond whose *cis-trans* configuration is crucial for their bioactivity, the discussions on the thermodynamically stable configuration of these simple molecules can provide the important information on the proper molecular structure of the bioactive ligands.

In the latter half of this thesis, the discussion was made on the three-dimensional molecular structure of bioactive peptide derivatives in relevance to their biological activities. The study was made on the series of bifunctional peptide derivatives that act as agonists for opioid receptors and as antagonists for neurokinin-1 (NK1) receptors. These compounds were designed and synthesized for a potential application as analgesics in various pain states and characterized using cell-membrane-based radioligand binding assays and isolated-tissue-based functional assays. The structural optimization was performed on the fifth residue and *C*-terminus of the lead peptide **TY001** (H-Tyr-*D*-Ala-Gly-Phe-Pro-Leu-Trp-O-3,5-Bzl(CF_3)$_2$) to find the potent bifunctional peptide derivatives. Moreover, in order to provide new insight into the determining factors of their membrane-bound molecular structure, which might play an important role in the ligand-receptor binding and further biological behavior, dodecylphosphocholine (DPC) micelle-bound three-dimensional structures of obtained potent peptide derivatives (**TY005**: Tyr-D-Ala-Gly-Phe-Met-Pro-Leu-Trp-O-3,5-Bzl(CF_3)$_2$; **TY027**: Tyr-D-Ala-Gly-

Phe-Met-Pro-Leu-Trp-NH-3,5-Bzl(CF_3)$_2$; and **TY025**: Tyr-D-Ala-Gly-Phe-Met-Pro-Leu-Trp-NH-Bzl) were determined based on the 2D NMR studies. Although their differences of the primary sequences were limited in the *C*-terminal benzyl moiety, the obtained NMR structures were unexpectedly different for each compound depending on their unique *C*-terminus. In particular, the effect of removal of trifluoromethyl groups was significant, resulting in a structural change of the whole molecule from a tandem-*β*-turn conformation (**TY005** and **TY027**) to a better-defined helical conformation (**TY025**). Therefore, trifluoromethyl groups at the *C*-terminus could be considered as the determining factor of the entire three-dimensional molecular structure of these analgesic peptide derivatives. Interestingly, **TY025** showed different biological charactor compared to those of **TY005** and **TY027**, with more potent opioid agonist activities as well as lower NK1 antagonist activities, in direct relation to the compound-specific molecular structures in DPC micelles. The simultaneous consideration of the micelle-bound structures and bioactivities provided in this study demonstrates the usefulness of this approach in explaining biological differences due to a "small" modification of a ligand. It was also suggested that this change in the three-dimensional molecular structure of ligand had an important relevance to the ligand-receptor binding to yield the bioactivities at the opioid and NK1 receptors.

Through these discussions, this thesis could provide important insights and basic information of the factors determining a molecular structure to understand wide-range of chemical phenomena at the molecular level to control their properties and characters, especially for understanding the ligand's binding at the targeted receptor and for efficient and rational design of next generation drug candidates.

ABSTRACT (in Japanese)

Studies on the Factors Determining Molecular Structures of
1,2-Dihaloethenes, 1,2-Dihalodiazenes and Analgesic Peptide Derivatives.

1,2-ジハロエテン、1,2-ジハロジアゼンおよび
鎮痛効果を有するペプチド誘導体の分子構造を決定する因子の研究

薬剤の生理作用は、薬剤がターゲットとなる受容体やイオンチャネルなどのたんぱく質に存在する鍵穴のような結合部位にぴったりとあう「鍵」として働き、生理作用を発揮するという「鍵と鍵穴」理論で説明されることが多い。しかし、病気ごとに違い、複雑に入り組んだ「鍵穴」にぴったりとはまる構造を持つ「鍵」となりうる分子を見つけることは膨大な研究資源と時間をつぎ込んでも決して容易ではなく、現在の創薬研究では何千、何万もの異なった「鍵」の中から目的の鍵を見つけ出すという、気の遠くなるような作業が行われている。また、この「鍵」はどの鍵穴にでもはまるマスターキーではなく、ある鍵穴だけにはまる選択性の高い化合物であることが副作用を抑制するために望ましい。また、この創薬化学研究は有機化学合成だけではなく、創薬ターゲットに関する薬理学的知識や化合物の生体内における吸収、分布、代謝、排泄等の挙動についての知識、特許的な知識なども要求される総合的な研究活動であり、こういったバックグラウンドを全てふまえて「鍵」となる分子構造を持つ薬剤候補化合物を適切にデザインし合成していく必要がある。このため、置換基レベルから分子全体にいたるまで、三次元構造を決定する因子について理解することは非常に重要だと考えられる。

ここで分子構造とは、原子や化学結合の三次元的な配列のことをいう。ある分子に固有の分子構造は、その分子構造に由来する電子構造とあいまって、その分子や分子の集合体に固有の様々な性質を決定する要因となる。また、包接体の形成、受容体との結合による生理活性の発現、溶液への溶解性など近接する分子間の相互作用の結果生み出される化学的現象の決定的な因子になるとも考えられている。

この分子構造は、量子力学的な概念から原子･分子の表面軌道（一番外の電子殻にある価電子軌道）の相互作用が最安定となる構造と考えることができる。このため量子化学的理論

に基づいたさまざまなモデルが現在までに提唱されてきたが、そのうち最も広く受け入れられているもののひとつが、「分子構造は非共有電子対や結合電子対の交換反発で決まる」とした原子価殻電子対反発（VSEPR) モデルである。例えばエタンの重なり配座よりねじれ配座の方が安定になる理由は、このVSEPRモデルによれば隣接するC－H･･･C－H結合間の交換反発の結果であると考えられる。しかし電子の非局在化（超共役理論）に基づいて、ねじれ配座の安定化の原因は隣接C－H結合間のアンチペリプラナー効果（AP effect）であるとの解釈も可能で、この二つの理論の間で長年議論が展開されてきた。この論文の前半部分では、VSEPRモデルでは説明ができない1,2-ジハロエテンおよび1,2－ジハロジアゼンの*cis*-effectと呼ばれる現象を理論化学的に考察することにより、これらの分子においては交換反発よりも電子の非局在化が熱力学的に安定な分子構造を決定する際に重要な因子になっていることを示した。

Cis-effectとは二重結合を持つ分子において*cis*体が*trans*体よりも熱力学的に安定になる現象をいう。1,2－ジハロエテン(XHC=CHX, X = F, Cl or Br)および1,2－ジフルオロジアゼン(FN=NF) の場合、VSEPRモデルによればハロゲン非共有電子対間の交換反発が大きい*cis*体のほうが対応する*trans*体よりも不安定化されていると考えられる。しかし、これらの化合物では実験的に*cis*体が*trans*体よりも熱力学的に安定になるか、ほぼ同じ安定性を示すことが示されている。この原因を分子軌道法計算とNatural Bond Orbital（NBO) 理論を用いて検証した。まず電子相関を考慮した高レベルの分子軌道法計算によって、1,2－ジハロエテンや1,2－ジフルオロジアゼンだけでなく、1,2－ジクロロジアゼンや1,2－ジブロモジアゼンでも*cis*体が*trans*体よりも熱力学的に安定であることが示された。さらにNBO法を用いた分子軌道計算により、電子の非局在化による安定化エネルギーがこれら化合物の*cis*体を対応する*trans*体よりも安定にしており、交換反発による影響は二次的なものであることを定量的に示した。ここで1,2－ジハロエテンにおいては、ハロゲン非共有電子対がC=C結合の反結合性軌道へと非局在化する軌道相互作用（LP effect) とAP effectの二つの非局在化メカニズムが重要で、LP effectを介する安定化エネルギーの方がAP effectよりも大きい。ここで*cis*体のLP effectが*trans*体よりも大きい理由は、軌道位相理論において*cis*体でのみLP effectの軌道位相が連続していることから説明できる。1,2－ジハロエテンの電子的等価体である1,2－ジハロジアゼンにおいてもLP effect、AP effectの両方が*cis*体を*trans*体よりも熱力学的に安定にする。しかし1,2－ジハロエテンの場合とは逆に、AP effectを介する安定化エネルギーの方がLP effectより

も大きい。この逆転の原因として、1,2－ジハロジアゼンにおいては窒素原子の非共有電子対がAP effectに寄与することと、N－X（X = F, Cl or Br) 結合がC－X結合に比べて長くハロゲン非共有電子対とN=N結合の反結合性軌道との軌道の重なりが小さくなることの二つが考えられる。以上の結果から、1,2－ジハロエテンや1,2－ジハロジアゼンといった小さく簡単な分子において、電子の非局在化が熱力学的に安定な分子構造を決定する主要因子であることを示した。また電子的等価体のような電子構造的に類似していると考えられる分子間でも、熱力学的に安定な分子構造を決定する因子に違いがあることも明らかとなった。また分子内の*cis-trans*異性が生理活性に大きく影響することは様々なリガンドや生理活性物質についてよく知られているため、これらの知見はより高い生理活性をもつ化合物をデザインするための有用な情報になるとも考えられる。

ここで分子構造の変化は分子間認識、例えば生理活性リガンドの受容体への結合にも決定的な影響を及ぼす。例えば官能基の導入や置換によってリガンドの受容体における生理活性が大きく変化することがあるが、この現象はリガンドの三次元的な分子構造変化の結果として受容体への親和性が変化することにより起こると考えられる。しかしリガンド－受容体結合体のX線結晶構造を得ることは簡単ではなく、リガンド単体として水溶液中で得られる三次元構造は必ずしも受容体に結合した構造とは一致しないため、実験的に得られるリガンドの三次元構造から生理活性を推測することは簡単ではなかった。このため、リガンドの受容体結合構造の推測に一般的に用いられる手段の一つがリガンドの受容体たんぱく質に対する結合計算である。この計算方法では、一般的に以下の三段階のステップでリガンド－受容体の結合構造を得る。まずホモロジーモデリング計算と呼ばれる方法により受容体たんぱく質の三次元的分子構造を求める。これは進化的類縁関係（ホモロジー）を持っているたんぱく質どうしは構造が類似している、という経験的事実に基づき、構造を知りたいたんぱく質（ターゲット）のアミノ酸配列をデータベースで検索を行ない、既に立体構造がX線構造解析などで決定されているたんぱく質の中から配列の類似率の高いものを選び出し、それを鋳型にしてモデリング計算を行なう方法である。次に、得られた受容体の立体構造の中でリガンドが結合する「鍵穴」となるべき結合部位を推定する。最後にどのようにリガンドが「鍵穴」に結合するかをモデリング計算で求め、リガンド－受容体間の相互作用エネルギーなどを指標にリガンド－受容体の結合構造を得る。このドッキング計算で最も重要なのはホモロジーモデリング計算によっていかに信頼性の高い受容体たんぱく質の立体構造を得ることが

できるかという点であるが、近年計算機のスペックが大幅に向上したことやアルゴリズムの改良などにより、受容体の種類によってはかなり高い確率で高活性なリガンドの構造を推定することができるようになってきている。しかし、精度の高いホモロジーモデリングを行うにはターゲットとなるたんぱく質に高いホモロジーを持つ他のたんぱく質のX線構造や高活性の既知リガンド化合物などさまざまな情報が必要なため、こういった計算を行うことができる受容体は限られているのが現状である。また、受容体のホモロジーモデリングをうまく行うことができても、鍵穴にはまるべきリガンド化合物がフレキシブルな構造を持つ場合にはドッキング計算を行うのが難しく、結合構造が得られたとしても計算の信頼性が低い場合が多い。このため、特にペプチドなどのフレキシブルな構造を持つ生理活性化合物においては、生理活性と立体構造との相関についてあまりよく分かっていないのが現状であるといえる。

ここで、Met-エンケファリン（Tyr-*D*-Ala-Gly-Phe-Met）を二つの*D*-Penで置換して誘導化し、ジスルフィド結合を用いて環化したDPDPE（Tyr-*cyclo*[*D*-Pen-Gly-Phe-*D*-Pen]）は、μオピオイド受容体（MOR）に比べてδオピオイド受容体（DOR）に対する高い親和性を持つオピオイドアゴニストである（リガンド結合評価系におけるKi = 10 nM, hDOR; 3700 nM, rMOR、オピオイド受容体はモルヒネが結合する受容体）。このDPDPEは環化によってフレキシビリティが下がっていることもあり、ホモロジーモデリングによるDORとのドッキング計算が行われている。DPDPEの受容体結合構造は環化部位でもある*D*-Pen^{2}から*D*-Pen^{5}の間にβターンを持っており、この二次構造がDORへの結合とMORとの選択性発現に重要な役割を果たしている可能性がある。このDORのリガンド結合部位は受容体膜貫通ドメイン内にある。また、ニューロキニン1（NK1）受容体阻害剤であるL-732,138（Ac-Trp-O-3,5-Bzl(CF_3)$_2$； Ki = 0.73 nM, hNK1、但し3,5-Bzl(CF_3)$_2$は3,5-bis-trifluoromethylbenzyl）はホモロジーモデリングの結果、C末のベンジル基を膜貫通ドメイン内、N末のアセチル基を膜貫通ドメインの外側に向ける形で受容体と結合していることが報告されている。さらに、NK1受容体のL-732,138アセチル基結合部位近傍には大きな空洞があり、L-732,138のN末側へシークエンスを延伸しても活性を維持することが可能と推測された。実際、L-732,138のN末側へシークエンスを伸ばしたCbz-Pro-Leu-Trp-O-3,5-Bzl(CF_3)$_2$が高い活性を持つNK1受容体阻害剤として報告されている。これらのようにリガンド結合部位が膜貫通ドメインあるいはその近傍にあることが分かっている膜結合型受容体においては、溶液中に存在するリガンドが直接受容体に結合するよりも、

生体膜中に移行したリガンドが膜中を二次元的に移動して受容体に結合するほうがエントロピー的に有利であると考えられる。また受容体の膜貫通ドメインは脂溶性の高いアミノ酸残基が多く、リガンド結合部位自体も脂溶性が高いことが多い。このため脂溶性が高い生体膜中の分子構造の方が水溶液中の構造よりも受容体に結合する構造と関連しており、生理活性の発現により大きな寄与があると仮定した。

この論文の後半部分では、この仮定に基づいて生体膜中のリガンドの三次元的な分子構造を決定している因子とその分子構造の変化が生理活性に及ぼす影響について、オピオイドアゴニスト（OA) 作用とNK1阻害作用を併せ持つ鎮痛ペプチド誘導体を用いて考察を行った。ペプチド誘導体は、オピオイドアゴニストファーマコフォア（OAP: Tyr-D-Ala-Gly-Phe）をN末に、NK1阻害ファーマコフォア（NAP: Pro-Leu-Trp-A-3,5-Bzl(B)$_2$, A = O or NH, B = H or CF_3）をC末に配置することにより設計した。副作用が少なく強力な鎮痛薬を目指してδ選択的なOA活性とNK1阻害活性を指標に構造の最適化を行った結果、C末（NAP）の分子構造のみが異なり、共通のOAPを持つ3つの高活性ペプチド誘導体TY005: Tyr-D-Ala-Gly-Phe-Met-Pro-Leu-Trp-O-3,5-Bzl(CF_3)$_2$; TY027: Tyr-D-Ala-Gly-Phe-Met-Pro-Leu-Trp-NH-3,5-Bzl(CF_3)$_2$; TY025: Tyr-D-Ala-Gly-Phe-Met-Pro-Leu-Trp-NH-Bzl （但し 3,5-Bzl(CF_3)$_2$ は 3,5-bis-trifluoromethylbenzyl）を得た。TY005はラット鎮痛モデルにおいて用量依存的な強い鎮痛効果を示し、これら誘導体の動物モデルにおける生理作用を確認することができた。興味深いことにこれら化合物はNK1阻害活性だけでなくOA活性にも大きな差があり、特にC末のCF_3基がオピオイド、NK1両方の受容体における活性に大きく関与していることが判明した。これら誘導体間ではOAPの一次配列は共通であるため、OA活性の変化は明らかにOAPから遠く離れたC末の構造変換によって惹起されたリガンドの高次分子構造変化によると考えられる。そこで先ほどの仮定の通りに生体膜中の分子構造が受容体に結合した分子構造と関連していると考え、生体膜を模したドデシルホスホコリン（DPC) ミセル中における誘導体の分子構造を二次元NMR法を用いて解析した。その結果、CF_3基を持つTY005とTY027は二つのβターンを持つ二次構造を示したのに対し、CF_3基を持たないTY025はヘリカルな二次構造を持つ全く違った立体構造をとっていることが明らかとなったが、化合物間のオピオイド受容体における活性の違いはこれら立体構造の違いと関連していると考えることができる。このように擬似生体膜中でのリガンドの分子構造変化が受容体への親和性や生理活性の変化と関連しており、生体膜中の分子構造の重要性を示唆する結果を得た。またC末の置換基、特

にCF$_3$基がこれら鎮痛ペプチド誘導体の生体膜中の分子構造を決定する重要な因子となっており、生理活性の発現にも重要な役割を果たしていることも明らかとなった。ここで得られたリガンドの生体膜中の分子構造決定因子とその生理活性への影響に関する研究結果は、新たな薬剤の設計や開発において重要な知見を提供できると考えられる。

以上のように本論文ではシンプルな分子である1,2－ジハロエテン、1,2－ジハロジアゼンおよび比較的大きな分子である鎮痛ペプチド誘導体の分子構造を決定する因子について、量子理論化学から構造生物化学的なアプローチを用いて幅広く議論を行った。シンプルな分子における安定構造の決定因子は生理活性化合物の分子構造を置換基レベルで議論する際に重要である。一方でペプチド誘導体の三次元分子構造と生理活性の相関についての議論は、構造的に比較的自由度の高いリガンドの生理活性を制御する際に重要な知見になるといえる。そしてこれらの議論はいずれも「鍵穴」である生体内の受容体に結合するリガンドの構造を理論だって考え、さらに活性の高い化合物を論理的かつ効率的に創出するための重要な手がかりになると考えられる。近年、製薬業界では新規に認可される薬剤の数が減ってきていると言われているが、創薬化学に携わる有機化学者はこういった分子構造レベルの知見、情報を新規生理活性化合物のデザインに役立てていくことによって、より良い新しい薬剤を作り出す努力をしていくべきだと考えている。

ACKNOWLEDGMENTS

I would like to thank several extraordinary people who allowed this fruitive study to complete for the Ph.D. program.

I am sincerely grateful to Prof. Shuji Tomoda for giving me his professional guidance along the degree program. I am especially thankful for the generous support of Prof. Victor J. Hruby in the variety of fields from the scientific discussions to the training of my English skills. Their support, patience and guidance have provided the stable platform on which these studies could be initiated and completed. I also would like to show my largest appreciation for the kind generosity of my advisory committee consisting of Prof. Takayuki Kawashima, Prof. Kazuo Tachibana, Prof. Kaoru Yamauchi and Prof. Hayato Tsuji. I would like to dedicate this thesis to the memory of Prof. Henry "Hank" I. Yamamura who passed away peacefully on the evening of September 4, 2008.

I would like to thank Prof. Keiichiro Ogawa, Prof. Michio Iwaoka, Prof. Takatoshi Senju and Prof. Daisuke Kaneno for kind advice and support in the theoretical works presented in the first half of this dissertation. I believe that I can't complete this work without their constant suggestions and leadings. I also appreciate for the indispensable support and help from my outstanding collaborators, Prof. Frank Porreca, Prof. Henry I. Yamamura, Prof. Josephine Lai, Prof. Todd W. Vanderah and Prof. Neil E. Jacobsen during my stay in the University of Arizona. I thank the Arizona PPG team members, including Prof. Padma Nair, Prof. Josef Vagner, Dr. Shou-wu Ma, Dr. Edita Navratilova, Peg Davis Sharif Moye, Suneeta Tumati, and Tally Largent-Milnes for their professional efforts as well as for academic, practical and social advice with the warmest friendships. At one time or another, I performed experiments with them and include these works in the latter half of this dissertation.

I would like to thank for generous help and support from Ajinomoto Co., Inc., including Dr.

Kunisuke Izawa, Dr. Takashi Tsuji, Mr. Hiroaki Takano, Mr. Masataka Shoji and Mr. Koichi Fujita, to have treasurable and invaluable research opportunities.

I especially wish to thank my supportive family members. My parents, Hajime and Akiko Yamamoto, helped me to develop my personality and provided my academic education. The biggest thank-you to Naomi, a partner of my life and the best supporter of my research, has been contributing on the completion of this work with her kind and indispensable help. Her contribution has encouraged and supported me greatly.

Finally, I would be very pleased if this thesis repaied even a small part of the many contributions made by my friends.

LIST OF ABBREVIATIONS

Abbreviations used for amino acids and designation of peptides follow the rules of the IUPAC-IUB Commission of Biochemical Nomenclature in *J. Biol. Chem.* **1972**, *247*, 977-83. The following additional abbreviations are used:

AcOH	acetic acid
AIBN	azobisisobutyronitrile
AP effect	antiperiplanar interactions
B3LYP	Beck's three-parameter functional in conjunction with the Lee-Yang-Parr gradient-corrected correlation functional
B3PW91	Beck's three-parameter hybrid functional and Perdew and Wang's 1991 gradient-corrected correlation functional
Boc	*tert*-butyloxycarbonyl
BP86	Becke88–Perdew86 gradient corrected functional
BSA	bovine serum albumin
Bzl	benzyl
CHO	Chinese hamster ovary
Cl-HOBt	1-hydroxy-6-chlorobenzotriazole
CSI	chemical shift index
DAMGO	[*D*-Ala^2, NMePhe^4, Gly^5-ol]enkephalin
DCM	dichloromethane
DFT	density functional theory
DIEA	diisopropylethylamine

DMEM	Dulbecco's modified Eagle's medium
5-DOXYL	5-doxylstearic acid
DPC	dodecylphosphocholine
DPDPE	*cyclo*[*D*-Pen^2, *D*-Pen^5]enkephalin
DQF-COSY	double quantum filtered correlation spectroscopy
EDC	1-ethyl-3-[3-dimethylaminopropyl]carbodiimide hydrochloride
ESI	electrospray ionization
Fmoc	fluorenylmethoxycarbonyl
GTPγS	guanosine-5'-O-(3-thio)triphosphate
GPCR	G-protein coupled receptor
GPI	guinea pig isolated ileum
HCTU	1H-Henzotriazolium-1-[bis(dimethylamino)methylene]-5-chloro-hexafluorophosphate-(1-),3-oxide
hDOR	human δ opioid receptor
HEPES	4-(2-hydroxyethyl)-1-piperazineethanesulfonic acid
HF	Hartree-Fock
hNK1	human neurokinin-1
HOBt	1-hydroxybenzotriazole
HRMS	high-resolution mass spectroscopy
i.th.	intrathecal
LMMP	longitudinal muscle with myenteric plexus
LP effect	delocalization of halogen lone-pair into the antibonding orbital of the C=C or N=N bonds
MP2	second-order Møller-Plesset perturbation theory
MP4(SDTQ)	fourth-order Møller–Plesset perturbation theory with account for single,

	double, triple, and quadruple excitations
MVD	mouse vas deferens
NBO	natural bond orbital
NMM	*N*-methylmorpholine
NMR	nuclear magnetic resonance
NOE	nuclear Overhauser effect
NOESY	nuclear Overhauser enhancement spectroscopy
NPA	natural population analysis
PyBOP	benzotriazol-1-yl-oxytripyrrolidinophosphonium hexafluorophosphate
QCISD(T)	quadratic configuration interaction with single, double and triple excitations added
rMD	restricted molecular dynamics
rMOR	rat μ opioid receptor
rmsd	root mean square deviation
rNK1	rat neurokinin-1
RP-HPLC	reverse phase high performance liquid chromatography
SAR	structure-activity relationships
SCF	self-consistent field
SEM	mean standard error
SP effect	synperiplanar interaction
SPPS	solid phase peptide synthesis
TFA	trifluoroacetic acid
TM domain	trans-membrane domain
TOCSY	total correlation spectroscopy
TPPI	time-proportional phase increment

Trp-NH-3,5-Bzl(CF_3)$_2$	3,5-(bistrifluoromethyl)-benzyl amide of tryptophan
Trp-O-3,5-Bzl(CF_3)$_2$	3,5-(bistrifluoromethyl)-benzyl ester of tryptophan
VSEPR	valence-shell electron-pair repulsion
ZPE	zero point energy

TABLE OF CONTENTS

Chapter 1

Introduction

1.1. Introduction

The interaction of a drug on its targeting receptor has been described using the "key and lock" concept in which the receptor is a lock that only a certain drug (key) can fit in for inducing the biological actions.[1] However, many drugs are not as specific as a key and interact with more than one type of receptor and influence physiological or biochemical processes that were not targeted. This leads to undesirable side-effects of drugs, or toxicity. Therefore, pharmaceutical companies have been paid huge efforts to find a specific "key" with a proper molecular structure which binds exclusively to their intended receptor to eliminate possible adverse effects. An appropriate structure of drug is also necessary for its proper delivery to the targeting cells or organs, based on the pharmacokinetics of a drug including absorption, metabolism, distribution and excretion. Therefore, the molecular structure of a drug is the critical regulating factor for these two important biochemical properties; the specific binding at the targeting receptor and the effective drug-delivery.

The chemical definition of molecular structure is the three-dimensional arrangement of the atoms and chemical bonds which constitute a molecule. Several intrinsic molecular characters and properties, such as stability, reactivity, polarity or magnetism, are derived from the molecular electronic state which originates from the molecular structure.[2, 3] In the host-guest molecular recognition, including a formation of inclusion compound and a ligand-receptor docking to yield bioactivities, the molecular structure also plays a critical role. In fact, the medicinal chemist often experiences that the proper modification of molecular structure in the biologically active ligand significantly improves the bioactivity. Such a relationship between molecular structure and bioactivity is called the "structure-activity relationship (SAR)" which is one of the most important concepts in the pharmaceutical science.[1] According to this concept, it is really important to understand the molecular structure of a ligand from the functional group level to the whole molecular conformation, for obtaining a highly

bioactive drug candidate.

From the quantum-chemical views, a molecular structure could be predicted with the molecular orbital (MO) theory as the maximum stabilizing interactions of the valence orbitals.[4] Therefore, various quantum-chemical models were addressed to date to explain the structure of a molecule. Among them, the valence shell electron pair repulsion (VSEPR) theory is one of the widely-accepted models, since this theory could explain many chemical phenomena with a simple rule.[2, 3, 5] The basic assumption of this theory is that "a molecular structure is determined as a result of the exchange repulsion between a pairs of electrons in the valence shell of a central atom". A rotational barrier of central carbon-carbon bond in ethane (C_2H_6) between the stable 'staggered' conformation and the unstable 'eclipsed' conformation (roughly 3 kcal mol^{-1}) is one of good examples.[2, 3, 5, 6] Generations of chemistry students have been taught that energy barriers like those found in ethane arise from steric effects (exchange repulsion) related to repulsive interactions between the neighboring C−H…C−H bonds based on the VSEPR theory. However, this energetic barrier could also be explained reasonably with the electron delocalization (hyperconjugative theory) in which the antiperiplanar-type electron transfer from a bonding orbital of C−H to an antibonding orbital of the neighboring C−H stabilizes the staggered conformation.[6] As such, even for an internal rotational barrier of a simple ethane, the origin has been discussed for decades.

The "*cis*-effect" is the physicochemical phenomenon in which the *cis*-form of a molecule with a double bond often shows higher thermodynamic stability than the corresponding *trans*-isomer.[7-22] This phenomenon is clearly against the VSEPR theory, since the exchange repulsions between two neighboring substituents should be larger in the *cis*-isomers compared to the ones in the *trans*-isomers. In the first half of this dissertation, the discussion will bee made on the origin of the *cis*-effects in 1,2-dihaloethenes (XHC=CHX, X = F, Cl or Br)[23] and 1,2-dihalodiazenes (XN=NX, X = F, Cl or Br)[23-25] to provide new theoretical insights to support the importance of the hyperconjugative mechanisms rather than the exchange repulsion in these systems to determine the thermodynamically more stable

molecular structures. Because of their structural simplicity and generality, the discussion made in this thesis regarding the orbital-orbital interactions can be a guide to new aspect of modern organic chemistry to understand larger and more complex molecular systems. In fact, many bioactive compounds have a double bond whose configuration has the critical importance in their bioactivities.[26-30] Therefore, this discussion regarding the thermodynamically stable configuration of these simple molecules with a double bond can provide important and basic insights on the proper molecular structure of the bioactive compounds.

In the latter half of this thesis, the discussion was made on the entire three-dimensional molecular structure (molecular conformation) of a bioactive ligand in relevance to their biological activities. As mentioned above, the substitutions or replacements of functional groups in a bioactive compound could yield some shifts of the biological activity, according to the SAR concept. In fact, the substitution or replacement of a functional group could change the three-dimensional molecular-structure of a ligand, leading to the perturbation of ligand's affinity on the corresponding receptor to change the biological activities.[1] Therefore, many studies have been conducted to estimate the bioactivity of a molecule based on its three-dimensional molecular structural information.[1] However, the molecular structure of a ligand observed in aqueous solution is generally different from the docking conformation at the receptor and obtaining the X-ray crystal structure of the ligand-receptor complex is far from easy.

One of the well-developed methodologies to evaluate the three-dimensional molecular structure of a ligand at their targeting receptor is the docking calculation.[31, 32] The first step of the docking calculation is so-called homology modeling which develops a three-dimensional model of the targeted receptor from an amino acid sequence based on the structures of homologous proteins.[33, 34] In this step, an X-ray structure of a protein possessing high homology with the targeted receptor was used as the conformational template. Then, the binding site of the targeted receptor was estimated. At the final step, the ligand was docked onto the estimated binding site to calculate the docking conformation of

ligand-receptor complex.[35] The most important process in this docking procedure is the estimation of three-dimensional structure of targeted receptor with high reliability. Along with the recent development of computational technology and calculation algorithm, the accuracy of docking calculation has been improved if an X-ray structure of protein with high homology to the targeted receptor could be available. However, the reliability of the calculated docking conformation is insufficient if the appropriate template could not be obtained. Moreover, it is still difficult to perform a reliable docking calculation for a ligand with high flexibility.[36, 37] Therefore, the effect of the three-dimensional molecular structure of highly flexible ligand, including a peptide, on their bioactivities still remain ill-defined and further study should be needed.

In order to obtain the structural information regarding the interaction between receptor and peptide ligand, the membrane-bound conformation of the ligand, which binds to the membrane-associated G-protein coupled receptors (GPCRs), was thought. Many GPCRs, including opioid receptors and NK1 receptors, have their ligand binding sites in or near the trans-membrane (TM) domains.[38-41] Since the docking event of such a receptor and a ligand must take place near the membrane, ligand-membrane interactions should be important, and this research topic has been occasionally explored for decades.[42, 43] In fact, it has been pointed out that the membrane promotes ligand-receptor docking,[44-47] and that the ligand adoption into membrane followed by membrane-catalyzed two-dimensional search should be more efficient than the three-dimensional ligand-receptor binding through solvent space.[43, 48-50] Moreover, most of the amino acid sequences of the TM domain of these receptors as well as of their ligand-binding site are lipophilic. Hence, understanding ligand-membrane interactions and membrane-bound structures of flexible ligands is indispensable for further insight into their diverse biological behaviors.[48-50] Based on these considerations, it was hypothesized that the three-dimensional molecular conformation of a ligand in membrane might be related to its docking conformation on the receptor. In the light of this hypothesis, the factors determining the three-dimensional molecular structure in membrane were studied using two-dimensional NMR experiments in the membrane-

mimicking dodecylphosphocholine (DPC) micelles,[51, 52] in relation to their observed bioactivities. The compounds for these NMR experiments were chosen through the extensive SAR study based on the lead peptide **TY001** (H-Tyr-*D*-Ala-Gly-Phe-Pro-Leu-Trp-O-3,5-Bzl(CF_3)$_2$), which was designed as the bifunctional compound for the opioid agonist and NK1 antagonist activities to be a novel pain-relieving drug candidate.

Chapter 2

Studies on the Factors Determining Thermodynamically Stable Molecular Structure of 1,2-Dihaloethenes and 1,2-Dihalodiazenes: the Origin of Their "*cis*-Effect"

2.1. The Origin of *cis*-Effect in 1,2-Dihaloethenes: The Quantitative Comparison of Electron Delocalizations and Steric Exchange Energies.

2.1.1 Background

The interaction between two electronic orbitals has been attracting the attention in modern organic chemistry, because of their important roles in the molecular structure, stability and reactivity.[53, 54] Two major quantum models based on the orbital-orbital interactions have been advocated to dictate the structural stabilization of molecules; the VSEPR (valence shall electron pair repulsion) theory and hyperconjugation (electron delocalization).[55] The former is destabilizing force explained by Pauli exclusion principle, in which pairs of electrons can not occupy the same space. The latter one arises from electron transfer from one occupied orbital to another unoccupied orbital, which leads to the stabilization of the molecule. Both of these interactions exist in a molecule to have an effect on their energetic stability, structure and reactions. Therefore, the discussions have been made to determine which force is the dominant factor in many molecular systems. One of the good examples is the ongoing discussion about the origin of rotational barrier of ethane.[6, 56-64] Both of the orbital interactions could give a reasonable explanation on its rotational barrier, but most of the textbooks explain that the origin is attributed to the exchange repulsion.[2, 3, 5] However, in recent years, some scientists have begun to believe that this rotational barrier comes mostly from the attractive hyperconjugation between the C-H bonds and not from repulsive steric repulsion.[2, 3, 5, 6, 59-64] As such, even for the simple ethane, the discussion on the dominant factor of rotational barrier still does not have dinitive conclusion.

1,2-Dihaloethenes (XHC=CHX; **1**: X = F, **2**: Cl and **3**: Br) are also simple molecules with the characteristic energy differences between their two isomers. According to the Pauli exclusion principle, electronically more condensed *cis*-isomers should be less stable than the corresponding

trans-isomers. However, it was reported that the *cis*-isomers are experimentally more stable than the *trans*-isomers (**1** and **2**) or that both have almost the same stability (**3**).[23, 65, 66] This phenomenon is called "*cis*-effect", and its origin has been discussed over 40 years.[7-22] In this work, it is believed that this phenomenon is the key for understanding the dominant orbital-orbital interaction in a molecule to determine the thermodynamically stable molecular structure. With this motivation, the study was performed on the energetic origin of their *cis*-effect.[11, 12]

In this section, high level *ab initio* and density functional theory (DFT) calculations with the natural bond orbital (NBO) analysis[6, 61, 62, 67-71] were conducted to estimate the hyperconjugations and steric exchange energies in the *cis*- and *trans*-isomers of **1**-**3**, to provide a convincing clue for the origin of the *cis*-effect. The orbital phase theory[72-81] was applied for further understanding about their internal hyperconjugation. The obtained results obviously showed that the *cis*-stabilizing hyperconjugations in the 1,2-dihaloethenes overwhelms the counteracting steric exchange energies, giving rise to their *cis*-effect.

2.1.2. Theoretical Details

2.1.2.1. Computational Methods

All *ab initio* and DFT calculations including NBO analysis were performed with Gaussian 03 program packages.[82] Geometries for those calculations were edited using Spartan program package[83]. Pre-NBO orbitals were plotted using Orbplot 2.0.[84] These initial structures were optimized at HF, MP2, B3LYP and B3PW91 level using 6-311++G(3df,3pd) basis set with 6D option. The single-point energies were calculated at MP3/6-311++G(3df,3pd), MP4(STDQ)/6-311++G(3df,3pd) and BP86/6-311++G(3df,3pd) levels on MP2-opmitized structures, to accurately evaluate the influence of electron correlations on the *cis*-*trans* energy differences. Furthermore, the NBO 2nd-order perturbation analysis[68-71] as well as the natural steric analysis[85-87] was performed at MP2/6-

311++G(3df,3pd)//MP2/6-311++G(3df,3pd) level to quantitatively determine the energetic contributions of each orbital-orbital interactions. Natural population analysis (NPA) was also calculated at the same level to confirm the dominant factor of the *cis*-effect in terms of the electronic population.[69, 70] Frequency calculations were performed on all the optimized geometries to avoid imaginary frequencies in all the 1,2-dihaloethenes **1**–**3**.

NBO 2nd-order perturbation energy (E_2), which is often applied to organic molecules[11-13, 62, 88], is expressed by the following formula,

$$E_2 = q_i \frac{F_{ij}^{\ 2}}{\varepsilon_j - \varepsilon_i}$$

where, q_i is the electron population of the ith donor orbital, ε_i and ε_j are the energy levels of the ith and jth orbital, and F_{ij} is the (i, j) element of the Fock matrix which can be approximated in terms of overlapping two corresponding NBOs.

2.1.2.2. Orbital Phase Theory

The orbital phase theory has been shown to underlie the stabilities of various chemical systems through the delocalization process.[72-81] According to the principle, the orbital phase of cyclic orbital interactions is an important factor in promoting orbital-orbital interactions. The requirement for orbital phase continuity to stabilize the molecule through the effective delocalization process is as follows: (a) the electron-donating orbitals (denoted by D-D) should be out of phase; (b) the accepting orbitals (denoted by A-A) should be in phase; and (c) the donating and accepting orbitals (D-A) should be in phase.

Trans-1,2-dihaloethenes has through-bond π orbital interaction in which two halogen π lone pairs (p and q) interact with π-bonding and antibonding orbitals of the N=N bond (π and π^*) (Figure 2.1.1). As can be seen in Figure 2.1.1a, the orbitals p, q, and π are occupied by two electrons in the ground state

G. The process of delocalization from the halogen π lone pair into the π antibonding orbital of the C=C bond ($n_{X\pi} \rightarrow \pi_{CC}^*$), in which one electron of p or q moves into the vacant π^* orbital, is denoted as p-π^* or q-π^* interaction (T_1 or T_2). From the point of view of orbital interactions, delocalizations are achieved via the mixing process of G with the T_1 or T_2 state. Moreover, the locally excited state (E) is formed when one electron in the π-orbital subsequently shifts into a singly occupied p or q orbital of T_1 or T_2, which are denoted as π-p or π-q interactions. Consequently, the cyclic -G-T_1-E-T_2- configuration (or -π-p-π^*-q- interaction) occurs in the *trans*-1,2-dihaloethenes. In this configuration, halogen lone pairs (p and q) and the π bonding orbital of C=C (π) are clearly electron-donating orbitals (denoted as D) and only the π-antibonding orbital of C=C (π^*) is an acceptor orbital (denoted as A). Hence, stabilization via through-bond electron delocalization is more effective when the orbital phases of these donors and acceptors are continuous, but as depicted in Figure 2.1.1b, the orbital continuity is not satisfied in this through-bond system of *trans*-1,2-dihaloethenes.

However, the mechanism in *cis*-1,2-dihaloethene systems is different because the consideration of through-space interactions between two halogen lone pairs is required. This *cis*-specific interaction could be denoted as p-q interaction in Figure 2.1.2a, in which one electron of a doubly occupied p/q orbital moves into a singly occupied q/p orbital. The existence of this interaction changes the mechanism of the electron delocalization system and the triangle interaction, -G-T_1-T_2- (-π^*-p-q-), is newly provided (Figure 2.1.2b). According to Figure 2.1.2c, the -G-T_1-T_2- configuration is clearly continuous. Because of this speculation, halogen π lone-pair delocalization into the π-antibonding orbital of the C=C bond (π-LP effect: $n_{X\pi} \rightarrow \pi_{CC}^*$) in *cis*-1,2-dihaloethenes could be predicted to be greater than in *trans*-isomers. In this model, the smaller energy gap between the halogen π lone-pair and the π-antibonding orbital of C=C bond (denoted as ΔE in Figure 2.1.2d) strengthens the -G-T_1-T_2- (-π^*-p-q-) type triangle interaction, while the larger ΔE weakens the corresponding triangle interaction.[79] Similar models could be provided for the σ-LP effect system of 1,2-dihaloethenes as

well as for the 1,2-dihalodiazene systems whose orbital-orbital interactions are discussed in the next section.

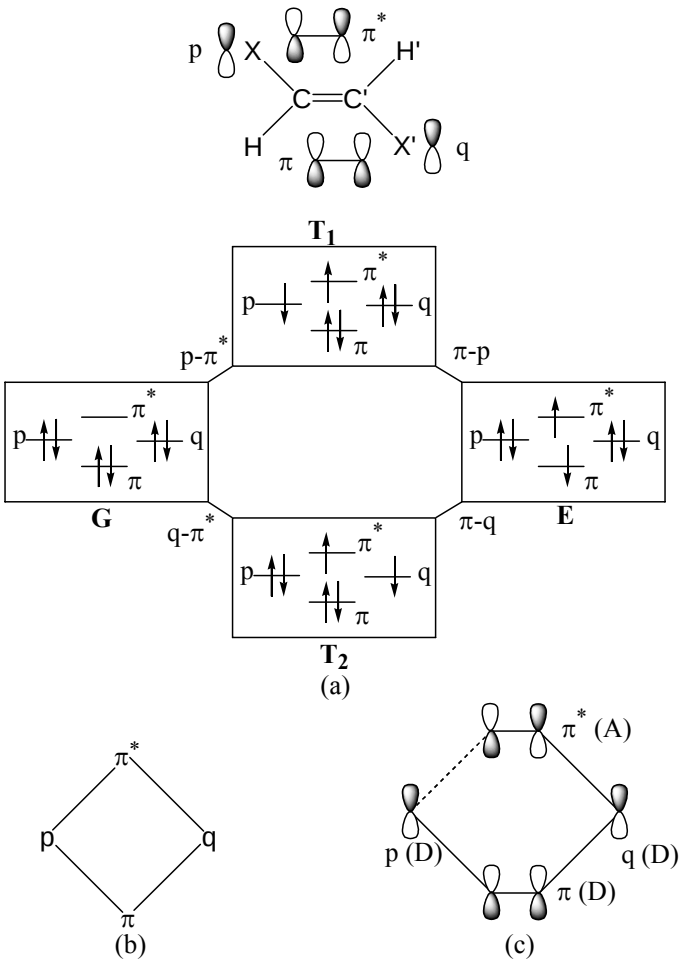

Figure 2.1.1. Through-bond interactions in the π-LP effect of *trans*-1,2-dihaloethenes. (a) Mechanism of electron delocalizations, (b) cyclic orbital interaction, (c) orbital phase discontinuity.

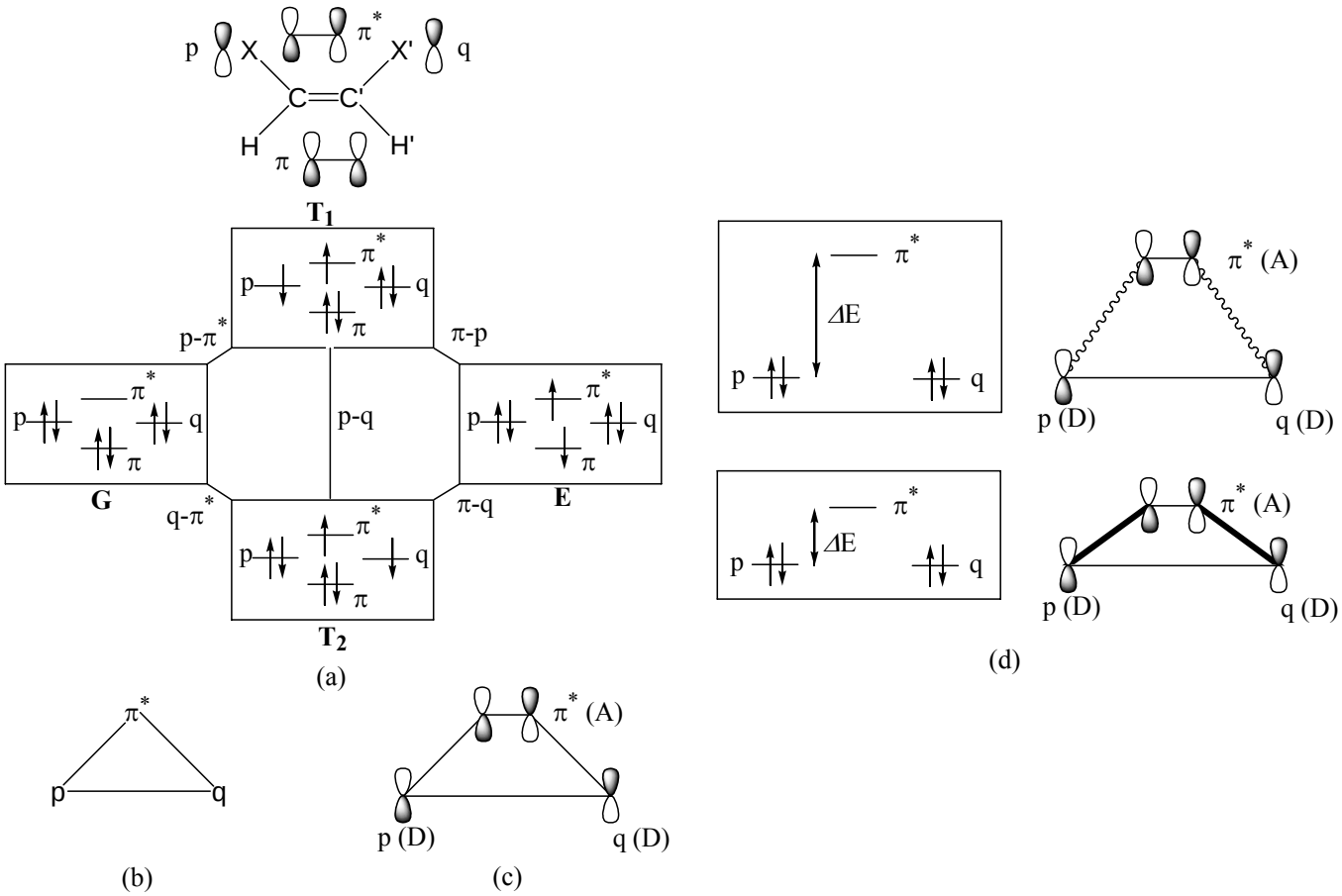

Figure 2.1.2. Through-space interactions in the π-LP effect of *cis*-1,2-dihaloethenes. (a) Mechanism of electron delocalizations, (b) cyclic orbital interaction, (c) orbital phase properties. (d) The energy gap (*Δ*E) between halogen π lone pair (p and q) and antibonding orbital of C=C bond (π^*) changes the strength of triangle orbital interaction -p-π^*-q-. The large energy gap leads to the weakened orbital interaction (up; denoted as wavy line), while the small energy gap results in the strengthened orbital interaction (below; denoted as bold line).

2.1.3. Results and Discussions

2.1.3.1. Geometries and Single-Point Energies

The geometry optimizations of **1-3** were performed with HF, MP2, B3LYP and B3PW91 methods using 6-311++G(3df,3pd) basis set and obtained structural parameters are listed in Table 2.1.1. The available experimental spectral data for **1**-**3** are also shown in the same Table.

The discussion was begun with 1,2-difluoroethenes (**1**) because they are the simplest and widely investigated molecules, in which the *cis*-form of **1** was experimentally determined to be 0.78 ± 0.04 kcal mol^{-1} more stable than the corresponding *trans*-isomer. A comparison of these experimental values with HF-optimized geometries is far from satisfaction because all of the bonds of HF structures were exceedingly shorter than those of experiments. On the other hand, the remaining three optimized geometries (B3PW91, B3LYP, and MP2) agreed well with the experiment (Table 2.1.1). This result dictates that the electron correlation plays a critical role on the molecular structures of **1**. Similarly, in 1,2-dichloroethenes (**2**) and 1,2-dibromoethenes (**3**), the HF methods predicted far shorter $d_{C=C}$ lengths (1.305-1.309 Å) than the experiments (1.332-1.36 Å), while the other methods (B3LYP, B3PW91 and MP2) showed good fit to the experimental structural parameters. This tendency dictates the necessity of post-SCF methods in geometry optimizations of these compounds (**1**-**3**).

Table 2.1.1. Structural parameters for 1,2-dihaloethenes **1** (F), **2** (Cl) and **3** (Br).[a]

		cis					*trans*				
	method [b]	$d_{C=C}$	d_{C-X}	d_{C-H}	θ_{CCH}	θ_{CCX}	$d_{C=C}$	d_{C-X}	d_{C-H}	θ_{CCH}	θ_{CCX}
1 (F)	HF	1.305	1.313	1.069	122.27	122.92	1.304	1.318	1.070	124.90	120.50
	MP2	1.327	1.335	1.078	122.27	122.50	1.326	1.341	1.078	125.10	119.92
	B3LYP	1.321	1.339	1.079	122.82	122.62	1.320	1.344	1.079	125.32	120.25
	B3PW91	1.321	1.332	1.081	122.32	122.91	1.320	1.337	1.081	125.09	120.35
	expl. [c, d]	1.330(11)	1.342(5)	1.099(6)	124.1(4)	122.0(2)					
	expl. [e]						1.324	1.345(5)	1.089	124	119.6(4)
2 (Cl)	HF	1.309	1.715	1.069	120.07	125.67	1.306	1.723	1.069	123.68	121.80
	MP2	1.334	1.706	1.079	120.03	124.48	1.332	1.715	1.079	123.09	121.39
	B3LYP	1.325	1.721	1.079	120.36	125.37	1.322	1.731	1.078	123.80	121.79
	B3PW91	1.325	1.709	1.081	120.18	125.23	1.323	1.718	1.080	123.51	121.82
	expl. [f]	1.337(4)	1.717(2)		120(3)	124.0(2)	1.332(8)	1.725(2)		124(3)	120.8(6)
3 (Br)	HF	1.308	1.874	1.070	120.01	126.59	1.305	1.886	1.068	124.30	121.66
	MP2	1.334	1.865	1.080	120.00	125.30	1.331	1.875	1.079	123.65	121.25
	B3LYP	1.322	1.886	1.079	120.53	126.24	1.319	1.899	1.077	124.77	121.45
	B3PW91	1.323	1.872	1.081	120.45	125.95	1.320	1.883	1.079	124.38	121.56
	expl. [g, d]	1.36(3)	1.87(2)			124(2)					

[a] Structural parameters (d; distance and θ; angle) are given in Å and degree. [b] all geometry optimizations were performed with 6-311++G(3df,3pd) basis set. [c] Electron diffraction data: Ref. 89. [d] Experimental errors were derived from the literature (Ref. 90) and its appendix. [e] Infrared spectra data: Ref. 91. [f] Electron diffraction data: Ref. 92. [g] Electron diffraction data: Ref. 93.

Further evaluations of the four theoretical methods used in the structural optimizations were made in terms of their calculated energy differences between the *cis*- and *trans*-isomers of 1,2-dihaloethenes (**1**-**3**) (Table 2.1.2; the positive number indicates the *cis*-preferable energetic difference). The experimental energy difference in 1,2-difluoroethenes (**1**) is nicely reproduced in the calculated results regardless of the theoretical method used in the optimization (0.77-1.00 kcal mol^{-1}), indicating that post-SCF method is not significantly important for the *cis*-*trans* energy gap in **1**. However, careful selection of the calculation method has to be made in the cases of **2** and **3**. The HF level calculation showed that their *trans*-isomers were more stable than the corresponding *cis*-isomers (−0.31 and −1.28 kcal mol^{-1} for **2** and **3**, respectively), which is clearly inconsistent with the experimental data (0.44 ± 0.09 and 0.09 ± 0.24 kcal mol^{-1}, respectively). Although two DFT results, B3LYP and B3PW91, showed better energy differences than the HF method, they still predicted that the *trans*-1,2-dibromoethene was more stable than its *cis*-counterpart (−0.71 and −0.47 kcal mol^{-1}, respectively). However, the consideration of electron correlation through the MP2 method provided the results closer to the experiment than the DFT calculations. In fact, the MP2-optimized *cis*-form of **3** was found to be 0.28 kcal mol^{-1} more stable than its *trans*-form. Accordingly, comparing the three post-SCF methods used in the geometry optimizations from the energetic viewpoint, the MP2-structures were chosen as the best ones. Therefore, following single-point energy calculations with several post-SCF methods were performed on the MP2 geometries.

As seen in Table 2.1.2, the MP3 energetic differences didn't show good agreement with the experiment in 1,2-dibromoethenes (**3**), but the result for 1,2-dichloroethenes (**2**) was improved from that of MP2 calculation. While, the very high MP4(SDTQ) level calculations with 6-311++G(3df,3pd) basis set reproduced the experimental values of **1**-**3** almost perfectly (0.89, 0.54 and 0.04 kcal mol^{-1} for **1**, **2** and **3**, respectively). Especially, the good agreement in 1,2-dibromoethenes **3** is noteworthy because no literature ever confirmed this subtle *cis*-effect, in which experimental errors exceeded the *cis*-*trans* energy difference (0.09 ± 0.24 kcal mol^{-1}).These results clearly proved that the *cis*-1,2-

dibromoethene has almost same stability as that of corresponding *trans*-isomer in spite of the repulsive forces between two bromine atoms, and high level electron correlation method is necessary to reproduce the experimental value.

A comparison of structural data at MP2 level showed three interesting trends (Table 2.1.1): First, the CCX angles (θ_{CCX}) of cis-isomers (122.5°: **1**, 124.5°: **2** and 125.3°: **3**, respectively) are greater than those of trans-isomers (119.9°: **1**, 121.4°: **2** and 121.3°: **3**, respectively) in all the 1,2-dihaloethenes. As for the bond lengths, cis-isomers (1.327 Å: **1**, 1.334 Å: **2** and 1.334 Å: **3**, respectively) have longer $d_{C=C}$ than corresponding trans-isomers (1.326 Å: **1**, 1.332 Å: **2** and 1.331 Å: **3**, respectively). Adversely, C–X bond lengths d_{C-X} are longer in trans-isomers (1.341 Å: **1**, 1.715 Å: **2** and 1.875 Å: **3**, respectively) than in cis-isomers (1.335 Å: **1**, 1.706 Å: **2** and 1.865 Å: **3**). In fact, these structural tendencies based on the MP2 structures are also found in all the other geometries including calculated and experimental ones. These structural trends might imply the origin of the cis-effect, and NBO 2nd-order perturbation analysis at MP2/6-311++G(3df,3pd)//MP2/6-311++G(3df,3pd) level was performed to evaluate their energetic element(s) (Table 2.1.3).

Table 2.1.2. Relative electronic energy differences (including the ZPE) between *cis*- and *trans*-1,2-dihaloethenes **1** (F), **2** (Cl) and **3** (Br) (kcal mol^{-1}).[a]

Optimized	Single point	**1** (F)	**2** (Cl)	**3** (Br)
HF	HF	0.83	−0.31	−1.28
B3PW91	B3PW91	0.88	0.24	−0.47
B3LYP	B3LYP	0.77	0.09	−0.71
	BP86	0.87	0.37	−0.41
	MP2	0.99	0.76	0.27
	MP3	0.76	0.24	−0.29
	MP4(SDTQ)	0.90	0.54	0.04
MP2	BP86	0.77	0.30	−0.37
	MP2	1.00	0.80	0.28
	MP3	0.76	0.23	−0.38
	MP4(SDTQ)	0.89	0.54	0.04
exp. [b]		0.78 ± 0.04	0.44 ± 0.09	0.09 ± 0.24

[a] All the calculations were performed with 6-311++G(3df,3pd) basis set. [b] The difference in electronic energy between the *cis*-*trans* isomers; Ref. 23.

2.1.3.2. Natural Bond Orbital 2nd–Order Perturbation Analysis

According to the results of NBO 2nd–order perturbation analysis, four types of the important hyperconjugations, antiperiplanar (AP), synperiplanar (SP), σ-lone pair (σ-LP), and π-lone pair (π-LP) effect, were identified to describe the mechanism of the *cis*-effect in 1,2-dihaloethenes **1-3** (Figure.2.1.3). The energy difference of the *i*th and *j*th orbital (ε_i - ε_j) and Fock matrix elements (*Fij*) of two interacting orbitals, both of which were used in the energetic calculation of NBO 2nd–order perturbation analysis, are found in the Tables 2.1.4 and 2.1.5.

Table 2.1.3. NBO 2nd-order perturbation analysis of *cis*- and *trans*-1,2-dihaloethenes **1** (F), **2** (Cl) and **3** (Br) (kcal mol^{-1})[a]

		Periplanar effect				
		AP effect		SP effect		Total [b]
1 (F)	*cis*	7.93 ($\sigma_{CH}\rightarrow\sigma_{C'F'}^{*}$)	1.56 ($\sigma_{CF}\rightarrow\sigma_{C'H'}^{*}$)	0.23 ($\sigma_{CH}\rightarrow\sigma_{C'H'}^{*}$)	0.10 ($\sigma_{CF}\rightarrow\sigma_{C'F'}^{*}$)	19.64
	trans	4.59 ($\sigma_{CH}\rightarrow\sigma_{C'H'}^{*}$)	2.78 ($\sigma_{CF}\rightarrow\sigma_{C'F'}^{*}$)	1.43 ($\sigma_{CH}\rightarrow\sigma_{C'F'}^{*}$)	– [c] ($\sigma_{CF}\rightarrow\sigma_{C'H'}^{*}$)	17.60
		Δ_{AP} [d] = 4.24		Δ_{SP} [d] = −2.20		$\Delta_{AP\&SP}$ [d] = 2.04
2 (Cl)	*cis*	9.62 ($\sigma_{CH}\rightarrow\sigma_{C'Cl'}^{*}$)	3.28 ($\sigma_{CCl}\rightarrow\sigma_{C'H'}^{*}$)	0.79 ($\sigma_{CH}\rightarrow\sigma_{C'H'}^{*}$)	0.03 ($\sigma_{CCl}\rightarrow\sigma_{C'Cl'}^{*}$)	27.44
	trans	5.65 ($\sigma_{CH}\rightarrow\sigma_{C'H'}^{*}$)	6.17 ($\sigma_{CCl}\rightarrow\sigma_{C'Cl'}^{*}$)	0.58 ($\sigma_{CH}\rightarrow\sigma_{C'Cl'}^{*}$)	0.14 ($\sigma_{CCl}\rightarrow\sigma_{C'H'}^{*}$)	25.08
		Δ_{AP} [d] = 2.16		Δ_{SP} [d] = 0.20		$\Delta_{AP\&SP}$ [d] = 2.36
3 (Br)	*cis*	10.55 ($\sigma_{CH}\rightarrow\sigma_{C'Br'}^{*}$)	4.02 ($\sigma_{CBr}\rightarrow\sigma_{C'H'}^{*}$)	0.94 ($\sigma_{CH}\rightarrow\sigma_{C'H'}^{*}$)	0.06 ($\sigma_{CBr}\rightarrow\sigma_{C'Br'}^{*}$)	31.14
	trans	5.85 ($\sigma_{CH}\rightarrow\sigma_{C'H'}^{*}$)	8.09 ($\sigma_{CBr}\rightarrow\sigma_{C'Br'}^{*}$)	0.44 ($\sigma_{CH}\rightarrow\sigma_{C'Br'}^{*}$)	0.37 ($\sigma_{CBr}\rightarrow\sigma_{C'H'}^{*}$)	29.50
		Δ_{AP} [d] = 1.26		Δ_{SP} [d] = 0.38		$\Delta_{AP\&SP}$ [d] = 1.64

		LP Effect		
		$n_{\sigma}\rightarrow\sigma_{CC}^{*}$	$n_{\pi}\rightarrow\pi_{CC}^{*}$	Total [b]
1 (F)	*cis*	8.89	25.77	69.32
	trans	8.12	24.00	64.24
		1.54	3.54	Δ_{LP} [d] = 5.08
2 (Cl)	*cis*	7.86	25.41	66.54
	trans	6.79	22.88	59.34
		2.14	5.06	Δ_{LP} [d] = 7.20
3 (Br)	*cis*	5.97	20.73	53.40
	trans	5.18	18.22	46.80
		1.58	5.02	Δ_{LP} [d] = 6.60

[a] at MP2/6-311++G(3df,3pd)//MP2/6-311++G(3df,3pd). AP: antiperiplanar effect; SP: synperiplanar effect. [b] Total value of periplanar effects or LP effects. The values are doubled because two sets of the same interactions exist. [c] – denotes the negligible interactional energy less than 0.02 kcal mol^{-1}. [d] Δ_{AP}, Δ_{SP} and Δ_{LP} denote the *cis*-*trans* energy difference in the total value of each interaction.

Table 2.1.4. (ε_i - ε_j) values (the energy difference of the *i*th and *j*th orbital) of NBO 2nd-order perturbation analysis in *cis*- and *trans*-1,2-dihaloethenes **1**-**3** at MP2/6-311++G(3df,3pd)//MP2/6-311++G(3df,3pd) level (a.u.).

1 (F)						
Isomers	Periplanar Effects				LP Effects	
	AP Effects		SP Effects		$n_\sigma \rightarrow \sigma_{CC}^*$	$n_\pi \rightarrow \pi_{CC}^*$
cis	$\sigma_{CH} \rightarrow \sigma_{C'F'}^*$ 1.33	$\sigma_{CF} \rightarrow \sigma_{C'H'}^*$ 1.92	$\sigma_{CH} \rightarrow \sigma_{C'H'}^*$ 1.37	$\sigma_{CF} \rightarrow \sigma_{C'F'}^*$ 1.87	1.47	0.84
trans	$\sigma_{CH} \rightarrow \sigma_{C'H'}^*$ 1.37	$\sigma_{CF} \rightarrow \sigma_{C'F'}^*$ 1.86	$\sigma_{CH} \rightarrow \sigma_{C'F'}^*$ 1.32	$\sigma_{CF} \rightarrow \sigma_{C'H'}^*$ -	1.47	0.84

-: the NBO 2nd-order perturbation energy was less than 0.02 kcal mol^{-1}

2 (Cl)						
Isomers	Periplanar Effects				LP Effects	
	AP Effects		SP Effects		$n_\sigma \rightarrow \sigma_{CC}^*$	$n_\pi \rightarrow \pi_{CC}^*$
cis	$\sigma_{CH} \rightarrow \sigma_{C'Cl'}^*$ 1.14	$\sigma_{CCl} \rightarrow \sigma_{C'H'}^*$ 1.59	$\sigma_{CH} \rightarrow \sigma_{C'H'}^*$ 1.39	$\sigma_{CCl} \rightarrow \sigma_{C'Cl'}^*$ 1.34	1.29	0.62
trans	$\sigma_{CH} \rightarrow \sigma_{C'H'}^*$ 1.40	$\sigma_{CCl} \rightarrow \sigma_{C'Cl'}^*$ 1.32	$\sigma_{CH} \rightarrow \sigma_{C'Cl'}^*$ 1.14	$\sigma_{CCl} \rightarrow \sigma_{C'H'}^*$ 1.58	1.30	0.62

3 (Br)						
Isomers	Periplanar Effects				LP Effects	
	AP Effects		SP Effects		$n_\sigma \rightarrow \sigma_{CC}^*$	$n_\pi \rightarrow \pi_{CC}^*$
cis	$\sigma_{CH} \rightarrow \sigma_{C'Br'}^*$ 1.06	$\sigma_{CBr} \rightarrow \sigma_{C'H'}^*$ 1.52	$\sigma_{CH} \rightarrow \sigma_{C'H'}^*$ 1.41	$\sigma_{CBr} \rightarrow \sigma_{C'Br'}^*$ 1.17	1.26	0.58
trans	$\sigma_{CH} \rightarrow \sigma_{C'H'}^*$ 1.42	$\sigma_{CBr} \rightarrow \sigma_{C'Br'}^*$ 1.15	$\sigma_{CH} \rightarrow \sigma_{C'Br'}^*$ 1.06	$\sigma_{CBr} \rightarrow \sigma_{C'H'}^*$ 1.51	1.26	0.58

Table 2.1.5. *F(i, j)* (the (i, j) element of the Fock matrix) of NBO 2nd-order perturbation analysis in *cis*- and *trans*-1,2-dihaloethenes **1-3** at MP2/6-311++G(3df,3pd)//MP2/6-311++G(3df,3pd) level (a.u.).

1 (F)						
Isomers	Periplanar Effects				LP Effects	
	AP Effects		SP Effects		$n_\sigma \rightarrow \sigma_{CC}^*$	$n_\pi \rightarrow \pi_{CC}^*$
cis	$\sigma_{CH} \rightarrow \sigma_{C'F'}^*$ 0.092	$\sigma_{CF} \rightarrow \sigma_{C'H'}^*$ 0.049	$\sigma_{CH} \rightarrow \sigma_{C'H'}^*$ 0.016	$\sigma_{CF} \rightarrow \sigma_{C'F'}^*$ 0.012	0.102	0.133
trans	$\sigma_{CH} \rightarrow \sigma_{C'H'}^*$ 0.071	$\sigma_{CF} \rightarrow \sigma_{C'F'}^*$ 0.064	$\sigma_{CH} \rightarrow \sigma_{C'F'}^*$ 0..039	$\sigma_{CF} \rightarrow \sigma_{C'H'}^*$ -	0.098	0.128

-: the NBO 2nd-order perturbation energy was less than 0.02 kcal mol^{-1}

2 (Cl)						
Isomers	Periplanar Effects				LP Effects	
	AP Effects		SP Effects		$n_\sigma \rightarrow \sigma_{CC}^*$	$n_\pi \rightarrow \pi_{CC}^*$
cis	$\sigma_{CH} \rightarrow \sigma_{C'Cl'}^*$ 0.092	$\sigma_{CCl} \rightarrow \sigma_{C'H'}^*$ 0.065	$\sigma_{CH} \rightarrow \sigma_{C'H'}^*$ 0.030	$\sigma_{CCl} \rightarrow \sigma_{C'Cl'}^*$ 0.006	0.090	0.113
trans	$\sigma_{CH} \rightarrow \sigma_{C'H'}^*$ 0.079	$\sigma_{CCl} \rightarrow \sigma_{C'Cl'}^*$ 0.081	$\sigma_{CH} \rightarrow \sigma_{C'Cl'}^*$ 0.023	$\sigma_{CCl} \rightarrow \sigma_{C'H'}^*$ 0.013	0.084	0.108

3 (Br)						
Isomers	Periplanar Effects				LP Effects	
	AP Effects		SP Effects		$n_\sigma \rightarrow \sigma_{CC}^*$	$n_\pi \rightarrow \pi_{CC}^*$
cis	$\sigma_{CH} \rightarrow \sigma_{C'Br'}^*$ 0.095	$\sigma_{CBr} \rightarrow \sigma_{C'H'}^*$ 0.070	$\sigma_{CH} \rightarrow \sigma_{C'H'}^*$ 0.032	$\sigma_{CBr} \rightarrow \sigma_{C'Br'}^*$ 0.008	0.077	0.099
trans	$\sigma_{CH} \rightarrow \sigma_{C'H'}^*$ 0.081	$\sigma_{CBr} \rightarrow \sigma_{C'Br'}^*$ 0.086	$\sigma_{CH} \rightarrow \sigma_{C'Br'}^*$ 0.019	$\sigma_{CBr} \rightarrow \sigma_{C'H'}^*$ 0.210	0.072	0.093

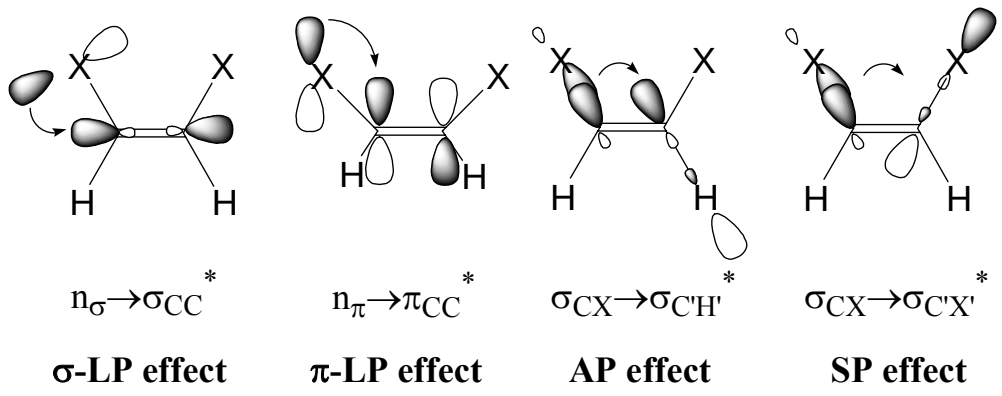

Figure. 2.1.3. Definitions of the lone pair (n_σ and n_π) delocalization effect (σ- or π-LP effect), the antiperiplanar hyperconjugation effect (the AP effect) and the synperiplanar hyperconjugation effect (the SP effect) within the NBO framework for *cis*-1,2-dihaloethenes (X=F, Cl or Br).

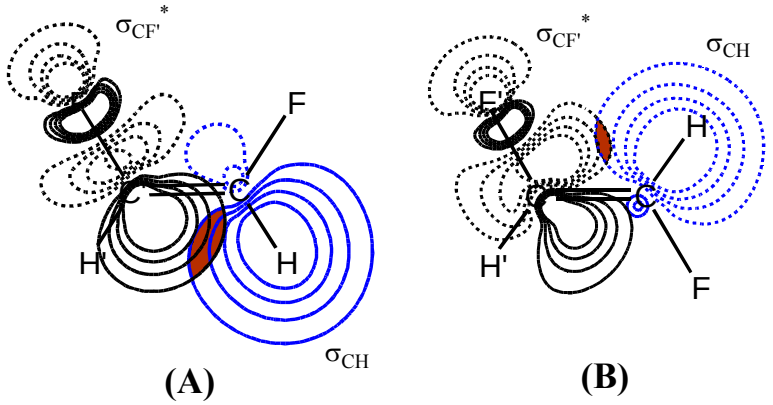

Figure. 2.1.4. pre-NBO interactions of $\sigma_{CH} \rightarrow \sigma_{C'F'}^*$ hyperconjugation for *cis*- (A) and *trans*-1,2-difluoroethenes (B). The hyperconjugation is anti-periplanar (AP) interaction in the *cis*-isomer whereas the corresponding *trans*-isomer has syn-periplanar (SP) interaction. Orbital contours were calculated from the same level for both isomers and the overlap of two orbitals were hatched for clearity.

The first two are antiperiplanar and synperiplanar σ_{CX}–$\sigma_{C'X'}^*$ (X, X'= H, F, Cl or Br) interactions across the C=C bond (AP and SP effects), in which doubly occupied orbital of C-X bond (X = H, F, Cl or Br) was interacted with the adjacent unoccupied orbital of C'-X' bond (X' = H', F', Cl' or Br'). The 2nd-order perturbation energies for these periplanar type hyperconjugations are given in Table 2.1.3 which shows that the magnitudes of each SP effects are uniformly less than 1.5 kcal mol^{-1} and much smaller than those of AP effects (1.56-10.55 kcal mol^{-1}). This predominance of AP effects over SP effects could be explained by the orbital overlaps. As seen in Figure 2.1.4, the overlap of the main lobe of the C-H bonding orbital (σ_{CH}) with the antibonding orbital of C'-X' bond ($\sigma_{C'X'}^*$) in the *cis*-isomer (AP effect) is much greater than one in the corresponding *trans*-isomer (SP effect) (Please see F_{ij} values in the Table 2.1.5). Due to the electronegativity of fluorine atom in **1**, σ_{CF} has much lower orbital energy and thus less ability as an electron donor than σ_{CH}, while the $\sigma_{C'F'}^*$ could be better electron acceptor than $\sigma_{C'H'}^*$ for the same reason. Therefore, the most significant combination of occupied and unoccupied orbitals to be interacted is $\sigma_{CH}\rightarrow\sigma_{C'F'}^*$. In fact, the most efficient AP effect in 1,2-difluoroethene (**1**) was $\sigma_{CH}\rightarrow\sigma_{C'F'}^*$ in the *cis*-isomer (7.93 kcal mol^{-1}) and total amount of AP effect made *cis*-isomer 4.24 kcal mol^{-1} more stable than the corresponding *trans*-isomer. As halogen atom becomes less electronegative, the energetic level of C−X bonding orbital (σ_{CX}) gets higher. While, the larger halogen atom provides weaker bonding energy and longer length of C−X bond, leading to the smaller energetic gap between the σ_{CX} and the $\sigma_{C'X'}^*$. Therefore, as halogen atom gets heavier, both the electron donating ability of σ_{CX} and accepting ability of $\sigma_{C'X'}^*$ get larger, and thus the energetic values of $\sigma_{CH}\rightarrow\sigma_{C'X'}^*$ interactions in *cis*-isomers get greater (9.62 and 10.55 kcal mol^{-1} for X = Cl and Br, respectively; the energetic differences of two orbitals are available in Table 2.1.4). These changes of energy levels in the bonding and antibonding orbitals of C-X bonds also could be confirmed from the energetic values of $\sigma_{CX}\rightarrow\sigma_{C'X'}^*$ in the *trans*-isomers which increased as the halogen atom got larger (2.78, 6.17 and 8.09 kcal mol^{-1} for X = F, Cl and Br, respectively), leading to

the gradually decreasing *cis*-preference energy of AP effect (4.24, 2.16 and 1.26 kcal mol^{-1} for X = F, Cl and Br, respectively). As a result, the summation of AP and SP periplanar effects made *cis*-isomers 2.04, 2.36 and 1.64 kcal mol^{-1} more stable than the *trans*-isomers for **1**, **2** and **3**, respectively. Accordingly, these periplanar effects were proved to be one of the important origins of the *cis*-effect.

Second and more important ones are the σ and π halogen lone pairs delocalizations into σ and π C=C antibonding orbitals (LP effect). The $n_{\sigma} \rightarrow \sigma_{CC}^{*}$ (σ-LP effect) interactions were the *cis*-preferable by 1.54, 2.14 and 1.58 kcal mol^{-1} for X = F, Cl and Br, respectively. The energetic amount of this interaction in 1,2-difluoroethenes (**1**) was the largest among the 1,2-dihaloethenes **1**-**3** (8.89 kcal mol^{-1} for *cis*- and 8.12 kcal mol^{-1} for *trans*-isomer), presumably because of their shortest C−X bond lengths which led to the largest orbital-orbital overlaps. The influence of the $n_{\pi} \rightarrow \pi_{CC}^{*}$ (π-LP effect) interactions were found to be noteworthy, because they stabilized the *cis*-isomers more than the corresponding *trans*-isomers by 3.54, 5.06 and 5.02 kcal mol^{-1}, respectively. Furthermore, the total energetic differences of σ- and π-LP effects (5.08, 7.20 and 6.60 kcal mol^{-1}, respectively) were greater than those of periplanar effects (2.04, 2.36 and 1.64 kcal mol^{-1}, respectively), and thus the LP effect could be treated as the major origin of the *cis*-effect in all the 1,2-dihaloethenes **1**-**3**. Moreover, the total energetic amount of these LP effects (69.32, 64.24, 66.54, 59.34, 53.40 and 46.80 kcal $mol^{-1}$for *cis*-**1**, *trans*-**1**, *cis*-**2**, *trans*-**2**, *cis*-**3** and *trans*-**3**, respectively: Table 2.1.3) was apparently greater than those of periplanar effects (19.64, 17.60, 27.44, 25.08, 31.14 and 29.50 kcal $mol^{-1}$for *cis*-**1**, *trans*-**1**, *cis*-**2**, *trans*-**2**, *cis*-**3** and *trans*-**3**, respectively). Those great influences of the LP effect could be seen in their structural parameters, because the LP effect seemed to elongate more the C=C bond lengths and made the C−X bond lengths shorter in the *cis*-isomers. The larger LP effect as well as the greater repulsive forces (dipole-dipole and Pauli repulsions) between two halogen atoms invoked wider CCX angles in the *cis*-isomers than in the *trans*-isomers. In fact, those structural trends could be seen in all the calculated and experimental geometries of **1**-**3** (Table 2.1.1). The reason why the σ- and π-LP

effects were greater in *cis*-isomers than in *trans*-isomers was clearly elucidated with the orbital phase theory, as explained in the Section 1.1.2.2. Total summations of periplanar and LP effects of *cis*-isomer exceeded those of *trans*-isomer by 7.12, 9.56 and 8.24 kcal mol^{-1} for **1**, **2** and **3**, respectively, which suggests that these hyperconjugation effects is the incontestable driving forces to produce the *cis*-effect.

Following the NBO 2nd-order perturbation analysis, natural population analysis (NPA) was performed to estimate the importance of those electron delocalization systems from a different perspective. As can be seen in Table 2.1.6, all the carbon atoms in the *trans*-isomers had more positive charges than those in the *cis*-isomers. While, the halogen atoms in the *trans*-isomers were found to be more negative than those in the *cis*-isomers. This observation clearly indicated that the more halogen lone pair electrons moved into carbon atoms in the *cis*-isomers, which could be taken as the obvious evidence of greater LP effect. Moreover, the positive charges of chlorine and bromine atoms in both *cis*- and *trans*-isomers in **2** and **3** might show that those heavy halogen atoms act as good electron donors, as supporting the predominance of LP effects.

In order to obtain the steric exchange contribution to the 1,2-dihaloethene systems, the natural steric analysis[85-87] was applied on **1**-**3** (Table 2.1.7). In 1,2-difluoroethene (**1**) with the smallest halogen atoms, total amount of steric exchange energy in the c*is*-isomer was slightly (0.30 kcal mol^{-1}) greater than that of *trans*-isomer. However, as halogen atom becomes larger, the *cis*-*trans* difference of steric exchange energies increased steadily (3.94 and 5.56 kcal mol^{-1} for **2** and **3**, respectively), primarily owning to the interatomic repulsion of the two halogen atoms in the *cis*-isomers (0.83, 2.85 and 3.34 kcal mol^{-1} for **1**, **2** and **3**, respectively). As a consequence, the differences of total steric exchange energies were *trans*-stabilizing by 0.30, 3.94 and 5.56 kcal mol^{-1} for **1**, **2** and **3**, respectively, which obviously counteract against *cis*-preferable hyperconjugation mechanisms, especially in the compounds with larger halogen atoms. However, it should be noted that the amounts of steric exchange energies were apparently smaller than those of hyperconjugations

(7.12, 9.56 and 8.24 kcal mol^{-1} for **1**, **2** and **3**, respectively), suggesting that the steric repulsion might not be an essential factor of *cis*-*trans* energetic differences in the 1,2-dihaloethene systems, but as a mere subordinate mechanism. As a consequence, the summation of the *cis*-*trans* energetic differences in the hyperconjugations and steric exchange energies were 6.82, 5.62 and 2.68 kcal mol^{-1} for **1**, **2** and **3**, respectively, which gradually decreased as the halogen atom got larger. Although some other *trans*-stabilizing forces, such as dipole-dipole moment and electrostatic repulsion, might be expected, this energetic tendency in the framework of NBO analysis successfully reproduced the one in the experimentally observed *cis*-*trans* energetic gaps for **1**-**3** (Table 2.1.2).[23]

Table 2.1.6. Natural population analysis of *cis*- and *trans*-1,2-dihaloethenes **1** (F), **2** (Cl) and **3** (Br) (a.u.).[a]

	atom	*cis*	*trans*	$\Delta_{cis\text{-}trans}$ [b]
1 (F)	C	0.2204	0.2232	–0.0028
	F	–0.3813	–0.3847	0.0034
	H	0.1609	0.1615	–0.0006
2 (Cl)	C	–0.2193	–0.2089	–0.0104
	Cl	0.0147	0.0051	0.0096
	H	0.2046	0.2038	0.0009
3 (Br)	C	–0.2973	–0.2839	–0.0134
	Br	0.0873	0.0745	0.0128
	H	0.2100	0.2094	0.0006

[a] at MP2/6-311++G(3df,3pd)//MP2/6-311++G(3df,3pd). [b] $\Delta_{cis\text{-}trans}$ denotes differences between *cis*- and *trans*-isomers

Table 2.1.7. Natural steric analysis of *cis*- and *trans*-1,2-dihaloethenes **1** (F), **2** (Cl) and **3** (Br) (kcal mol^{-1})[a]

		total steric exchange energy	steric exchange energy between two lone pairs
1 (F)	*cis*	81.29	0.83
	trans	80.99	0.67
	$\Delta_{cis\text{-}trans}$ [b]	0.30	0.16
2 (Cl)	*cis*	77.20	2.85
	trans	73.26	0.69
	$\Delta_{cis\text{-}trans}$	3.94	2.16
3 (Br)	*cis*	71.57	3.34
	trans	66.02	0.41
	$\Delta_{cis\text{-}trans}$	5.56	2.93

[a] at MP2/6-311++G(3df,3pd)//MP2/6-311++G(3df,3pd). [b] $\Delta_{cis\text{-}trans}$ denotes differences between *cis*- and *trans*-isomers

2.1.4. Summary of the Section

The MO calculations were performed to estimate the contribution of hyperconjugations and steric exchange energy in the energetic difference of *cis*- and *trans*-isomers of 1,2-dihaloethenes (XHC=CHX; **1**: X = F, **2**: Cl and **3**: Br). According to the NBO 2nd-order perturbation analysis, two types of hyperconjugations were found important: the periplanar interactions between C−X bond (X= H, F, Cl or Br) and C'−X' bond (X'= H', F', Cl' or Br') locating at a *anti* or *syn* position across the C=C bond (AP and SP effect); the second and greatest one was the electron delocalizations from halogen lone pairs into σ and π antibonding orbitals of the C=C bond (LP effect). This greater LP effect in the *cis*-isomer was clearly explained with the orbital phase theory, i.e., the cyclic orbital interaction was continuous only in the *cis*-isomers of **1**-**3**. While, the steric exchange energy was found as a *trans*-stabilizing force especially for the 1,2-dihaloethenes with large halogen atoms, based on the

natural steric analysis. However, the total energetic gain of steric exchange energies was apparently less than those of *cis*-preference hyperconjugations for all the 1,2-dihaloethenes. Therefore, the periplanar and LP effects could be regarded as the origin of *cis*-effect and the latter was the predominant one. The *cis*-*trans* differences in the bond lengths and atomic charges supported the fact. The central point of this section is that the hyperconjugation has the largest responsibility for the *cis*-*trans* energy differences as well as for determining the thermodynamically more stable molecular structure in 1,2-dihaloethene systems.

2.2. Theoretical Investigations on the Thermodynamic Stability of *cis*- and *trans*-Isomers in 1,2-Halodiazenes

2.2.1. Background

The nitrogen–nitrogen double bond is popular in textbooks for general organic chemistry. Several diaryl azocompounds are widely used as dyes and pH indicators.[2, 3, 5] Diethyl azodicarboxylate (DEAD) reacts with phosphine to form an important intermediate in the Mitsunobu reaction.[94-98] Azobisisobutyronitrile (AIBN) is a frequently used radical initiator, which decomposes into nitrogen and two cyanoisopropyl radicals when it is heated or light-irradiated. As such, many molecules possessing an N=N bond are known to be stable under normal conditions and are used for many purposes. Thus, the understanding of their electronic structure as well as the factors determining their geometries has been important and has been studied for decades. 1,2-Difluorodiazenes (FN=NF; **4**) are known to be the only stable dihalodiazenes. A trace of 1,2-dichlorodiazenes (ClN=NCl; **5**) seems to have been detected,[99] but nothing has been reported on 1,2-dibromodiazenes (BrN=NBr; **6**), experimentally and theoretically. Morokuma[100, 101] and Schneider[102] independently calculated the dissociation energy barriers of 1,2-difluorodiazenes (**4**) and 1,2-dichlorodiazenes (**5**), and reached the same conclusion; the former ones (**4**) had large barriers for N–F bond cleavage, while those of N–Cl bond in the 1,2-dichlorodiazenes (**5**) were small and they instantaneously decompose into nitrogen gas and two chlorine radials. Their discussions on the potential energy surface of **2** were comprehensive and reasonable, but the critical explanation for the chemical weakness of the N–Cl bond was missing.

Because of their availability and simple molecular structures, 1,2-difluorodiazenes (**4**) are well-studied molecules possessing an interesting chemical feature called the "*cis*-effect," which has been known for 40 years.[23, 103] The *cis*-effect of **4** is a physicochemical phenomenon in which its *cis*-isomer

was experimentally reported to be more stable than the corresponding *trans*-isomer by 3.050 ± 0.400 kcal mol^{-1}.[23] Furthermore, even though no experimental results have been reported, previous calculations showed that the 1,2-dichlorodiazenes (**5**) also have the *cis*-preferable energetic gap between the two isomers (6.8 kcal mol^{-1}).[24] Since the *cis*-isomers of 1,2-dihalodiazenes are electronically more condensed and have greater dipole–dipole repulsion between the two N–X bonds, this phenomenon is obviously at odds with the valence-shell electron-pair repulsion (VSEPR) theory and hence the origin of this mysterious *cis*-effect has been a long-standing question in the field of basic chemistry.[23, 65] Wolfe insisted that the sum of the repulsive forces among two nitrogen lone pairs and two N–F bonds was greater in the *trans*-isomer, which led the *cis*-isomer to be more stable.[104-106] Epiotis performed the Hartree-Fock (HF) level calculations with 4-31G basis set and qualitatively ascribed the *cis*-effect to two delocalization mechanisms: the nitrogen lone-pair delocalization into the antibonding orbital of the neighboring N–F bond, ($n_N \rightarrow \sigma_{N'F'}^*$; AP effect) and the out-of-plane lone-pair delocalization of F ($n_{F\pi}$) into the antibonding π-orbital of the N=N bond ($n_{F\pi} \rightarrow \pi_{NN'}^*$; π-LP effect). However, the contributions of these delocalization mechanisms were not evaluated quantitatively.[21, 22, 107] Skancke indicated that π delocalizations including $n_{F\pi} \rightarrow \pi_{NN}^*$ were the origin.[108] Recently, Anders performed high-level post-SCF calculations (MP2, B3LYP and BP86) with 6-311++G(3df,3pd) basis set and concluded that the *cis–trans* energy difference came from the lone pair–lone pair repulsion, antiperiplanar interactions, and Coulombic repulsion or attraction between diazene substituents.[24] As such, a number of theories and calculations have been independently or qualitatively performed to explain this phenomenon, but the origin of the *cis*-effect in 1,2-dihalodiazenes is still controversial.

Here, high-level *ab initio* and density functional theory (DFT) calculations have been combined with natural bond orbital (NBO) analysis[6, 61, 62, 67-71] and orbital phase theory[72-81] to quantitatively investigate this puzzling *cis–trans* energy gap in 1,2-dihalodiazenes (XN=NX; X = **4**: F, **5**: Cl or **6**: Br), just as shown in the *cis*-effect on 1,2-dihaloethenes,[11, 12] where the dominant factor was halogen

lone pair delocalized into the antibonding orbitals of the C=C bond (LP effect, please see the Section 2.1). The origin of their *cis*-effect could be considered as the factors determining thermodynamically stable molecular structure in these systems. The unsubstituted 1,2-diazenes (HN=NH: **7**) were used as reference compounds because previous infrared and near-ultraviolet absorption spectrum showed that the *trans*-isomer of **7** was the most stable isomer[109-113] and several theoretical calculations proved the *trans*-preference energy difference.[24, 114] Moreover, the electronic structures of 1,2-dihalodiazenes were extensively examined from the viewpoint of orbital–orbital interactions to clarify the reason for the particular instability of 1,2-dibromodiazenes (**6**) compared to the reported degradability of 1,2-dichlorodiazenes (**5**), and the fair stability of 1,2-difluorodiazenes (**4**). For further understanding of the electronic structures of 1,2-dihalodiazenes **4-6,** their calculated trends in the geometries and orbital-orbital interactions were compared to those of the 1,2-dihaloethenes which were the electronic isosteres to the 1,2-dihalodiazenes (please see the Section 2.1).[11, 12]

2.2.2. Theoretical Details

2.2.2.1. Computational Methods

All the *ab initio* and DFT calculations including NBO analysis were performed using the similar procedure for the 1,2-dihaloethenes (Section 2.1.2.1) . The geometries for the calculations were edited using the vi text editor or Spartan program package.[83] These initial structures were optimized at HF, MP2, B3LYP, and B3PW91 levels using very large 6-311++G(3df,3pd) basis set with 6D option. Then, single-point energies were calculated on B3LYP-optimized structures to accurately evaluate the influence of the electron correlations on *cis–trans* energy differences. Furthermore, NBO 2nd-order perturbation analysis[6, 61, 62, 67-71] were performed at the BP86/6-311++G(3df,3pd)//B3LYP/6-311++G(3df,3pd) level to quantitatively determine the contributions of two-electron–two-orbital interactions. Natural population analysis (NPA) was also performed at the same level to confirm the

mechanism of the *cis*-effect from the viewpoint of the electron population.[69, 70] Frequency calculations were performed on all the optimized geometries to avoid imaginary frequencies in all the 1,2-disubstituted and unsubstituted diazenes **4**–**7**.

2.2.3. Results and Discussions

2.2.3.1. Geometry Optimization

It has been reported that a high-level theoretical method with sufficient electron correlation should be conducted to reproduce the experimental geometries of 1,2-difluorodiazenes (**4**).[24, 115, 116] In fact, optimized structures of **4** at the HF level gave far shorter N–F (1.323 and 1.324 Å for *cis*- and *trans*-isomers, respectively) and N=N bonds (1.189 and 1.186 Å, respectively) than the experimental parameters (N–F bonds: 1.384 or 1.409 Å for *cis*-isomer, 1.398 Å for *trans*-isomer; N=N bonds: 1.214 or 1.209 Å for *cis*-isomer, 1.224 Å for *trans*-isomer) (Table 2.2.1). On the other hand, the remaining three geometries based on the post-SCF methods, MP2, B3LYP, and B3PW91, were clearly closer to the experiment and proved the strong influence of electron correlation on both the N–F and N=N bonds. Among these structures, MP2-optimized ones had rather longer N=N bonds (1.229 and 1.238 Å for *cis*- and *trans*-isomers, respectively) and shorter N–F bonds (1.375 and 1.373 Å, respectively) compared to the experimental results, presumably because of the overestimation of electron correlation. The applied DFT methods, B3LYP and B3PW91, showed good agreement with the experimental geometries, but the B3LYP structures were chosen for further single-point energy calculations, since the reliability of this method has already been reported for 1,2-difluorodiazene system (**4**).[116] The structure optimizations were also conducted at the same level for 1,2-dichlorodiazene (**5**), 1,2-dibromodiazene (**6**) and the reference compound 1,2-diazene (**7**) (Table 2.2.1).

Table 2.2.1. Calculated bond length and angles of 1,2-substituted and unsubstituted diazenes, XN=NX (X=F, Cl, Br or H)[a]

X	Method	*cis*			*trans*		
		N=N	N-X	∠N-N-X	N=N	N-X	∠N-N-X
4 (F)	HF[b]	1.189	1.323	114.6	1.186	1.324	107.5
	MP2[b]	1.229	1.375	114.2	1.238	1.373	104.9
	B3LYP[b]	1.209	1.387	115.1	1.216	1.381	105.8
	B3PW91[b]	1.209	1.373	115.1	1.216	1.368	105.9
	BP86[c]	1.218	1.402	115.8	1.232	1.402	104.9
	expl.[d]	1.214(5)	1.384(10)	114.5(5)			
	expl.[e]	1.209	1.409	114.4	1.224	1.398	105.5
5 (Cl)	HF[b]	1.184	1.719	122.0	1.186	1.716	111.2
	MP2[b]	1.221	1.755	121.2	1.241	1.740	108.5
	B3LYP[b]	1.191	1.795	122.6	1.206	1.782	109.5
	B3PW91[b]	1.196	1.764	122.2	1.211	1.753	109.5
6 (Br)	HF[b]	1.169	1.913	124.0	1.175	1.906	111.3
	MP2[b]	1.194	1.980	123.9	1.222	1.946	108.4
	B3LYP[b]	1.167	2.022	125.3	1.179	2.017	109.6
	B3PW91[b]	1.174	1.977	124.7	1.188	1.973	109.6
7 (H)	HF[b]	1.210	1.015	112.9	1.208	1.012	108.1
	MP2[b]	1.254	1.035	111.6	1.255	1.030	105.8
	B3LYP[b]	1.235	1.039	112.9	1.236	1.033	107.0
	B3PW91[b]	1.232	1.038	112.8	1.233	1.033	106.9
	expl.[f]				1.252(2)	1.028(5)	106.51(28)

[a] Structural data are given in angstrom and degrees. [b], 6-311++G(3df,3pd) basis set was used. [c] 6-311++G(3df,3pd) basis set was used, Ref. 24. [d] Microwave spectroscopy data, Ref. 117. [e] Electron diffraction data, Ref. 118. [f] Infrared absorption spectra data, Ref. 119.

For the obtained B3LYP optimized structures, N=N bond length of *cis*-1,2-diflurodiazene (1.209 Å) is shorter than that of the corresponding *trans*-isomer (1.216 Å), both of which showed good agreement with the experiments (1.214 or 1.209 Å for *cis*-isomer, 1.224 Å for *trans*-isomer, respectively) (Table 2.2.1). On the other hand, N–F bond length in the *cis*-isomer (1.387 Å) is longer than its *trans*-counterpart (1.381 Å) (experimental values: 1.384 or 1.409 Å for *cis*-isomer, 1.398 Å for

trans-isomer). These structural trends were clearly opposite to the 1,2-dihaloethenes where C=C bonds in the *cis*-isomers and C–X bonds in the *trans*-isomers were longer than those in the other isomers (Section 1.1).[11, 12] Changes in their structural parameters might imply differences in their electronic states. The NNF angles in the *cis*-isomer like those in 1,2-dihaloethenes are greater and indicate the existence of repulsive forces (N–F dipole moment repulsion and lone pair/lone pair repulsion) or hyperconjugation mechanisms possessing structural influences on the molecules (Section 2.1).[11, 12] These trends were also found in both the 1,2-dichlorodiazenes (**5**) and the 1,2-dibromodiazenes (**6**) with the N=N bonds being shorter going down the periodic table: N=N bond lengths are 1.209, 1.191, and 1.165 Å in *cis*-**4**, *cis*-**5,** and *cis*-**6**, respectively. The same trend was found for their *trans*-isomers (Table 2.2.1). Moreover, it should be noted that the molecules possessing larger halogen atoms have wider NNX angles: 115.1, 122.6, and 125.3º in *cis*-**4**, *cis*-**5** and *cis*-**6**, respectively. Their *trans*-isomers also showed the same tendency (Table 2.2.1).

2.2.3.2. *Cis-trans* Energy Differences

Subsequent single-point energy calculations were performed on the B3LYP/6-311++G(3df,3pd) geometries using a variety of methods (Table 2.2.2). In the 1,2-difluorodiazenes (**4**), the HF calculations showed poor results compared to the experimental value (Table 2.2.2), even with the very large 6-311++G(3df,3pd) basis set. This result indicated that the electron correlation, which might have a relationship with van der Waals forces, has a strong influence on the *cis–trans* energy difference. As Jursic[114] and Anders[24] described, the BP86 method, a non-local DFT, reproduced the experimental energy difference almost perfectly. All of the MP2, B3LYP, and B3PW91 level calculations were good, but they were not comparable with the BP86 result. MP4(SDTQ) and QCISD(T), which are extremely high-level *ab initio* methods, provided a similar energy difference as MP2 and B3LYP calculated methods.

Table 2.2.2. Calculated *cis–trans* energy differences (including the ZPE) of 1,2-substituted and unsubstituted diazenes, XN=NX (X=F, Cl, Br or H) (kcal mol^{-1}, the positive number indicates *cis*-preference)

Method [a]	**4** (F)	**5** (Cl)	**6** (Br)	**7** (H)
HF [b]	−1.82	−3.03	−3.14	–6.07
B3LYP [c]	1.67	4.14	4.73	–5.03
B3PW91 [d]	1.64	4.16	4.77	–5.08
MP2 [e]	1.30	3.75	5.36	–5.42
MP4(SDTQ) [c]	1.85	4.36	6.15	–5.14
QCISD(T) [c]	1.43	3.52	4.63	–5.06
MP4(SDTQ) [e]	1.71	4.20	5.78	–5.18
QCISD(T) [e]	1.37	3.58	4.70	–5.07
BP86 [c]	3.15	7.04	8.19	–4.62
expl.[f]	3.050 ± 0.400			

[a] All single point energy calculations were performed using 6-311++G(3df,3pd) basis set. [b] HF/6-311++G(3df,3pd) optimized geometries were used. [c] B3LYP/6-311++G(3df,3pd) optimized geometries were used. [d] B3PW91/6-311++G(3df,3pd) optimized geometries were used. [e] MP2/6-311++G(3df, 3pd) optimized geometries were used. [f] Ref. 23.

Based on the energies calculated at the BP86 level, *cis*-1,2-dichlorodiazene was 7.04 kcal mol^{-1} more stable than the corresponding *trans*-isomer, consistent with the electronic energy difference of 6.8 kcal mol^{-1} reported by Anders.[24] Furthermore, 1,2-dibromodiazenes (**6**) show the largest 8.19 kcal mol^{-1} *cis*-preference energy difference, implying that the *cis–trans* energy gap increased as the size of the substituted halogen atoms increased. The 1,2-diazenes (**7**) showed good agreement with experiments in which the *trans*-isomer was the most stable one.[109-113] The calculated *trans*-preference energy difference in **7** was 4.62 kcal mol^{-1} which was close to the previously reported energy difference of 4.9 kcal mol^{-1} based on the high-level theoretical method.[24] These opposing results among 1,2-dihalodiazenes (**4**-**6**) and 1,2-diazenes (**7**) clearly imply that their substituents play

key roles in energetic conversion between their *cis*- and *trans*-isomers.

2.2.3.3. Natural Bond Orbital 2nd-Order Perturbation Analysis

In order to determine the dominant factors in their *cis–trans* energy differences, the NBO 2nd-order perturbation analysis was performed at the BP86/6-311++G(3df,3pd)//B3LYP/6-311++G(3df,pd) level (Table 2.2.3).

First, the delocalization of halogen lone pairs into the antibonding orbitals of the N=N bond (LP effect) was found to be an important *cis*-stabilizing mechanism for 1,2-dihalodiazenes (**4**–**6**) (Figures 2.2.3 and 2.2.4), as explained above with the orbital phase theory, (the cyclic orbital interaction was continuous only in the *cis*-isomers of **4**–**6**; please see the Section 2.1.2.2). Moreover, the heavier halogen atom provides the smaller orbital-orbital energy gaps for the $n_{X\pi} \rightarrow \pi_{NN'}^{*}$ interactions (π-LP effect) (Table 2.2.4), leading to the stronger -G-T_1-T_2- (-π-p-q-) type triangle orbital interactions and the larger *cis*-stabilizing energies. However, the overlap of π halogen lone pair ($n_{X\pi}$) and π antibonding orbital of N=N bond ($\pi_{NN'}^{*}$) decreased due to the longer N−X bond length as the halogen atom got heavier (see the Fock matrix element F_{ij} in Table 2.2.4). This decrease in the orbital-orbital overlap gave smaller energetic gain through the π-LP effect. Consequently, the energy differences of π-LP effect were 3.44, 3.02, and 2.80 kcal mol^{-1} *cis*-preferable for **4**, **5,** and **6**, respectively. On the other hand, the $n_{X\sigma} \rightarrow \sigma_{NN'}^{*}$ interaction (σ-LP effect) only stabilized the *cis*-isomer in 1,2-difluorodiazenes (**4**) by 3.14 kcal mol^{-1}, but it worked as a stabilizer for the *trans*-isomers relative to the *cis*-isomers in 1,2-dichlorodiazenes (**5**) and 1,2-dibromodiazenes (**6**) (their *trans* stabilizing effects are 0.68 and 1.60 kcal mol^{-1} for **5** and **6**, respectively). These results for the σ-LP effect were clearly at odds with orbital phase theory (please see the Section 2.1.2.2.), but this exception might be ascribable to the difference in N–X bond lengths between the two isomers. The combination of longer

N–X bond lengths and condensed halogen σ-lone pairs led to smaller orbital–orbital overlaps in the *cis*-isomers compared to those in the *trans*-isomers. In fact, the N–X bonds in the *cis*-isomers were longer than those in their *trans*-forms, especially in the compounds with heavier halogen atoms. Collectively, the total amount of σ- and π-LP effects was *cis*-preference by 6.58, 2.34 and 1.20 kcal mol^{-1} for **4**, **5** and **6**, respectively (Table 2.2.3). Clearly, these LP effects play effective roles in the *cis*-effect, especially for 1,2-difluorodiazenes (**4**). 1,2-Diazenes (**7**), possessing no halogen lone pairs, could not gain any stabilizing energy via LP effects. This should be an important reason for *trans*-preference in this molecule.

Table 2.2.3. NBO 2nd-order perturbation analysis calculations for 1,2-substituted or unsubstituted diazenes, XN=NX (X=F, Cl, Br or H) (kcal mol^{-1})[a]

X		AP&SP effects[b]			LP effect[c]			Total
		$n_N \rightarrow \sigma_{N'X'}^*$	$\sigma_{NX} \rightarrow \sigma_{N'X'}^*$	Subtotal[d]	$n_{X\sigma} \rightarrow \sigma_{NN'}^*$	$n_{X\pi} \rightarrow \pi_{NN'}^*$	Subtotal[d]	
4 (F)	*cis*	15.40	2.04	34.88	4.93	16.61	43.08	
	trans	2.83	6.40	18.46	3.36	14.89	36.50	
	Δ[e]			16.42			6.58	23.00
5 (Cl)	*cis*	20.83	3.60	48.86	2.10	11.54	27.28	
	trans	0.46	12.70	26.32	2.44	10.03	24.94	
	Δ[c]			22.54			2.34	24.88
6 (Br)	*cis*	19.46	10.79	60.50	0.66	6.67	14.66	
	trans	0.13	21.45	43.16	1.46	5.27	13.46	
	Δ[c]			17.34			1.20	18.54
7 (H)	*cis*	7.04	1.63	17.34	-	-	-	
	trans	1.72	6.03	15.50	-	-	-	
	Δ[c]			1.84	-	-	-	1.84

[a] BP86/6-311++G(3df,3pd)//B3LYP/6-311++G(3df,3pd). [b] antiperiplanar and synperiplanar interactions. [c] the delocalization of halogen lone pairs into the antibonding orbitals of the N=N bond. [d] total value of AP&SP effects or LP effect. The values are doubled because two sets of same interactions exist. [e] Δ denote *cis–trans* energy difference in the total value of AP&SP effects or LP effect.

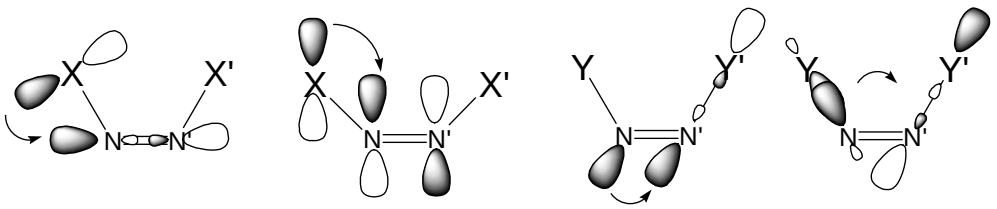

$n_{X\sigma} \rightarrow \sigma_{NN'}^{*}$ $n_{X\pi} \rightarrow \pi_{NN'}^{*}$ $n_{N} \rightarrow \sigma_{N'Y'}^{*}$ $\sigma_{NY} \rightarrow \sigma_{N'Y'}^{*}$

σ-LP effect **π-LP effect** **AP effect** **SP effect**

Figure 2.2.3. Definitions of the halogen lone pair ($n_{X\sigma}$ and $n_{X\pi}$) delocalization effects (σ- or π-LP effect), the antiperiplanar interaction (AP effect), and the synperiplanar interaction (SP effect) within the NBO framework for *cis*-XN=N'X' (X, X'= F, Cl or Br) or *cis*-YN=N'Y' (Y, Y'=F, Cl, Br or H).

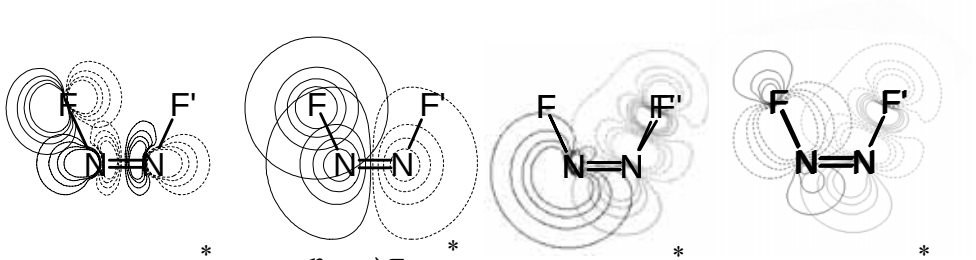

$n_{F\sigma} \rightarrow \sigma_{NN'}^{*}$ $n_{F\pi} \rightarrow \pi_{NN'}^{*}$ $n_{N} \rightarrow \sigma_{N'F'}^{*}$ $\sigma_{NF} \rightarrow \sigma_{N'F'}^{*}$

σ-LP effect **π-LP effect** **AP effect** **SP effect**

Figure 2.2.4. The fluorine lone pair ($n_{F\sigma}$ and $n_{F\pi}$) delocalization effect (σ- or π-LP effect), the antiperiplanar interaction (AP effect), and the synperiplanar interaction (SP effect) as pre-NBO interactions calculated at the BP86/6-311+G(3df)//B3LYP/6-311+G(3df) level for *cis*-1,2-difluorodiazene. Orbital contours were calculated at the same level for two interacting orbitals in each scheme.

Second, the most important hyperconjugation was found to be the $n_N \rightarrow \sigma_{N'X'}^{*}$ interaction in which two orbitals were located at the advantageous antiperiplanar position only in the *cis*-1,2-dihalodiazenes (AP effect: Figures 2.2.3 and 2.2.4), due to the larger orbital–orbital overlaps compared to the corresponding synperiplanar interaction (SP effect) in the *trans*-isomers. Another periplanar-type interaction $\sigma_{NX} \rightarrow \sigma_{N'X'}^{*}$ yielded smaller stabilizing energies in **4** and **5** than those of $n_N \rightarrow \sigma_{N'X'}^{*}$ interactions, to make their *trans*-forms more stable than the corresponding *cis*-isomers by

8.72 and 18.2 kcal mol^{-1}, respectively. As such, the combinations of n_N and $\sigma_{N'X'}^*$ were the most effective periplanar-type hyperconjugations in **4** and **5**, because of the smallest energy gaps between two interacting orbitals (Table 2.2.4). Here, an interesting trend was found in the $\sigma_{NX} \rightarrow \sigma_{N'X'}^*$ interactions: the stabilizing energy through this hyperconjugation increased as the halogen atom increased in size (Table 2.2.3). As clearly seen in Table 2.2.4, this trend mainly came from both the greater orbital–orbital overlaps (Fock matrix element, F_{ij}) and the smaller energy differences between two interacting orbitals (ε_i-ε_j) as the substituted halogen atom increases in size. It should be noted that the difference in orbital energy level (ε_i-ε_j) in the $\sigma_{NBr} \rightarrow \sigma_{N'Br'}^*$ interaction was smaller than that in $n_N \rightarrow \sigma_{N'Br'}^*$ in 1,2-dibromodiazenes (**6**) (Table 2.2.4), indicating that the energy level of bonding orbitals σ_{NBr} is higher than that of nitrogen lone pair n_N. This "strange" calculated result might be the theoretical evidence for the non-existence of 1,2-dibromodiazenes (**6**), because of the instability of N–Br bonds. Thus, even though 1,2-dibromodiazenes (**6**) have no imaginary frequencies at any level of calculation, **6** could be regarded as imaginary molecules. In 1,2-dichlorodiazenes (**5**), the orbital energy level of n_N was calculated to be slightly higher than that of σ_{NCl} (0.08 and 0.07 a.u. for *cis*- and *trans*-isomers, respectively, Table 2.2.4), but their differences were far smaller than those for stable 1,2-difluorodiazenes (**4**) (0.33 and 0.30 a.u., respectively), implying that N–Cl bonds are barely bound and the stabilities of 1,2-dichlorodiazenes (**5**) are very delicate. This observation for **5** is consistent with Morokuma's *ab initio* calculations[100, 101].

Table 2.2.4. Fock matrix elements (F_{ij}) and orbital-orbital energy differences (ε_i-ε_j) of AP, SP and LP effects in 1,2-substituted or unsubstituted diazenes, XN=NX (X = F, Cl, Br or H) via NBO 2nd perturbation analysis (a.u.)[a]

F_{ij}	*cis*				*trans*			
	$n_N \rightarrow \sigma_{N'X'}^*$	$\sigma_{NX} \rightarrow \sigma_{N'X'}^*$	$n_{X\sigma} \rightarrow {}^*\sigma_{NN'}$	$n_{X\pi} \rightarrow {}^*\pi_{NN'}$	$n_N \rightarrow \sigma_{N'X'}^*$	$\sigma_{NX} \rightarrow \sigma_{N'X'}^*$	$n_{X\sigma} \rightarrow {}^*\sigma_{NN'}$	$n_{X\pi} \rightarrow {}^*\pi_{NN'}$
4 (F)	0.081	0.038	0.059	0.061	0.036	0.066	0.047	0.058
5 (Cl)	0.089	0.041	0.038	0.043	0.014	0.075	0.040	0.040
6 (Br)	0.085	0.058	0.023	0.032	0.007	0.080	0.033	0.028
7 (H)	0.063	0.034	-[b]	-[b]	0.032	0.065	-[b]	-[b]

ε_i-ε_j	*cis*				*trans*			
	$n_N \rightarrow \sigma_{N'X'}^*$	$\sigma_{NX} \rightarrow {}^*\sigma_{N'X'}$	$n_{X\sigma} \rightarrow \sigma_{NN'}^*$	$n_{X\pi} \rightarrow {}^*\pi_{NN'}$	$n_N \rightarrow \sigma_{N'X'}^*$	$\sigma_{NX} \rightarrow \sigma_{N'X'}^*$	$n_{X\sigma} \rightarrow {}^*\sigma_{NN'}$	$n_{X\pi} \rightarrow {}^*\pi_{NN'}$
4 (F)	0.53	0.86	0.96	0.27	0.55	0.85	0.91	0.27
5 (Cl)	0.46	0.54	0.93	0.19	0.48	0.55	0.93	0.19
6 (Br)	0.44	0.36	0.98	0.18	0.44	0.37	1.04	0.18
7 (H)[a]	0.71	0.86	-[b]	-[b]	0.74	0.87	-[b]	-[b]

[a] BP86/6-311++G(3df,3pd)//B3LYP/6-311++G(3df,3pd). [b] no halogen atoms

Compared to the antiperiplanar-type interactions (AP effect), all of the corresponding synperiplanar interactions (SP effect) were small due to their smaller orbital–orbital overlaps (Table 2.2.3 and 2.2.4), and thus they could be classified as secondary periplanar hyperconjugation for the energetic difference between *cis*- and *trans*-isomers. As such, the AP effect is more important than the SP effect and the total amount of these periplanar interactions is greater in the *cis*-isomers for all the 1,2-dihalodiazenes (**4**: 16.42; **5**: 22.54; **6**: 17.34 kcal mol^{-1}, respectively: Table 2.2.3). The combination of these strong periplanar-type hyperconjugations in the 1,2-dihalodiazene systems obviously promote the triple bond-like nature of the N=N bond and make the N′–X′ bond easier to cleave. In other words, these periplanar interactions could be considered as an "intra-molecular S_N2 type reaction" in which the nitrogen lone pair is regarded as a nucleophile to attack the adjacent N′–X′ bond. As a result, strong

periplanar interactions could promote the decomposition of 1,2-dihalodiazenes to yield N_2 and two halogen radicals,[100-102] just as an AIBN decomposes into nitrogen gas and two cyanoisopropyl radicals, especially for the ones with larger halogen atoms. In fact, shorter N=N bond lengths and longer N–X bond lengths in all of the *cis*-isomers of **4**–**6** could be seen as the structural expression of electronic dominance of these periplanar interactions, especially AP effects, as the primary origin of the *cis*-effect in 1,2-dihalodiazene systems (Table 2.2.1). Furthermore, the enhanced triple bond-like nature of the N=N bond should ensure that the nitrogen atom is close to *sp* hybridization, resulting in wider NNX angles as found in the geometries obtained for **4**–**6**.

However, in the case of 1,2-diazenes (**7**), the *cis*-stabilizing energy difference of AP and SP effects drastically decreased to only 1.84 kcal mol^{-1}. This significant difference compared to that in the 1,2-dihalodiazenes (**4**–**6**) could be ascribed to the higher σ_{NH}^* orbital energy level than those of σ_{NX}^* (X=F, Cl or Br) due to the higher electronegativity of the halogen atoms. This difference yielded a larger orbital–orbital energy gap (ε_i-ε_j) for both periplanar-type $n_N \rightarrow \sigma_{N'H'}^*$ and $\sigma_{NH} \rightarrow \sigma_{N'H'}^*$ hyperconjugations which led to a smaller amount of stabilizing energy on 1,2-diazenes (**7**) compared to their halogenated derivatives **4**–**6** (Tables 2.2.3 and 2.2.4). These small periplanar effects as well as the non-existence of an LP effect in the simple 1,2-diazenes (**7**) were ascribable to the *trans*-preference energy gap between the two isomers.

The additional natural population analysis (NPA) calculations showed apparent existence of N−X dipoles in **4**-**7** (Table 2.2.5), which repel each other only in the *cis*-isomers to produce the *cis*-destabilizing energies. Furthermore, the NPA results supported the dominance of periplanar-type interactions, because all of the nitrogen atoms in the *cis*-isomers had more positive charges than those in the corresponding *trans*-isomers for all 1,2-dihalodiazenes (**4**–**6**) and 1,2-diazenes (**7**) (Table 2.2.5). This tendency implied that the nitrogen atoms in the *cis*-isomers were better electron donors than those in the corresponding *trans*-isomers for **4**–**7** due to the dominant delocalization from the nitrogen lone

pair to the antibonding orbital of N–X (X = F, Cl, Br or H). Interestingly, this trend was completely opposed to the results for 1,2-dihaloethenes in which the LP effect was the major origin of the *cis*-effect and the carbon atoms in the *cis*-isomers had more negative charges than those in the corresponding *trans*-isomers (Section 2.1).[11, 12] Furthermore, as mentioned above, the *cis–trans* difference in the structural parameters also showed opposite tendencies between the 1,2-dihalodiazenes and the 1,2-dihaloethenes, reflecting the difference in their dominant hyperconjugation mechanisms to determine their geometrical characteristics. Thus, although the 1,2-dihalodiazenes were electronic isosteres to the 1,2-dihaloethenes, the electronic structure and geometrical natures of the two isomers were found to be completely opposite. This reversion seems to be due to the strong electron-donating effect of the nitrogen lone pairs compared to the ordinary covalent bonds (C–H or C–X; X = F, Cl or Br) in 1,2-dihaloethenes. The longer N–X bond length compared to the C–X bond could also contribute to the difference in the hyperconjugative systems, owing to the production of a smaller LP effect in the 1,2-dihalodiazene systems compared with those in the 1,2-dihaloethenes. As a result, 1,2-dihalodiazenes have a larger AP effect than LP effect, whereas 1,2-dihaloethenes show a greater LP effect than AP effect, but both of these molecules have an apparent *cis*-effect through lone-pair hyperconjugation mechanisms which work as counterparts against existing repulsive forces in the *cis*-isomers. Moreover, these differences in the electronic structure of 1,2-dihalodiazenes and 1,2-dihaloethenes might have a critical influence on their thermodynamic stability and existence under normal conditions.

Table 2.2.5. Natural Population Analysis of 1,2-substituted or unsubstituted diazenes, XN=NX (X=F, Cl, Br or H)[a]

X	atom	*cis*	*trans*	Δ[b]
4	N	0.20631	0.18856	0.01775
(F)	F	–0.20631	–0.18856	–0.01775
5	N	–0.08340	–0.13522	0.05182
(Cl)	Cl	0.08340	0.13522	–0.05182
6	N	–0.07207	–0.12570	0.05363
(Br)	Br	0.07207	0.12570	–0.05363
7	N	–0.27376	–0.29482	0.02106
(H)	H	0.27376	0.29482	–0.02106

[a] BP86/6-311++G(3df,3pd)//B3LYP/6-311++G(3df,3pd) level. [b] Δ denotes differences between *cis*- and *trans*-isomers

In order to obtain the steric contribution to the 1,2-dihalodiazene systems, the natural steric analysis[85-87] was applied on **4**-**7** (Table 2.2.6). The result showed some *cis*-destabilizing steric exchange energies between the halogen lone pairs (1.94, 3.06 and 2.45 kcal mol^{-1} for **4**, **5** and **6**, respectively). The total amounts of intra-molecular steric repulsion energies were estimated to be 0.00, −2.82, −0.15 kcal mol^{-1} for **4**, **5** and **6**, respectively (positive number indicates *cis*-destabilizing energy). Although they have some effects on the *cis*-*trans* energetic difference for **4**-**6**, the amounts of steric repulsion energies were far smaller and had only the secondary influences on their *cis*-*trans* energies compared to those of hyperconjugations. Therefore, these results strongly supported the energetic dominance of hyperconjugations on the 1,2-dihalodiazene systems **4**-**6**. On the other hand, the steric exchange energy of unsubstituted diazene **7** was *cis*-destabilizing by 2.27 kcal mol^{-1} which was comparable to the energetic amount of hyperconjugations (1.84 kcal mol^{-1}, Table 2.2.3), indicating the relatively small contributions of hyperconjugations in this system.

Table 2.2.6. The total steric exchange energy of *cis*- and *trans*-1,2-substituted or unsubstituted diazenes, XN=NX (X=F, Cl, Br or H) (kcal mol^{-1})[a]

		Total steric exchange energy	steric exchange energy between halogen lone pairs
4 (F)	*cis*	82.83	2.58
	trans	82.83	0.64
	Δ [b]	0.00	1.94
5 (Cl)	*cis*	79.37	3.48
	trans	82.19	0.42
	Δ [b]	−2.82	3.06
6 (Br)	*cis*	76.48	2.55
	trans	76.63	0.10
	Δ [b]	−0.15	2.45
7 (H)	*cis*	40.09	-[c]
	trans	37.82	-[c]
	Δ [b]	2.27	-[c]

[a] calculated at the BP86/6-311++G(3df,3pd)//B3LYP/6-311++G(3df,3pd) level using the natural steric analysis. [b] Δ denote *cis–trans* energy difference (the positive number indicates larger steric repulsion in the *cis*-isomer compared to the corresponding *trans*-form). [c] no halogen atoms.

2.2.4. Summary of the Section

The *cis–trans* energy differences in 1,2-dihalodiazenes (halogen = F, Cl or Br) were investigated using the *ab initio* and DFT calculations. It was found that not only 1,2-difluorodiazenes (**4**) and 1,2-dichlorodiazenes (**5**), but also 1,2-dibromodiazenes (**6**) have the *cis*-preferable energy differences of 3.15, 7.04, and 8.19 kcal mol^{-1}, respectively, at the BP86/6-311++G(3df,3pd)//B3LYP/6-311++G(3df,3pd) level calculations. According to subsequent NBO 2nd-perturbation analysis, the combined *cis*-preference energies, namely the periplanar effects (AP&SP effects: 16.42, 22,54, and 17.34 kcal mol^{-1} for **4**, **5** and **6**, respectively) and the halogen lone pair effects (LP effect: 6.58, 2.34

and 1.20 kcal mol^{-1}), stabilizes the *cis*-isomers by 23.00, 24.88 and 18.54 kcal mol^{-1}, respectively, compared with their *trans*-counterparts. These large stabilizing energies for the *cis*-isomers should override various repulsive destabilization energies, such as Pauli repulsion between the halogen lone pairs and the electrostatic repulsive forces between the N–X (X = F, Cl or Br) dipoles, to produce the *cis*-effect in the 1,2-dihalodiazenes. The fact that the parent diazene (HN=NH) exists exclusively as the *trans*-form may suggest that the AP effects ($n_N \rightarrow \sigma_{N'H'}^*$) alone could not cause *cis*-preference. In addition, extraordinarily high energy levels of N–Br bonding orbitals in 1,2-dibromodiazenes (**6**) were found to indicate their non-existence as a result of strong interactions, which decreased the bonding character between nitrogen and bromine atoms, while the N–F bond in 1,2-difluorodiazenes (**4**) was calculated to be stable and the N–Cl bond in 1,2-dichlorodiazenes (**5**) was degradable. These observations are in good agreement with previous experimental and theoretical results that 1,2-difluorodiazenes were found to be stable under normal conditions, 1,2-dichlorodiazenes was barely exist, and 1,2-dibromodiazenes have never been reported to date. These results and discussions could provide an important insight on the factors determining the thermodynamically stable molecular structures in these systems. Moreover, these findings, primarily derived from hyperconjugations, could also provide the basic information to elucidate the electronic structure of various molecules.

Chapter 3

Relationships of Molecular Structure and Biological Activities on the C-terminal Modified Peptide Derivatives for delta/mu Opioid Receptor Agonists and Neurokinin-1 Receptor Antagonists

3.1. Biological Evaluations of bifunctional C-terminal modified peptides for *δ/μ* opioid receptor agonists and neurokinin-1 receptor antagonists

3.1.1. Background

The opioid receptors are membrane-bound G-protein coupled receptors (GPCRs) and classified into at least three subtypes (μ, δ and κ, and possibly others) with endogenous peptides as their ligands such as endorphin, enkephalin and dynorphin.[40, 120, 121] It is well-known that an opiate, which is an agonist for these opioid receptors, produces analgesia, generally by the reduction of central autonomic and endocrine responses to a pain stimulus. The μ opiates have the strongest analgesic potency with several disadvantages such as constipation, respiratory depression, dysphoria, opioid-induced tolerance development and addiction.[122, 123] While selective δ opioid agonists showed several potential clinical advantages over their μ counterparts, since the analgesia mediated through the δ receptors is likely accompanied with fewer these adverse effects, although their potency is less than that of the μ receptor agonists. Therefore, understanding the binding property of selective δ opiate has been important, and selective δ opioid agonists with enhanced efficacy and no tolerance should be expected as novel and potent candidate for next generation analgesic drugs.

Substance P is a preferable ligand for NK1 receptor and a major neurotransmitter of pain signals. Interestingly, NK1 knockout mice did not show the rewarding properties for morphine.[124] Moreover, the co-administration of opioid agonists and NK1 antagonists showed enhanced antinociceptive potency in acute pain states and in prevention of opioid-induced tolerance in chronic preclinical trials.[125-129] These results suggested that contributions from pronociceptive signaling through the NK1 receptor can play a significant role in the outcome of analgesic actions of opioids acting at opioid receptors.[130-132] Such interactions of pro- and antinociceptive activity may have an anatomical basis as the expression of the NK1 and opioid receptors as well as the neurotransmitters show a significant

degree of overlap in the central nervous system.[128, 133-135] Thus, the opioid and NK1 receptors were expected to exist in the same synaptic cleft and play important roles for pain signal transmission (Figures 3.1.1 and 3.1.2). Therefore, bifunctional compounds possessing selective δ opioid agonists together with the NK1 antagonist activity could be a promising strategy to find potent analgesics.[136, 137]

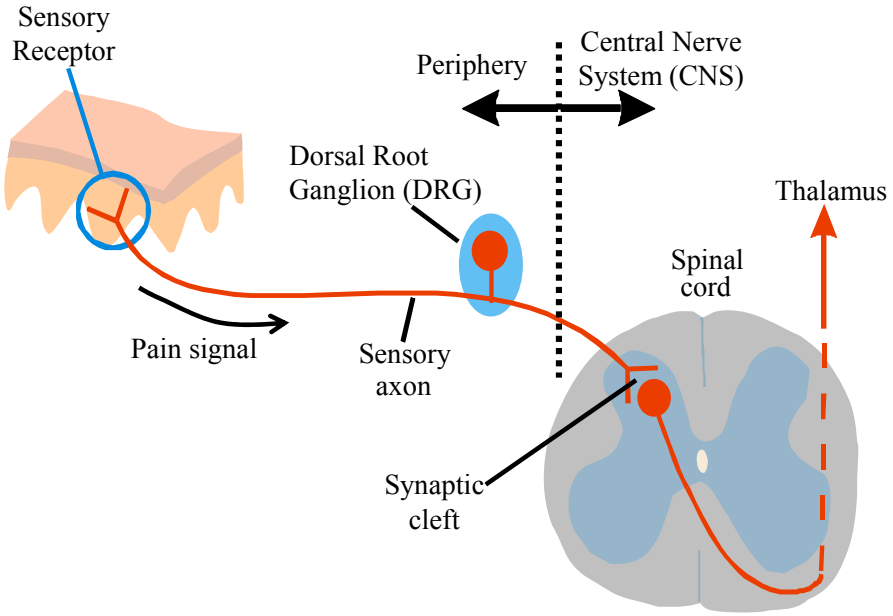

Figure 3.1.1. Nociceptive transmission pathway

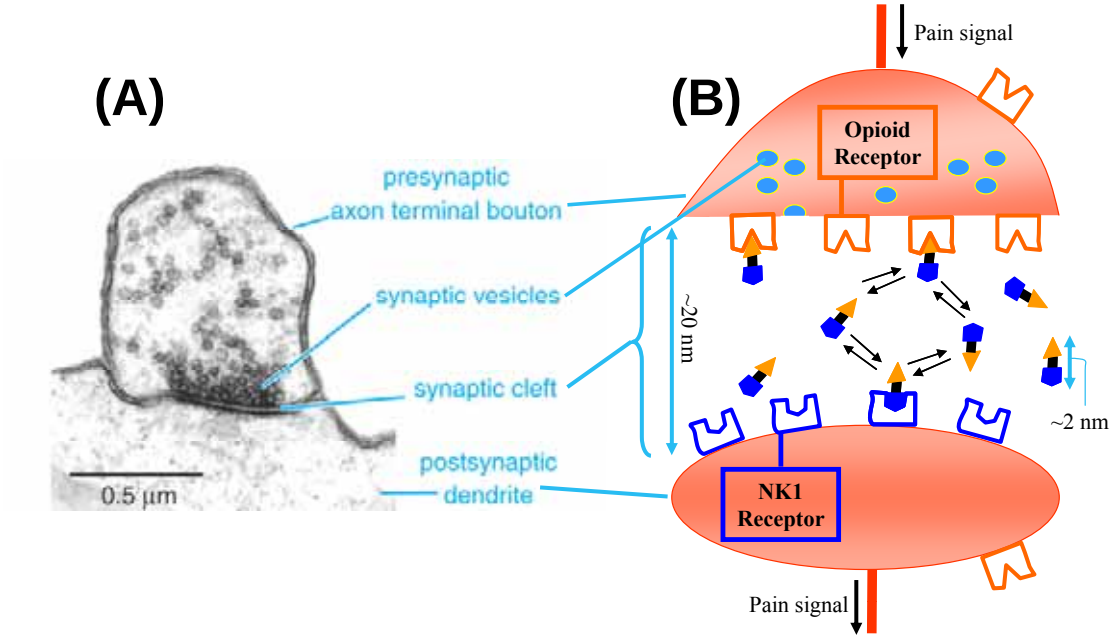

Figure 3.1.2. (A) The electron micrograph of spinal dorsal horn neurons which construct the synaptic cleft and have an important role in the pain signal transmission. (B) Schematic view of the synaptic cleft in relevance to the bifunctional concept of opioid agonist and NK1 antagonist.

In view of these discussions, novel chimeric molecules have been designed to possess two structural moieties for both δ-selective opioid agonist and NK1 antagonist pharmacophores. These chimeric molecules should be easier to administer and have lower risk of drug-drug interactions than co-administration of two different drugs, and are expected to have enhanced and concerted antinociceptive potency without the development of analgesic tolerance. To date, some molecules are already reported to have both δ/μ opioid agonist and substance P antagonist activities.[138-140] However, their activities are extensively biased for one of the receptors, and no molecule had sufficient and balanced activities for both of opioid and NK1 receptors. In the molecular design, H-Tyr-*D*-Ala-Gly-Phe sequence was chosen for the opioid agonist part which is a substituted "message" sequence of enkephalins (H-Tyr-Gly-Gly-Phe), but with the second amino acid being *D*-Ala. This sequence has high metabolic stability,[141] and has been used in several potent opioids including the δ selective agonist DADLE and the superpotent δ/μ dual agonist biphalin (Figure 3.1.3).[121, 142] As for the NK1 receptor antagonist part, the moiety from the 3,5-(bistrifluoromethyl)benzyl ester of *N*-acylated tryptophan was chosen (Figure 3.1.3).[41, 143-145] Modeling studies revealed that the two aromatic groups of L-732,138 (Ac-Trp-O-3,5-Bzl(CF_3)$_2$), which is one of the most thoroughly studied 3,5-(bistrifluoromethyl)benzyl esters of *N*-acylated tryptophan, binds to His^{197} and His^{265} of human NK1 receptors and bulky substituents seemed to be tolerated on the *N*-terminal acetyl moiety.[41] In fact, its derivative Cbz-Pro-Leu-Trp-O-3,5-Bzl(CF_3)$_2$, which has two more amino acids capped with a Cbz group at the *N*-terminal, maintains good affinity for NK1 receptors.[144, 145] Considering the reported structure-activity relationship (SAR) studies, the Pro-Leu sequence seems to have a positive influence on antagonistic activity at the NK1 receptor.[144, 145] According to these considerations, the Pro-Leu-Trp-O-3,5-Bzl(CF_3)$_2$ was used as the NK1 receptor antagonist structural pharmacophore.

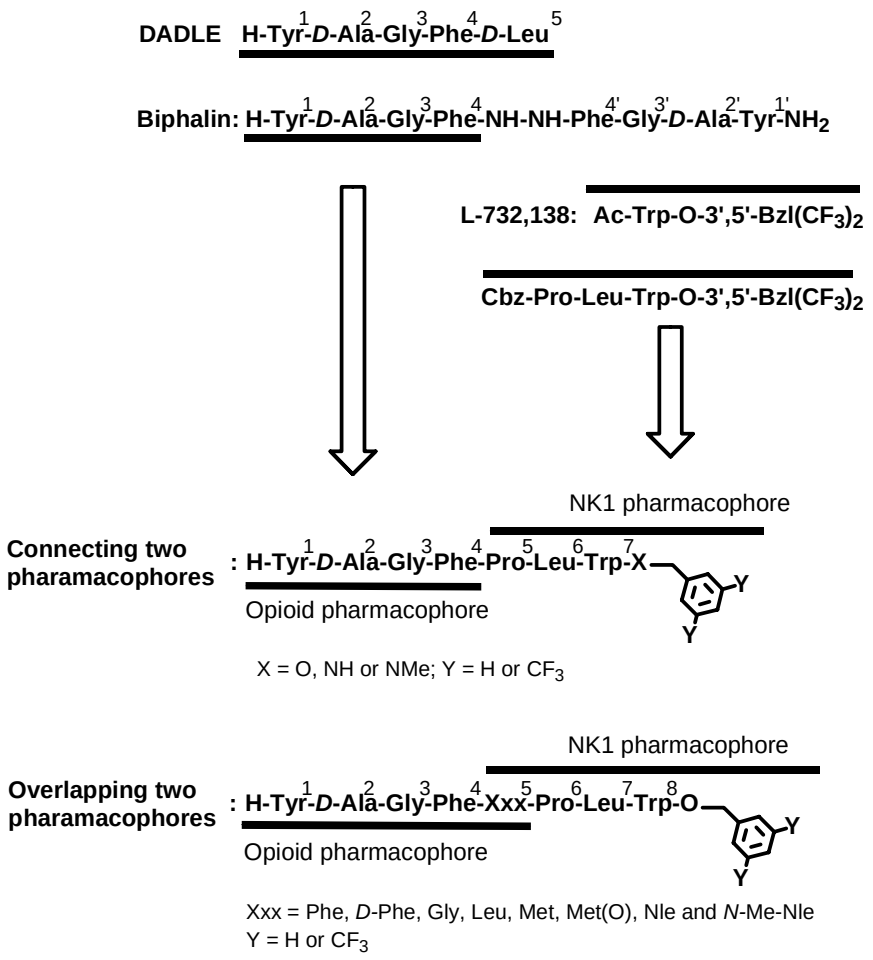

Figure 3.1.3. Design of bifunctional peptides possessing sequences for both δ/μ opioid agonist and neurokinin-1 antagonist.

In this section, the synthesis and SAR studies were reported on the bifunctional peptide **TY001** (H-Tyr-*D*-Ala-Gly-Phe-Pro-Leu-Trp-O-**3,5**-Bzl(CF_3)$_2$), in which two pharmacophores were simply connected into one molecule with a single bond (Figure 3.1.3). The optimization was first focused on its *C*-terminus, where the NK1 antagonist pharmacophore was incorporated, because of the interest on the shift of biological behaviors in the presence or absence of highly lipophilic two trifluoromethyl groups. The connecting position of two pharmacophores was another part to be optimized, because of its important role as an "address" region for both of opioid agonist and NK1 antagonist activities.

3.1.2. Results and Discussion

3.1.2.1. Synthesis of Peptide Derivatives Using Solution Phase Chemistry

The bifunctional peptides were synthesized using stepwise solution phase PyBOP/HOBt-chemistry (Figure 3.1.4). The synthesis was started from the coupling reaction of Boc-Pro-Leu-OH and tryptophan 3,5-(bistrifluoromethyl)benzyl ester hydrochloride followed by deprotection of the Boc group using 4 M hydrogen chloride in 1,4-dioxane. [144, 145] After subsequent chain elongation, the 3,5-(bistrifluoromethyl)benzyl ester of the tetra- or penta-peptide structure was obtained to be coupled with Boc-Tyr-*D*-Ala-Gly-OH. The final crude peptides were obtained upon treatment of trifluoroacetic acid to remove the protecting groups. Peptide intermediates were isolated by precipitation from cold ether or petroleum ether, and the obtained final crude peptides were purified by RP-HPLC to give pure (>98%) peptides.

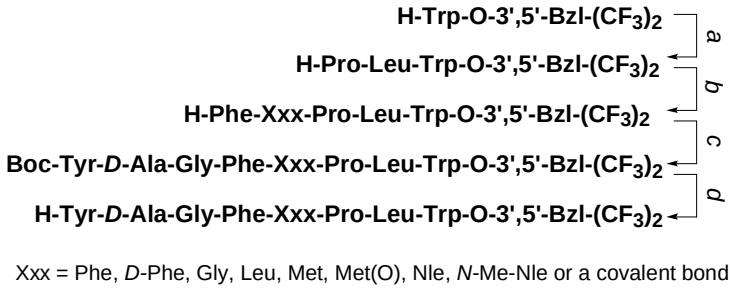

(a) (i) Boc-Pro-Leu-OH, PyBOP, HOBt, DMF, 2h.; (ii) 4 M HCl / 1,4-dioxane, 2h. (b) Stepwise chain elongation using PyBOP/HOBt and 4M HCl / 1,4-dioxane chemistry with Boc-Phe-OH and Boc-Xxx-OH. (c) (i) Boc-Tyr-*D*-Ala-Gly-OH, PyBOP, HOBt, DMF, 2h.; (ii) 4 M HCl / 1,4-dioxane, 2h. (d) TFA, 1h.

Figure 3.1.4. Synthesis of bifunctional peptides using solution phase chemistry.

3.1.2.2. Synthesis of Peptide Derivatives Using Solid Phase Chemistry on 2-Chlorotrityl Resin.

A series of peptide derivatives also were obtained through a two-steps synthetic approach (Figure 3.1.5). The first step was the synthesis of Boc-Tyr(tBu)-*D*-Ala-Gly-Phe-Pro-Leu-Trp(Boc)-OH or Boc-Tyr(tBu)-*D*-Ala-Gly-Phe-Met-Pro-Leu-Trp(Boc)-OH as shared intermediates using N^{α}-Fmoc chemistry on a 2-chlorotrityl resin, which is a common support for batch SPPS of protected peptides with a free *C*-terminal.[146] First, Fmoc-Trp(Boc)-OH was introduced on a resin in the presence of DIEA in DCM. Resin-bound Fmoc-Trp(Boc) was treated with 20% piperidine/DMF to remove a N^{α}-Fmoc protecting group. Couplings of the following amino acids were carried out with standard *in situ* activating reagents used in routine Fmoc SPPS with HCTU, in the presence of DIEA, to generate Cl-HOBt esters. The resin-bound Boc-Tyr(tBu)-*D*-Ala-Gly-Phe-Pro-Leu-Trp(Boc) obtained was cleaved off the resin with 1% TFA in DCM in 30 min. The protected peptide was obtained after evaporation followed by precipitation with chilled petroleum ether. The resulting white solid was washed twice with chilled petroleum ether, then dried under vacuum to give the protected peptide with good purity (87 and 99% for Boc-Tyr(tBu)-*D*-Ala-Gly-Phe-Pro-Leu-Trp(Boc)-OH and Boc-Tyr(tBu)-*D*-Ala-Gly-Phe-Met-Pro-Leu-Trp(Boc)-OH, respectively) and moderate yield (75 and 57%, respectively: based on the substitution of the resin).

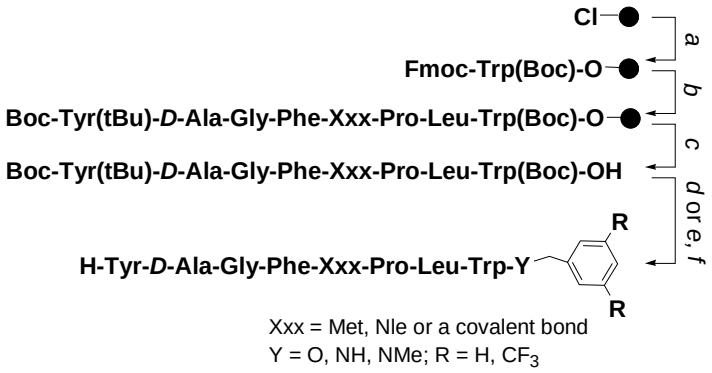

(a) Fmoc-Trp(Boc)-OH, DIEA, DCM, 2h. (b) Stepwise chain elongation using HCTU / 20% piperidine chemistry. (c) 1% TFA in DCM, 30min. (d) benzyl bromide or 3,5-bis(trifluoromethyl)benzyl bromide, Cs_2CO_3, DMF, 2h. (e) benzyl amine or 3,5-bis(trifluoromethyl)benzyl amine or (3,5-Bis(trifluoromethyl)benzyl)methylamine, Cl-HOBt, EDC, DMF, 1h. (f) 82.5% v/v TFA, 5% water, 5% thioanisol, 2.5% 1,2-ethanedithiol, 5% phenol, 1h.

Figure 3.1.5. Synthesis of bifunctional peptides using solid phase chemistry on 2-chlorotrityl resin.

The second step was esterification or amidation of the protected intermediate followed by side-chain deprotection in the solution phase. The esterification was performed employing cesium carbonate to form the cesium salt of the protected peptide to react with benzyl bromide or 3,5-bis(trifluoromethyl)benzyl bromide.[144, 145] The crude esters were obtained by one hour treatment with the cleavage cocktail (82.5% v/v TFA, 5% water, 5% thioanisole, 2.5% 1,2-ethanedithiol and 5% phenol) to quench the highly stabilized carbocations released from permanent protecting groups. Some acid mediated hydrolysis of *C*-terminal benzyl ester occurred during the final cleavage, but the purities of the final crude peptides were still moderate to good (67 ~ 84%). For the amidation, standard EDC/Cl-HOBt coupling chemistry with two equivalents of reactant amine was used. The crude amides were obtained with 98% to quantitative yield and good purity (75 ~ 93%). The crude peptides were purified by RP-HPLC (>99% purity).

3.1.2.3. Characterization of Synthesized Peptide Derivatives

The final peptides were characterized and their purities were confirmed by analytical HPLC, ^{1}H-NMR, HRMS and TLC (Table 3.1.1 and Table 3.3.1; Table 3.3.1 is displayed at the end of this chapter). ^{1}H-NMR studies showed that *cis/trans* isomerization at the Pro residue was found in some of the synthesized peptides. The ratio of two amide rotamers and their assignments are available in Table 3.3.1 at the end of this chapter.

Table 3.1.1. Sequence and analytical data of bifunctional peptide ligands

ID	Sequence	*m/z* [a] (M + H)$^+$		HPLC [b] log *k*'		TLC [c] (R_f)		
		Obs. (ESI)	Calc.	(A)	(B)	(I)	(II)	(III)
TY001	H-Tyr-*D*-Ala-Gly-Phe-Pro-Leu-Trp-O-3,5-Bzl(CF_3)$_2$	1079.4466	1079.4495	19.03	7.36	0.13	0.71	0.77
TY011	H-Tyr-*D*-Ala-Gly-Phe-Pro-Leu-Trp-**O-Bzl**	943.4719	943.4764	15.82	3.42	0.18	0.71	0.77
TY008	H-Tyr-*D*-Ala-Gly-Phe-Pro-Leu-Trp-**NH-Bzl**	942.4879	942.4942	13.80	4.28	0.07	0.57	0.78
TY010	H-Tyr-*D*-Ala-Gly-Phe-Pro-Leu-Trp-**NMe-Bzl**	956.5035	956.5188	14.97	4.97	0.11	0.58	0.81
TY012	H-Tyr-*D*-Ala-Gly-Phe-Pro-Leu-Trp-**NH-3,5-Bzl(CF_3)$_2$**	1078.4626	1078.4616	16.83	6.27	0.11	0.67	0.81
TY013	H-Tyr-*D*-Ala-Gly-Phe-Pro-Leu-Trp-**NMe-3,5-Bzl(CF_3)$_2$**	1092.4783	1092.4806	17.98	6.76	0.13	0.68	0.81
TY003	H-Tyr-*D*-Ala-Gly-Phe-**Phe**-Pro-Leu-Trp-O-3,5-Bzl(CF_3)$_2$	1226.5139	1226.5151	20.12	11.75	0.16	0.77	0.82
TY007	H-Tyr-*D*-Ala-Gly-Phe-***D*-Phe**-Pro-Leu-Trp-O-3,5-Bzl(CF_3)$_2$	1226.5127	1226.5151	20.95	13.26	0.19	0.72	0.88
TY006	H-Tyr-*D*-Ala-Gly-Phe-**Gly**-Pro-Leu-Trp-O-3,5-Bzl(CF_3)$_2$	1136.4745	1136.4681	18.46	10.16	0.04	0.45	0.72
TY004	H-Tyr-*D*-Ala-Gly-Phe-**Leu**-Pro-Leu-Trp-O-3,5-Bzl(CF_3)$_2$	1192.5286	1192.5307	19.51	11.42	0.23	0.81	0.79
TY005	H-Tyr-*D*-Ala-Gly-Phe-**Met**-Pro-Leu-Trp-O-3,5-Bzl(CF_3)$_2$	1210.4810	1210.4871	19.21	11.14	0.14	0.73	0.79
TY023	H-Tyr-*D*-Ala-Gly-Phe-**Met(O)**-Pro-Leu-Trp-O-3,5-Bzl(CF_3)$_2$	1226.4786	1226.4820	16.91	9.49	0.06	0.44	0.62
TY018	H-Tyr-*D*-Ala-Gly-Phe-**Nle**-Pro-Leu-Trp-O-3,5-Bzl(CF_3)$_2$	1192.5291	1192.5307	19.70	11.64	0.21	0.79	0.82
TY019	H-Tyr-*D*-Ala-Gly-Phe-***N*-Me-Nle**-Pro-Leu-Trp-O-3,5-Bzl(CF_3)$_2$	1206.5489	1206.5464	19.94	11.94	0.20	0.79	0.85
TY027	H-Tyr-*D*-Ala-Gly-Phe-**Met**-Pro-Leu-Trp-**NH-3,5-Bzl(CF_3)$_2$**	1209.3055	1209.5031	17.29	7.94	0.09	0.67	0.58
TY025	H-Tyr-*D*-Ala-Gly-Phe-**Met**-Pro-Leu-Trp-**NH-3,5-Bzl**	1073.3096	1073.5283	14.14	4.19	0.14	0.67	0.55

[a] High-resolution mass spectroscopy using electrospray ionization (ESI) method. [b] HPLC log *k'* = log [(peptide retention time - solvent retention time)/solvent retention time]. All the peptide derivatives showed > 98% purity. (A) 10-90% of acetonitrile containing 0.1% TFA within 40 min and up to 95% within additional 5 min, 1 mL/min, (B) 30-70% of acetonitrile containing 0.1% TFA within 20 min and up to 95% within additional 5 min, 1 mL/min. [c] (I) $CHCl_3$: MeOH : AcOH = 90 : 10 : 3, (II) EtOAc : *n*-BuOH : water : AcOH = 5 : 3 : 1 : 1, (III) *n*-BuOH : water : AcOH = 4 : 1 : 1.

3.1.3. Structure Activity Relationships

3.1.3.1. The *In Vitro* Assay Systems

Three different biological-assay systems were used for evaluating the synthesized peptides: cell-membrane-based radioligand binding assays ("binding assays"), cell-membrane-based GTPγS binding assays ("GTPγS binding assays") and tissue-based assays. The cell-membrane-based radioligand binding assays characterized the binding affinity of the test compound at the corresponding receptor, but the assays could not provide any information related to an agonism or an antagonism of the test compound. The cell-membrane-based GTPγS binding assays were used to determine the stimulative activity (EC_{50}) and potency (E_{max}) of the test compound at the level of receptor-G-protein using the GTP analogue guanosine-5'-*O*-(3-[^{35}S]thio)triphosphate ([^{35}S]GTPγ). These GTPγS binding assay systems could give the result only when the test compound was an agonist at the tested receptor. These two assay systems were performed on homogenated cell-membrane which stably expressed the corresponding receptors and provided the information about the molecular-level ligand-receptor interaction of the test compound. In the tissue-based assays, mouse vas deferens (MVD) and guinea pig isolated ileum (GPI) were used for testing both the agonist and antagonist activity of the compound. Different from the cell-membrane-based assays, the potential of tested compound was evaluated with the tissue-level response (muscular contraction of the tissue was used as the index), so the MVD and GPI assays could be considered as the closer systems to *in vivo* compared to the cell-membrane-based assays. It should be noted that the pharmacokinetical properties of the test compound, such as enzymatic cleavability and membrane permeability, might have more influences in tissue-based assays compared to the cell-membrane-based assays, since opioid and NK1 receptors exist in the nerve plexus of used tissues. Collectively, the combination of cell-membrane-based radioligand binding, GTPγS binding and tissue-based assays could provide their biological figures as an agonist

from the molecular-level and tissue-level standpoints. As for the characterization of their antagonist activities, both the radioligand binding and tissue-based assays should be required.

Therefore, for the estimation of opioid agonist activities, the opioid receptor binding affinities of the synthesized bifunctional peptides were evaluated using human δ-opioid receptors (hDOR) and rat μ-opioid receptors (rMOR) with the cells that stably express these receptors.[136, 147, 148] [^{3}H]DPDPE and [^{3}H]DAMGO were used as their radioligands, respectively. Their agonist efficacies were determined by GTPγS binding assays on the same transfected cells to the radioligand binding assays. [136, 147, 148] The tissue bioassays (MVD and GPI) also were performed to characterize agonist function of the peptides at δ and μ opioid receptors. [136, 147, 148]

As for the affinity at the rat and human NK1 (rNK1 and hNK1) receptors, receptor binding assays also were used on the transfected Chinese hamster ovary (CHO) cells that stably express rNK1 or hNK1 receptors, using [^{3}H]substance P as the standard radioligand.[136, 149] To estimate their antagonist activities against substance P stimulation on the NK1 receptors, tissue bioassays using the GPI were performed in the presence of naloxone to eliminate all the opioid-derived activities.[136, 149] All the synthesized peptides were confirmed to have no or negligible agonist activities against substance P stimulation at the tested concentration.

3.1.3.2. Structural Optimization at the *C*-terminus.

As shown in Table 3.1.2, the lead peptide **TY001** had good binding affinity for both the human and rat NK1 receptors and exhibited functional antagonism against substance P stimulation in guinea pig ileum (Table 3.1.4, *Ke* = 3.6 nM, GPI). Compared to L-732,138, **TY001**, whose sequence was longer than that of L-732,138, showed much less selectivity between the human and rat NK1 receptor homologs (35-fold selectivity for the human NK1 receptor vs. 200-fold selectivity in the case of L732,138). Peptide **TY001** also had moderate binding affinities at the DOR and MOR with 3.6-fold δ-

opioid selectivity over μ-receptor (K_i = 50 and 180 nM, respectively). In the MVD, GPI and GTPγS binding assays, the opioid agonist activities of **TY001** were consistent with the binding assays (Tables 3.1.3 and 3.1.4). Interestingly, the removal of the two trifluoromethyl groups from **TY001** (**TY011,** H-Tyr-*D*-Ala-Gly-Phe-Pro-Leu-Trp-O-Bzl) resulted in increasing opioid affinities especially at the MOR (K_i = 31 nM, DOR; 29 nM, MOR), suggesting the importance of trifluoromethyl groups for the opioid affinities (Table 3.1.2). In the functional tissue assays, both the activities in the MVD and GPI assays of **TY011** also were increased from those of **TY001** (IC_{50} = 40 nM, MVD; 74 nM, GPI). However, the removal of trifluoromethyl groups at the *C*-terminal ester resulted in reduced antagonist activities for the NK1 receptors, indicating much more critical role for the trifluoromethyl groups for the substance P antagonist pharmacophore. In fact, **TY011** showed the decreased affinities at the NK1 receptors from those of **TY001**, and these results were consistent with the *Ke* value in the GPI assay (K_i = 270 nM, rNK1; K_i = 100 nM, hNK1; *Ke* = 150 nM, GPI).

Table 3.1.2. Binding affinities of bifunctional peptides at δ/μ opioid receptors and NK1 receptors

ID	hDOR[a], [^{3}H]DPDPE[b]		rMOR[a], [^{3}H]DAMGO[c]		$K_i(\mu)$ /$K_i(\delta)$	hNK1[d], [^{3}H]Substance P[e]		rNK1[d], [^{3}H]Substance P[f]		K_i(rNK1) /K_i(hNK1)
	$LogIC_{50}$[g]	K_i (nM)	$LogIC_{50}$[g]	K_i (nM)		$LogIC_{50}$[g]	K_i (nM)	$LogIC_{50}$[g]	K_i (nM)	
TY001	–7.0 ± 0.10	50	–6.4 ± 0.20	180	3.6	–10.0 ± 0.14	0.046	–8.3 ± 0.06	1.6	35
TY011	–7.2 ± 0.14	31	–7.2 ± 0.17	29	0.94	–6.7 ± 0.07	100	–6.1 ± 0.04	270	2.7
TY008	–7.7 ± 0.09	10	–8.9 ± 0.09	0.65	0.065	–7.5 ± 0.03	14	30 ± 9.9 %[h]	-	-
TY010	–6.8 ± 0.24	77	–7.0 ± 0.33	46	0.60	–8.5 ± 0.04	1.6	33 ± 7.6 %[h]	-	-
TY012	–6.8 ± 0.08	72	–7.7 ± 0.21	9.5	0.13	–8.9 ± 0.06	0.61	–7.0 ± 0.06	33	54
TY013	–6.5 ± 0.09	31	–7.8 ± 0.13	6.8	0.22	–8.5 ± 0.06	1.4	–7.7 ± 0.03	6.1	4.4
TY003	–7.5 ± 0.14	15	–7.2 ± 0.10	28	1.9	–10.4 ± 0.03	0.021	–8.5 ± 0.07	0.88	42
TY007	–6.7 ± 0.13	93	–6.1 ± 0.15	380	4.1	–8.6 ± 0.04	1.3	–8.0 ± 0.10	3.0	2.3
TY006	–7.1 ± 0.06	36	–7.2 ± 0.15	27	0.75	–10.5 ± 0.04	0.016	–8.5 ± 0.02	1.0	63
TY004	–8.0 ± 0.07	5.0	–7.3 ± 0.07	23	4.7	–10.5 ± 0.04	0.016	–8.6 ± 0.13	0.80	50
TY005	–8.2 ± 0.06	2.8	–7.1 ± 0.11	36	13	–9.9 ± 0.25	0.082	–9.0 ± 0.10	0.29	3.5
TY023	–7.9 ± 0.04	4.8	–7.9 ± 0.07	5.5	1.1	–12.5 ± 0.13	0.00015	–9.1 ± 0.02	0.20	1300
TY018	–8.4 ± 0.15	1.8	–7.7 ± 0.05	9.7	5.4	–9.6 ± 0.04	0.14	–8.7 ± 0.19	0.60	4.3
TY019	–6.8 ± 0.13	77	–6.5 ± 0.09	140	1.8	–8.8 ± 0.03	0.82	–8.5 ± 0.03	0.71	0.86
TY027	–8.8 ± 0.07	0.66	–7.4 ± 0.05	16	24	–10.9 ± 0.10	0.0065	–7.6 ± 0.05	7.3	1100
TY025	–9.1 ± 0.09	0.44	–8.4 ± 0.03	1.8	4.1	–8.4 ± 0.42	3.20	–5.6 ± 0.06	700	220
Biphalin[i]		2.6		1.4	0.54					
DADLE[j]		1.3		16	12					
L-732,138						–8.8 ± 0.02	0.73	–6.4 ± 0.12	130	180

[a] Competition analyses were carried out using membrane preparations from transfected HN9.10 cells that constitutively expressed the δ and μ opioid receptors, respectively. [b] K_d = 0.45 ± 0.1 nM. [c] K_d = 0.50 ± 0.1 nM. [d] Competition analyses were carried out using membrane preparations from transfected CHO cells that constitutively expressed the human or rat NK1 receptors. [e] K_d = 0.40 ± 0.17 nM. [f] K_d = 0.16 ± 0.03 nM. [g] The IC_{50} ± standard errors are expressed as logarithmic values determined from the non-linear regression analysis of data collected from 2 independent experiments (4 independent experimental values per drug concentration). The K_i values are calculated using the Cheng and Prusoff equation to correct for the concentration of the radioligand used in the assay. [h] Inhibition % at 1μM. [i] Ref.150 [j] Ref.151

Table 3.1.3. Opioid agonist functional activities in [^{35}S]GTPγS binding assays

ID	hDOR[a]			rMOR[a]			$EC_{50}(\mu)/EC_{50}(\delta)$
	$LogEC_{50}$[b]	EC_{50} (nM)[c]	Emax (%)[d]	$LogEC_{50}$[b]	EC_{50} (nM)[c]	Emax (%)[d]	
TY001	–7.5 ± 0.28	35	16 ± 0.7	–6.8 ± 0.24	140	26 ± 2	4.0
TY011	–7.1 ± 0.14	85	131 ± 6	–7.4 ± 0.21	36	66 ± 4	0.42
TY008	–7.8 ± 0.28	17	56 ± 6	–8.2 ± 0.44	0.71	100 ± 16	0.067
TY010	–6.8 ± 0.16	150	70 ± 4	–7.5 ± 0.36	29	120 ± 16	0.19
TY012	–7.1 ± 0.13	80	161 ± 7	–7.2 ± 0.26	57	61 ± 4	0.71
TY013	–6.9 ± 0.21	120	137 ± 7	–7.1 ± 0.17	72	72 ± 3	0.60
TY003	–7.7 ± 0.20	21	39 ± 2	–7.2 ± 0.18	59	36 ± 2	2.8
TY007	–7.8 ± 0.36	17	23 ± 2	–6.5 ± 0.38	350	24 ± 3	2.0
TY006	–7.3 ± 0.24	50	34 ± 3	–7.4 ± 0.20	42	36 ± 3	0.84
TY004	–8.1 ± 0.18	9.6	43 ± 2	–7.5 ± 0.16	33	45 ± 3	3.4
TY005	–8.5 ± 0.21	2.9	45 ± 3	–7.5 ± 0.09	32	42 ± 2	11
TY023	–8.7 ± 0.20	1.8	52 ± 3	–7.5 ± 0.12	34	49 ± 2	19
TY018	–8.4 ± 0.11	4.0	130 ± 4	–7.6 ± 0.06	28	120 ± 2	6.9
TY019	–6.4 ± 0.27	360	290 ± 28	–6.8 ± 0.08	150	114 ± 3	0.42
TY027	–8.1 ± 0.14	8.9	58 ± 2	–7.3 ± 0.31	29	65 ± 4	3.3
TY025	–8.6 ± 0.13	2.6	290 ± 28	–7.7 ± 0.18	21	47	8.1
Biphalin	–9.0 ± 0.17	1.1	83	-	-	-	
DADLE	–8.8 ± 0.14	1.6	79 ± 3	–7.8 ± 0.12	17	69 ± 2	11

[a] [^{35}S]GTP-γ-S binding analyses were carried out using membrane preparations from transfected cells that constitutively expressed the respective opioid receptor type. [b] The log EC_{50} ± standard error are logarithmic values determined from the non-linear regression analysis of data collected from 2 independent experiments. [c] The EC_{50} value is converted from the respective log EC_{50}. [d] The E_{max} value is the saturable, maximum level of [^{35}S]GTP-γ-S binding in the cell membranes upon incubation with the peptide, expressed as [Net [^{35}S]GTP-γ-S bound / basal [^{35}S]GTP-γ-S bound] X 100 ± standard error.

Table 3.1.4. Functional assay result for bifunctional peptide ligands at opioid and Substance P receptors

ID	Opioid agonist[a]			Substance P antagonist[a]
	MVD (δ), IC_{50} (nM)[b]	GPI (μ), IC_{50} (nM)[b]	IC_{50}(GPI)/ IC_{50}(MVD)	GPI, *Ke* (nM)[d]
TY001	400 ± 23	520 ± 40	1.3	3.6 ± 1.1
TY011	40 ± 4.4	74 ± 25	1.9	150 ± 17
TY008	50 ± 10	13 ± 3.3	0.26	26 ± 3.9
TY010	41 ± 8.6	9.0 ± 0.5	0.22	59 ± 18
TY012	45 ± 6.3	350 ± 91	7.8	8.5 ± 2.1
TY013	150 ± 26	52 ± 9.4	0.35	6.9 ± 1.1
TY003	910 ± 190	7% at 1μM[c]	> 1.0	14 ± 4.9
TY007	410 ± 110	9% at 1μM[c]	> 2.4	70 ± 7.1
TY006	170 ± 26	380 ± 28	2.2	5.4 ± 1.4
TY004	100 ± 25	340 ± 71	3.4	19 ± 5.0
TY005	22 ± 1.2	360 ± 130	16	25 ± 8.8
TY023	33 ± 7.0	150 ± 51	4.7	7.8 ± 4.0
TY018	17 ± 2.4	370 ± 65	22	7.9 ± 1.9
TY019	190 ± 21	12% at 1μM[c]	> 5.3	4.6 ± 1.2
TY027	15 ± 2.0	490 ± 29	**33**	10 ± 2.1
TY025	4.8 ± 0.35	61 ± 9.6	**13**	9.9 ± 2.8
Biphalin	2.7 ± 1.5	8.8 ± 0.3	3.2	-
DADLE[e]	0.27 ± 0.06	24 ± 5.3	90	-
L-732,138	-	-	-	250 ± 87

[a] Calculated from four isolated tissues (n = 4). [b] Concentration at 50% inhibition of muscle concentration at electrically stimulated isolated tissues. [c] Contraction of isolated tissue relative to initial muscle contraction with KCl at antagonist concentration tested. [d] Inhibitory activity against the Substance P induced muscle contraction in the presence of 1 μM naloxone, *Ke*: concentration of antagonist needed to inhibit Substance P to its half activity. The *Ke* values were obtained from full concentration-effect curve for Substance P in the absence and presence of the test compounds in the presence of 1 μM naloxone to block opioid effects on the tissue. [e] Ref.151

In contrast to the large decreased activities of the *C*-terminal benzyl ester derivative without trifluoromethyl groups (**TY011**) for the substance P antagonist activity, the *Ke* value of its benzyl amide derivative (**TY008,** H-Tyr-*D*-Ala-Gly-Phe-Pro-Leu-Trp-NH-Bzl) was 26 nM, which was 6 and 10 times more active than those of **TY011** and L-732,138, respectively (Table 3.1.4). Since **TY008** had only low affinity for the rNK1 receptor (30% inhibition at 1.0 μM), the species difference between the guinea pig and the rat should be enhanced from that of **TY011** (more than 40-fold). As expected from the result of GPI assay, **TY008** showed a good affinity at hNK1 (K_i = 14 nM). Surprisingly, the opioid activities of **TY008** showed large increases from those of both **TY001** and **TY011,** especially at the MOR (Table 3.1.2). Its affinity at the DOR was 10 nM and subnanomolar-level affinity was found at the MOR (K_i = 0.65 nM), which were consistent with the results in the GTPγS bindings (EC_{50} = 17 nM, DOR; 0.71 nM, MOR) and the tissue assays (IC_{50} = 50 nM, MVD; 13 nM, GPI) (Tables 3.1.3 and 3.1.4). These results indicated that **TY008** was expected to work as a potent bifunctional peptide with μ-preferable opioid agonist and substance P antagonist activities in humans, but not in rats. However, a simple *N*-methylation in the *C*-terminal amide of **TY008** (**TY010,** H-Tyr-*D*-Ala-Gly-Phe-Pro-Leu-Trp-NMe-Bzl) decreased affinities at both the δ and μ opioid receptors (K_i = 77 nM, DOR; 46 nM, MOR) from those of **TY008** and this biological trend was maintained in the GTPγS binding assays. Contrary to the membrane-based assays, **TY010** showed good potencies in the tissue-based MVD and GPI assays (IC_{50} = 41 nM, MVD; 9.0 nM, GPI) (Table 3.1.4). The functional activity of **TY010** as a substance P antagonist was more than two times lower than **TY008** (*Ke* = 59 nM, GPI), though its K_i value at hNK1 was improved (1.6 nM). These biological results of the compounds with *C*-terminal modification (**TY008**, **010** and **011**) proved that the *C*-terminus may regulate opioid activities and selectivities, although it is structurally apart from the opioid pharmacophore, and trifluoromethyl groups played a critical role for it.

Although whose opioid selectivity was μ-selective, the introduction of amide at the *C*-terminus improved the bioactivities in the benzyl amide derivative **TY008.** Thus, the 3,5-bis(trifluoromethyl)-

benzyl amide derivative (**TY012,** H-Tyr-*D*-Ala-Gly-Phe-Pro-Leu-Trp-NH-3,5-Bzl(CF_3)$_2$) was next prepared**.** It also showed a μ-selective binding affinities with nanomolar-level affinity at the MOR and a moderate affinity at the DOR (K_i = 72 nM, DOR; 9.5 nM, MOR) (Table 3.1.1). However, in the tissue assays, IC_{50} value in MVD assay (45 nM) was better than that in the GPI assay (350 nM). Therefore, **TY012** could strongly bind at the MOR, but its functional activity to regulate a μ opioid signal in the tissue was apparently decreased. As for its substance P antagonist activity, ligand **TY012** had decreased affinities at both the hNK1 and rNK1 receptors from those of the *C*-terminal ester **TY001** (K_i = 0.61 and 33 nM, respectively) (Table 3.1.2). In the GPI assay, the substitution of a benzyl ester to amide with trifluoromethyl groups showed less influence on substance P antagonist activity compared to the results of **TY008** and **TY011** (*Ke* = 3.6 nM for **TY001**, 8.5 nM for **TY012**) (Table 3.1.4). Finally, the *N*-methylation in the *C*-terminal amide of **TY012** (**TY013,** H-Tyr-*D*-Ala-Gly-Phe-Pro-Leu-Trp-NMe-3,5-Bzl(CF_3)$_2$) was also tested. Relatively small difference (less than 2.5-fold) were found in the binding affinities at rMOR, hDOR and hNK1 receptors from those of **TY012**. For opioids, **TY013** showed moderate binding at the DOR and good affinity for the MOR (K_i = 31 nM, DOR; 6.8 nM, MOR), and this trend was maintained in the IC_{50} values in MVD and GPI assays (150 and 52 nM, respectively), although its functional activities were relatively low in the GTPγS binding (EC_{50} = 120 nM, DOR; 72 nM, MOR). The binding affinity of **TY013** at the hNK1 receptor was two times less than that of **TY012** (K_i = 1.4 nM), but its *Ke* value in the GPI assay with substance P stimulation was 6.9 nM, which was almost equipotent to **TY012** (Tables 3.1.2 and 3.1.4).

As a consequence of the modification on **TY001** (H-Tyr-*D*-Ala-Gly-Phe-Pro-Leu-Trp-O-3,5-Bzl(CF_3)$_2$) at its *C*-terminus, where the NK1 antagonist pharmacophore was incorporated, not only NK1 antagonist activity but also opioid activity and selectivity were shifted. The opioid agonist activities of **TY008** (H-Tyr-*D*-Ala-Gly-Phe-Pro-Leu-Trp-NH-Bzl), which had benzyl amide moiety with no trifluoromethyl groups, was improved from those of **TY001**, but its opioid selectivity was changed into μ-preference. The affinity of **TY008** for hNK1 receptor was decreased from that of

TY001 and it showed almost no affinity at the rNK1 receptor. **TY012** (H-Tyr-*D*-Ala-Gly-Phe-Pro-Leu-Trp-NH-3,5-Bzl(CF_3)$_2$) was also found as a potent bifunctional peptide derivative with opioid agonist and substance P antagonist activities whose opioid selectivity was still δ-selective in the tissue assays.

3.1.3.3. Structural Optimization at the Connecting Position of Two Pharmacophores.

Next position to be optimized was the connecting position between two pharmacophores in **TY001**, since this position was considered as the "address" region which could be fine-tuned for both of the opioid agonist and NK1 antagonist activities as well as their selectivities. Based on the "overlapping pharmacophore" concept, one amino acid residue was inserted in between the two pharmacophores (Figure 3.1.3). First, two newly designed peptides, H-Tyr-*D*-Ala-Gly-Phe-Phe-Pro-Leu-Trp-O-3,5-Bzl(CF_3)$_2$ (**TY003**) and H-Tyr-*D*-Ala-Gly-Phe-*D*-Phe-Pro-Leu-Trp-O-3,5-Bzl(CF_3)$_2$ (**TY007**), in which both on opioid agonist structure (H-Tyr-*D*-Ala-Gly-Phe) and on NK1 antagonist moiety (Pro-Leu-Trp-O-3,5-Bzl(CF_3)$_2$ were fused into one molecule with Phe or *D*-Phe as an "address" residue for both the pharmacophores. Interestingly, the binding affinities of **TY003** at both δ/μ opioid receptors were in the 10 nM range with 1.9-fold δ-opioid selectivity (K_i =15 nM, δ opioid; 28 nM, μ opioid) (Table 3.1.2). Peptide **TY003** also showed potent and slightly δ-selective opioid agonist efficacies in the GTPγS binding assays with the EC_{50} values of 21 and 59 nM at the DOR and MOR, respectively (Table 3.1.3). The binding affinity of **TY003** at hNK1 and rNK1 was improved from those of **TY001** (Table 3.1.2, 0.021 and 0.88 nM, respectively). Moreover, the GPI assay demonstrated that **TY003** acted as an effective antagonist against substance P stimulation (*Ke* = 14 nM) (Table 3.1.4). It should be noted that **TY003** had excellent affinity at rat NK1 receptors as well as good functional activity using guinea pig ileum tissue, which means that **TY003** had substance P antagonist activities in animal models for both of the species. Moreover, the affinity and bioactivity of

TY003 were greatly improved over those of L-732,138 whose IC_{50} value for the hNK1 and rNK1 was 0.73 and 130 nM in radioligand binding assays, respectively, and whose *Ke* value in the GPI tissue was 250 nM. Even though the peptide **TY003** was not very δ opioid selective, these results clearly demonstrated the success of the rationale of the overlapping-pharmacophore concept. However, the peptide possessing a *D*-amino acid in position 5 (**TY007**) was found to have drastically lower affinities than **TY003** (K_i = 93 nM, DOR; 380 nM, MOR; 1.3 nM, hNK1; 3.0 nM, rNK1), which suggested that the amino acid residue in position 5 was critical for the binding affinities, and the *L*-form was preferred over the *D*-form. It is reasonable to expect the position 5 of these peptides to play an important role not only at NK1 receptors, but also at δ/μ opioid receptors, since it can act as an "address" element for the NK1 antagonist pharmacophore as well as an "address" region for the opioid receptor.[121, 145, 152] Considering these results, the synthetic effort was focused on optimizing the position 5 of **TY003** to find a bifunctional compound possessing potent NK1 antagonist activity and effective δ/μ opioid agonist activities together with better δ-selectivity. First, Gly which is the simplest amino acid was introduced at position 5 of **TY003** (H-Tyr-*D*-Ala-Gly-Phe-Gly-Pro-Leu-Trp-O-3,5-Bzl$(CF_3)_2$; **TY006**). Although the binding assays (Table 3.1.2) of **TY006** showed lower affinity for δ opioid receptors (K_i = 36 nM) than did **TY003**, the affinities at both μ opioid and NK1 receptors were maintained (K_i = 27, MOR; 0.016 nM, hNK1; 1.0 nM, rNK1). The opioid agonist activities of ligand **TY006** in the MVD and GPI assays were much higher than expected from the binding assay results but were not greatly improved from the results of **TY003** (IC_{50}=170 and 380 nM, respectively). The antagonist activity of **TY006** against substance P stimulation in the GPI tissue assay also was higher than that of **TY003** (IC_{50} = 5.4 nM). These improvements in tissue assays might indicate that the aromatic side chain at position 5 led to low activity or to metabolical instability, and thus Leu and Met were chosen for the next substituents (H-Tyr-*D*-Ala-Gly-Phe-Leu-Pro-Leu-Trp-O-3,5-Bzl$(CF_3)_2$; **TY004** and H-Tyr-*D*-Ala-Gly-Phe-Met-Pro-Leu-Trp-O-3,5-Bzl$(CF_3)_2$; **TY005**). In these modifications, the 1-5 residues of two peptides (H-Tyr^1-*D*-Ala^2-Gly^3-Phe^4-Leu^5 of **TY004** and H-Tyr^1-*D*-Ala^2-Gly^3-

Phe^4-Met^5 of **TY005**) were similar to the endogenous opioid peptides Leu-enkephalin (H-Tyr-Gly-Gly-Phe-Leu-OH) and Met-enkephalin (H-Tyr-Gly-Gly-Phe-Met-OH), both of which have potent opioid activities as well as δ-opioid receptor selectivity. As can be seen in Table 3.1.2, binding affinity at DOR of **TY004** was improved from that of **TY006** (K_i = 5.0 nM) and its K_i value at MOR was 23 nM with 4.7-fold δ receptor selectivity over μ opioid. The agonist activities of ligand **TY004** in the GTPγS binding assays showed a similar tendency, with EC_{50} values of 9.6 and 33 nM, respectively (3.4-fold δ selectivity). This δ selectivity was maintained in the MVD and GPI assays (3.4-fold). The affinities at the NK1 receptors of **TY004** were retained relative to **TY006** (K_i = 0.016 and 0.80 nM for hNK1 and rNK1, respectively) with slightly decreased antagonist activity in the GPI assay (IC_{50} = 19 nM). In the case of peptide **TY005**, there was a large increase in δ opioid activity (K_i = 2.8 nM), and 13-fold δ selectivity was seen over MOR in the binding assays. The agonist activities for both DOR and MOR in GTPγS binding assays were consistent with the results of the binding assays (EC_{50} = 2.9 and 32 nM, respectively). Moreover, ligand **TY005** showed excellent functional opioid agonist activity in the MVD assay (IC_{50} = 22 nM) with better selectivity over that of the GPI assay (16-fold). Although the substance P antagonist activity of **TY005** in the GPI assay was less than that of **TY006**, it still retained good activity (*Ke* = 25 nM) with effective affinities for the NK1 receptors (K_i = 0.082 and 0.29 nM for hNK1 and rNK1, respectively). Moreover, the *Ke* value of **TY005** in the GPI assay against substance P stimulation was almost equivalent to its IC_{50} value in the MVD assay against opioid stimulation. Therefore, the peptide **TY005** could be considered as a highly active, highly balanced and δ selective bifunctional compound for the δ/μ opioid and NK1 receptors. Next, further modifications were made in position 5 on **TY005**. Improved activities and δ selectivity were sought. The oxidized form of ligand **TY005** at Met^5, H-Tyr-*D*-Ala-Gly-Phe-Met(O)-Pro-Leu-Trp-O-3,5-Bzl$(CF_3)_2$ (**TY023**), was synthesized and tested since it has been reported that methionine oxidation enhances opioid activities as well as δ selectivity for enkephalin analogues.[153, 154] In fact, this modification led to better binding affinity at the MOR than that of **TY005** (K_i = 5.5 nM), but a

decreased K_i value at DOR which led to almost equivalent affinities at both δ and μ opioid receptors (δ selectivity: 1.1-fold). As for the EC_{50} values in the GTPγS binding assays, ligand **TY023** unexpectedly showed the highest agonist activity at δ opioid receptors with the best δ selectivity (19-fold). However, this good δ selectivity was decreased to 4.7-fold in the tissue-based MVD and GPI assays (IC_{50} = 33 and 150 nM, respectively). The affinity of ligand **TY023** at the hNK1 and rNK1 receptors increased from that of **TY005** (K_i = 0.00015 and 0.20 nM, respectively), and its substance P antagonist activity in the GPI assay was also improved (*Ke* = 7.8 nM). Nle, which is a general bioisostere of Met, also was introduced at position 5 of the sequence (H-Tyr-*D*-Ala-Gly-Phe-Nle-Pro-Leu-Trp-O-3,5-Bzl(CF_3)$_2$; **TY018**). In the receptor binding assays, ligand **TY018** showed the best affinity for DOR (K_i = 1.8 nM) and its K_i value at MOR was less than 10 nM (9.8 nM; 5.4-fold δ selectivity). In the GTPγS binding assays, the δ selectivity of **TY018** was moderate (6.9-fold) just as in the receptor binding assays. However, the δ selectivity showed a distinct increase in tissue assays (22-fold), in which IC_{50} value in the MVD assay was better than that of **TY005** (17 nM). The hNK1 and rNK1 affinities of **TY018** were decreased, while its substance P antagonist activity was increased from that of **TY005** (*Ke* = 7.9 nM). Finally, the *N*-methylation of Nle^5 of **TY018** (H-Tyr-*D*-Ala-Gly-Phe-*N*-Me-Nle-Pro-Leu-Trp-O-3,5-Bzl(CF_3)$_2$; **TY019**) was tested, since a δ selective and potent enkephalin analogue has been reported with *N*-methylation at position 5.[155-157] However, although this modification led to the best substance P antagonist activity in the functional assay (*Ke* = 4.6 nM), ligand **TY019** showed a significant decrease of binding affinities at both DOR and MOR as well as agonist activities in the GTPγS binding assays, with low δ selectivity (1.8 and 0.4-fold, respectively). These results show that the introduction of *N*-methyl amino acid at position 5 decreases the activities not only at opioid receptors but also at NK1 receptors.

Consequently, **TY005** was chosen as the best compound because of its good δ selectivity in all *in vitro* and tissue assays as well as the high affinity and activity at the δ opioid receptor among the optimized bifunctional peptides at the fifth residue. Although the antagonist activity of **TY005** against

substance P stimulation in the GPI assay was moderate among the peptides tested, this activity should be enough since it was 12-fold more potent than L-732,138, whose biological activities *in vivo* were reported in several models with different species of animals.[125, 158, 159]

3.1.3.4. *In Vivo* Biological Activity of TY005

As discussed above, **TY005** was considered as the highly active, well-balanced and δ selective bifunctional compound for the δ/μ opioid and NK1 receptors. Thus, the anti-nociceptive efficacy of this compound was evaluated to confirm the proof-of-concept via intrathecal administration in male Sprague Dawley rats (Figure 3.1.5). This assay gave encouraging results. Peptide **TY005** showed a distinct anti-nociceptive effect with excellent dose-dependency (Figure 3.1.5). Moreover, throughout the *in vivo* studies, **TY005** showed no sign of toxicity at any concentration tested.

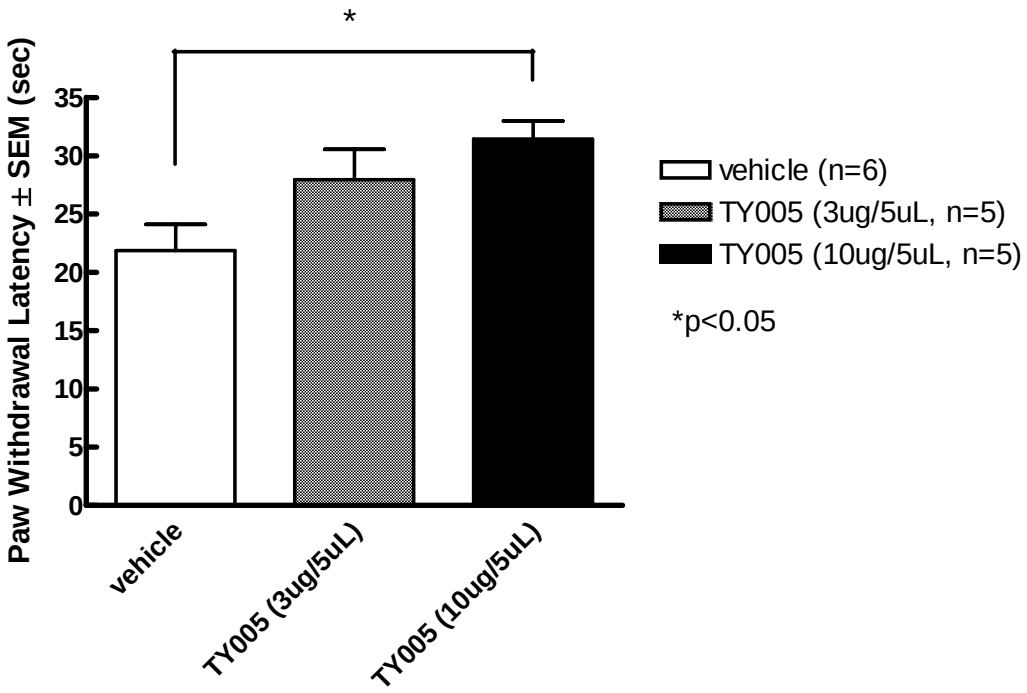

Figure 3.1.6. Antinociceptive effect of bifunctional peptide **TY005** (H-Tyr-*D*-Ala-Gly-Phe-Met-Pro-Leu-Trp-O-3,5-Bzl(CF_3)$_2$) in male Sprague Dawley rats. Naïve animals were given bifunctional peptide, TY005, intrathecally and subsequently tested for response to noxious thermal heat via infrared stimulation. Fifteen minutes after the introduction of **TY005**, the peak effect (shown here) was observed. Compared to vehicle, the bifunctional peptide significantly increased the paw withdrawal threshold in response to thermal stimulation, indicating an antinociceptive effect ($p<0.05$).

3.1.3.5. Structural Optimization at Both of the C-terminus and the Connecting Position of Two Pharmacophores.

Finally, all the obtained SAR information were combined and further optimization was performed on the *C*-terminus of **TY005** which has a Met^5 as the key amino acid residue for the δ-opioid selectivity and had potent analgesic activities *in vivo*. The *C*-terminus of **TY005** was modified based on the SAR on **TY001** to give two novel derivatives (Tyr-*D*-Ala-Gly-Phe-Met-Pro-Leu-Trp-NH-3,5-Bzl(CF_3)$_2$; **TY027** and Tyr-*D*-Ala-Gly-Phe-Met-Pro-Leu-Trp-NH-Bzl; **TY025**) (Table 3.1.1).

Compared to the subnanomolar-level affinities of the *C*-terminal ester derivative (**TY005**) at the rNK1 receptor, the *C*-terminal amide derivative (**TY027**) was 25 times less potent, but still showed binding affinities in the nanomolecular range (K_i = 7.3 nM) (Table 3.1.2). The binding affinity at the rNK1 of **TY025**, which had no trifluoromethyl group in the *C*-terminal benzyl moiety, was decreased to a K_i = 700 nM. However, in the functional assay using the GPI to examine their antagonist activities, the *Ke* value for **TY025** (10 nM) was similar to that for **TY027** (9.9 nM) and better than that for **TY005** (25 nM) (Table 3.1.7). Several factors, such as membrane permeability and metabolic stability might be responsible for this inconsistency, but one good explanation should be provided by the known species difference between rat and guinea pig NK1 receptors.[160] It is well known that the human NK1 receptor has higher homology to the guinea pig NK1 receptor than to the rat or mouse NK1, and some NK1 antagonists have a large species difference.[160] In fact, **TY025** showed a 220 times better K_i value at the hNK1 receptor (3.2 nM) compared to the value at the rNK1 receptor. Surprisingly, **TY027**, which is the *C*-terminal benzyl amide with two trifluoromethyl groups, showed the largest difference between the affinities at the rNK1 and at the hNK1 (1100-fold), and the K_i value for the hNK1 receptor was 6.5 pM suggesting that this analogue would be very potent in humans. Therefore, substitution of the *C*-terminal ester of **TY005** for an amide gave rise to increased species difference at the human and rat NK1 receptors.

For the δ and μ opioid agonist activities, **TY027** showed 24-fold δ selectivity, as expected from the existence of Met[5],[136] with four-fold higher affinity at the DOR (K_i = 0.66 nM) and two times higher affinity at the MOR (K_i = 16 nM) than **TY005** (Table 3.1.2)**.** It is interesting again that a small modification at the *C*-terminus, which is far from the opioid agonist pharmacophore, can influence the opioid activities so much. The elimination of two trifluoromethyl groups led to further increased affinity at both the DOR (K_i = 0.44 nM) and the MOR (K_i = 1.8 nM) with 4.1-fold δ-selectivity. The binding affinity results correlated well with the *in vitro* GTPγS binding assays, and the functional assays using GPI and MVD tissues (Tables 3.1.3 and 3.1.4).

Here, **TY027** showed potent activity in the MVD assay with the best δ selectivity (IC_{50} = 15 nM in MVD and 490 nM in GPI). The IC_{50} value of **TY025** in the GPI assay (IC_{50} = 61 nM) was a large increase from those of **TY005** and **TY027,** with the best IC_{50} value in the MVD assay among all the synthesized bifunctional peptides (4.8 nM). Therefore, **TY025** was found to be a bifunctional peptide possessing potent agonist activities for opioid receptors and moderate δ opioid selectivity together with a nanomolar level hNK1 antagonist activity. On the other hand, **TY027** was characterized as a very efficient hNK1 antagonist with potent and δ selective opioid agonist activities, which also has nanomolar level affinity at the rNK1 receptor. Thus, **TY027** can be considered as another promising candidate for an analgesic drug. Though both **TY027** and **TY025** have different biological profiles, they are expected to be potent analgesics for pain control in humans.

3.1.4. Summary of the Section

A series of bifunctional peptides with opioid agonist and NK1 antagonist bioactivities were designed with the concept of connecting or overlapping two pharmacophores. **TY001** (H-Tyr-*D*-Ala-Gly-Phe-Pro-Leu-Trp-O-3,5-Bzl(CF_3)$_2$) was synthesized as the lead peptide possessing the opioid agonist pharmacophore in the *N*-terminus and NK1 antagonist pharmacophore in the *C*-terminal half. The extensive structure-activity relationship (SAR) studies were performed on **TY001** to find a potent bifunctional peptide with high δ-opioid selectivity as a novel candidate of analgesic drug for several pain states. The first-phase optimization was performed on the *C*-terminus of **TY001** to show that the *C*-terminus acted as not only a critical pharmacophore for the NK1 antagonist activities, but as an address region for the opioid agonist pharmacophore which is structurally distant from the *C*-terminus. The second-phase optimization was done on the fifth residue which was inserted in between the two pharmacophores and serves as an address moiety for both receptor recognitions. The substitution of fifth residue had critical effects on both of activities at opioid receptors and NK1 receptors. Among the

optimized peptides on the position, **TY005** (H-Tyr-*D*-Ala-Gly-Phe-Met-Pro-Leu-Trp-O-3,5-Bzl(CF_3)$_2$) had excellent agonist activity for both δ opioid and μ opioid receptors with good δ opioid selectivity, and excellent antagonist activity for NK1 receptors. Moreover, **TY005** showed efficient and dose-dependent anti-nociceptive potency *in vivo* to confirm the proof-of-concept of the bifunctionalization. The final-phase structural tuning was focused on the *C*-terminus of **TY005** to yield two novel peptides **TY027** (Tyr^1-*D*-Ala^2-Gly^3-Phe^4-Met^5-Pro^6-Leu^7-Trp^8-NH-3,5-Bzl(CF_3)$_2$) and **TY025** (Tyr^1-*D*-Ala^2-Gly^3-Phe^4-Met^5-Pro^6-Leu^7-Trp^8-NH-Bzl). The bioactivities of **TY025** and **TY027** were evaluated and they both were found to be potent bifuctional peptides. It should be noted again that the structural modifications were limited only in their NK1 pharmacophores, but the bioactivities were shifted both for opioid and NK1. Interestingly, the biological activities of **TY025** showed different trends from those of **TY005** and **TY027**, with more potent δ/μ opioid agonist activities as well as lower NK1 antagonist activities, in direct relation to the removal of two trifluoromethyl groups in the *C*-terminus. The important result is that not only was the NK1 antagonist activities changed (the pharmacophore located at the *C*-terminus where the structure was modified), but also the opioid agonist activities (the pharmacophore was at the *N*-terminal half which was structurally preserved for all three derivatives) were shifted due to the local removal of trifluoromethyl groups, suggesting the large influence of these groups on both the bioactivities. In the light of these structure-activity relationship studies, the following NMR structural studies were performed on the highly bioactive peptide derivatives, **TY005**, **TY027** and **TY025** as reported in the next section, to figure out the factors determining their three-dimensional molecular structure which might be related to their observed biological activities.

3.2. The Small and Local Modification in the *C*-terminus of Bifunctional Peptide Led to Large Structural Change That Are Relevant to the Shift of Bioactivities

3.2.1. Background

The importance of peptide conformation (or three-dimensional molecular structure) has become increasingly appreciated recently, as their biological importance has been widely recognized.[161-165] As for the conformation of small and linear peptides, such as the endogenous opioid peptide enkephalin[166] and its analogues,[49, 50] have been thought to form "random" conformations in aqueous solution due to their high flexibility.[167] However, in the presence of trifluoroethanol (TFE) or membrane-mimicking surroundings, they could have structured conformations, since their secondary structural elements can be stabilized by the environmental effects.[49, 50, 168, 169] Therefore, the circumstances surrounding such a peptide should be important especially for their conformational definitions.[170]

Many G-protein coupled receptors (GPCRs), which are the typical membrane-bound proteins, have their ligand binding sites in or near the lipophilic trans-membrane (TM) domains.[38-41] Since the docking event of such a receptor and a ligand must take place near the membrane, ligand-membrane interactions should be important, and this research topic has been explored for decades.[42, 43] In fact, it has been pointed out that the membrane promotes ligand-receptor docking,[45-47, 171] and that the ligand adoption into membrane followed by membrane-catalyzed two-dimensional search should be more efficient than the three-dimensional ligand-receptor binding through solvent space (Figure 3.2.1).[43, 48-50] Hence, understanding ligand-membrane interactions and membrane-bound structures of ligands is indispensable for further insight into their diverse biological behaviors.[48-50]

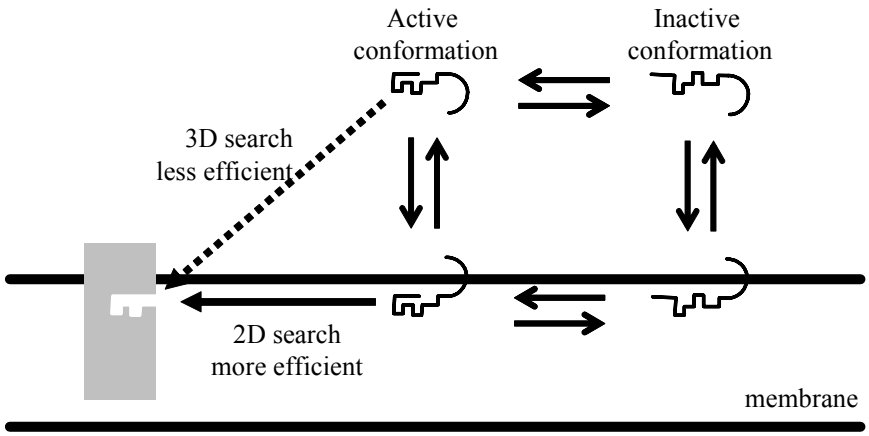

Figure 3.2.1. The interactive model of peptide ligand and membrane-bound protein.

The opioid and NK1 receptors are both GPCRs which have significant importance in pain signal transmission, and their ligand binding sites are found in or near the TM domains.[40,41] As reported in the previous section, the bifunctional peptide derivatives, which act as opioid agonists and NK1 antagonists, have been developed. The extensive discussions were made on their structure-activity relationships (SAR) which were based on their primary sequences (Section 3.1). However, their three-dimensional molecular structures in membrane and compound-membrane interactions should also be important for further understanding the biological activities of ligands both *in vitro* and *in vivo*. In the previous section, Tyr^1-*D*-Ala^2-Gly^3-Phe^4-Met^5-Pro^6-Leu^7-Trp^8-O-3,5-Bzl$(CF_3)_2$ (**TY005**), which has a Met^5 as the key amino acid residue for the δ-opioid selectivity and showed potent analgesic activities *in vivo*,[136, 149, 172] was modified into two derivatives (Figure 3.2.2). The ester moiety of **TY005** was changed into amide connection to yield **TY027** (Tyr^1-*D*-Ala^2-Gly^3-Phe^4-Met^5-Pro^6-Leu^7-Trp^8-NH-3,5-Bzl$(CF_3)_2$) which had improved affinities for DOR, MOR and hNK1 receptors with decreased affinity at rNK1 receptor. The δ opioid selectivity of **TY027** (24-fold over μ opioid) also was improved compared to that of **TY005** (13-fold). While, the removal of two trifluoromethyl groups in **TY027** (**TY025;** Tyr^1-*D*-Ala^2-Gly^3-Phe^4-Met^5-Pro^6-Leu^7-Trp^8-NH-Bzl) gave rise to the significantly increased agonist activities for MOR, resulting in decreased δ selectivity to 4.1-fold compared to **TY027**. The affinities of **TY025** at NK1 receptors were lower than those of **TY005** and **TY027**.

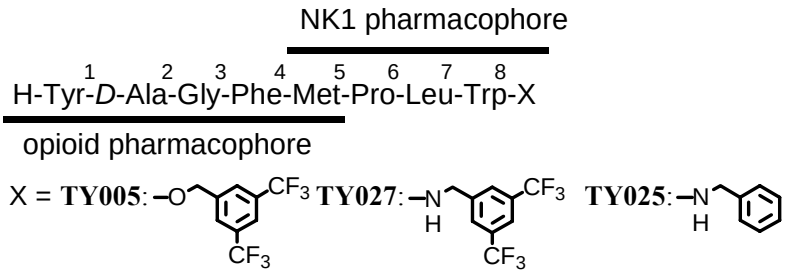

Figure 3.2.2. Sequence of the bifunctional ligands synthesized and examined

In fact, the main intension for these structural modifications was to seek for induced conformational changes in the presence of lipid media, and to examine the influences of such changes on manipulating bioactivities. Therefore, the NMR conformation of **TY005, TY027** and **TY025** was determined in aqueous solution with membrane-mimicking perdeuterated dodecylphosphocholine (DPC) micelles. Fluorescence experiments as well as additional NMR studies using paramagnetic agents also were performed to determine the difference in membrane-compound interactions.

In this section, the new findings, that small and local structural modifications which were made only at the *C*-terminus of peptide sequence induced large conformational changes in membrane-mimicking DPC micelles,[51, 52, 173-176] was reported in the direct relevance to their observed biological activity shifts.

3.2.2. Results and Discussion.

3.2.2.1. Secondary Structure Analysis Based on Assigned ^{1}H NMR.

NMR experiments were performed to obtain structural information in DPC micelles with previously reported procedure.[51, 52] Two-dimensional NMR studies including TOCSY, DQF-COSY and NOESY were performed on all three bifunctional peptide derivatives in pH 4.5 buffer (45 mM CD_3CO_2Na/HCl, 1 mM NaN_3, 90% H_2O/10% D_2O) with 40-fold perdeuterated DPC micelles. At concentrations above

the critical micelle point, DPC forms micelles with an aggregate number of 50 to 90, corresponding to one or two peptide molecules per micelle.[177] All ^{1}H chemical shift assignments of **TY005, TY027** and **TY025** can be found in Table 3.3.2 at the end of this section.

The NOESY data showed the reasonably good quality as seen in Figure 3.2.3 (Side-chain region and H^N-H^N region of the NOESY spectrum were also found in Figure 3.3.1 at the end of this section). A total of 136, 155 and 184 non-redundant NOE restraints were used for **TY005, TY027** and **TY025**, respectively, based on the NOESY cross-peak volumes including sequential (50, 63 and 72, respectively), medium-range (2-4 residues; 31, 36, and 46, respectively) and long-range (1, 0 and 3, respectively) restraints. The distribution of these restraints along the peptide chain is shown in Figure 3.2.4D. Only one dihedral angle restraint was used: the Leu φ angle in **TY025**. The total numbers of restraints were 136, 155 and 185, respectively (15.1, 17.2 and 20.4 per residue). The large numbers of NOEs per residue for small and linear peptides suggest that the peptide derivatives exist in well-defined conformations in the DPC micelles.

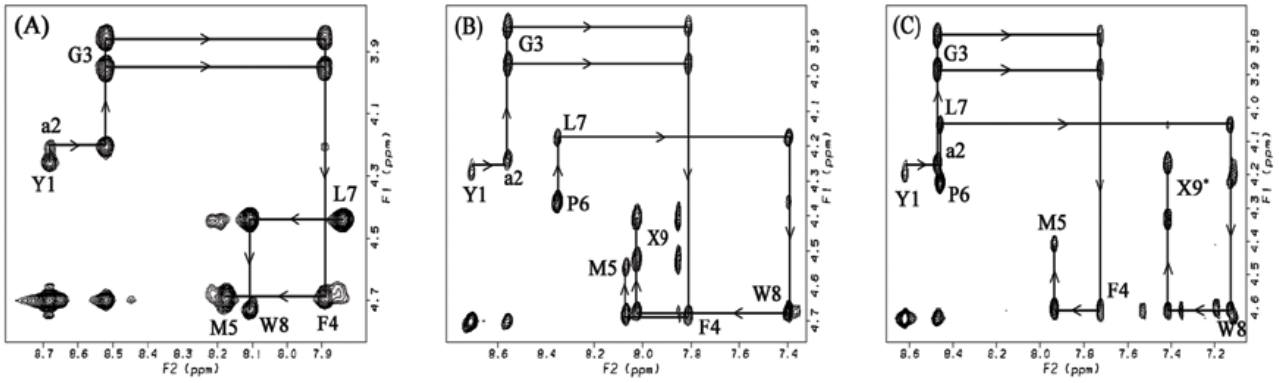

Figure 3.2.3. Fingerprint (H^N-H^α) region of the NOESY spectrum of (A) **TY005**, (B) **TY027** and (C) **TY025** in DPC micelles. Intraresidue H^N-H^α NOE cross-peaks are labeled with residue number, and arrows indicate the connectivity path from N-terminal to *C*-terminal. X9 represents the cross-peaks derived from the corresponding *C*-terminal H^N and benzyl protons.

The interresidual NOE connectivities and the $^3J_{HN\text{-}H\alpha}$ coupling constants of all of the peptide derivatives are illustrated in Figure 3.2.4. The *C*-terminal benzyl moiety of **TY027** and **TY025** are represented as residue 9. The $^3J_{HN\text{-}H\alpha}$ coupling constants for all residues in all three peptide derivatives were within the range of 6–8 Hz except for Leu[7] in **TY025**. This is most likely due to conformational averaging of the peptides in solution.[178] The observed NOE patterns, including $d_{NN}(i, i + 1)$, $d_{\alpha N}(i, i + 1)$ and some medium-range (i, i + 2 or 3) connectivities, suggest the possibility of β-turn structures[179] around residues 1-4 in all three peptide derivatives as well as around residues 5-8 in **TY027**. A few longer-range $d_{\alpha N}(i, i + 3)$ and $d_{\alpha N}(i, i + 4)$ connectivities found in **TY025** indicate the existence of a helical structure[179] in this molecule, consistent with its H^α CSI pattern (Figure 3.2.4C).

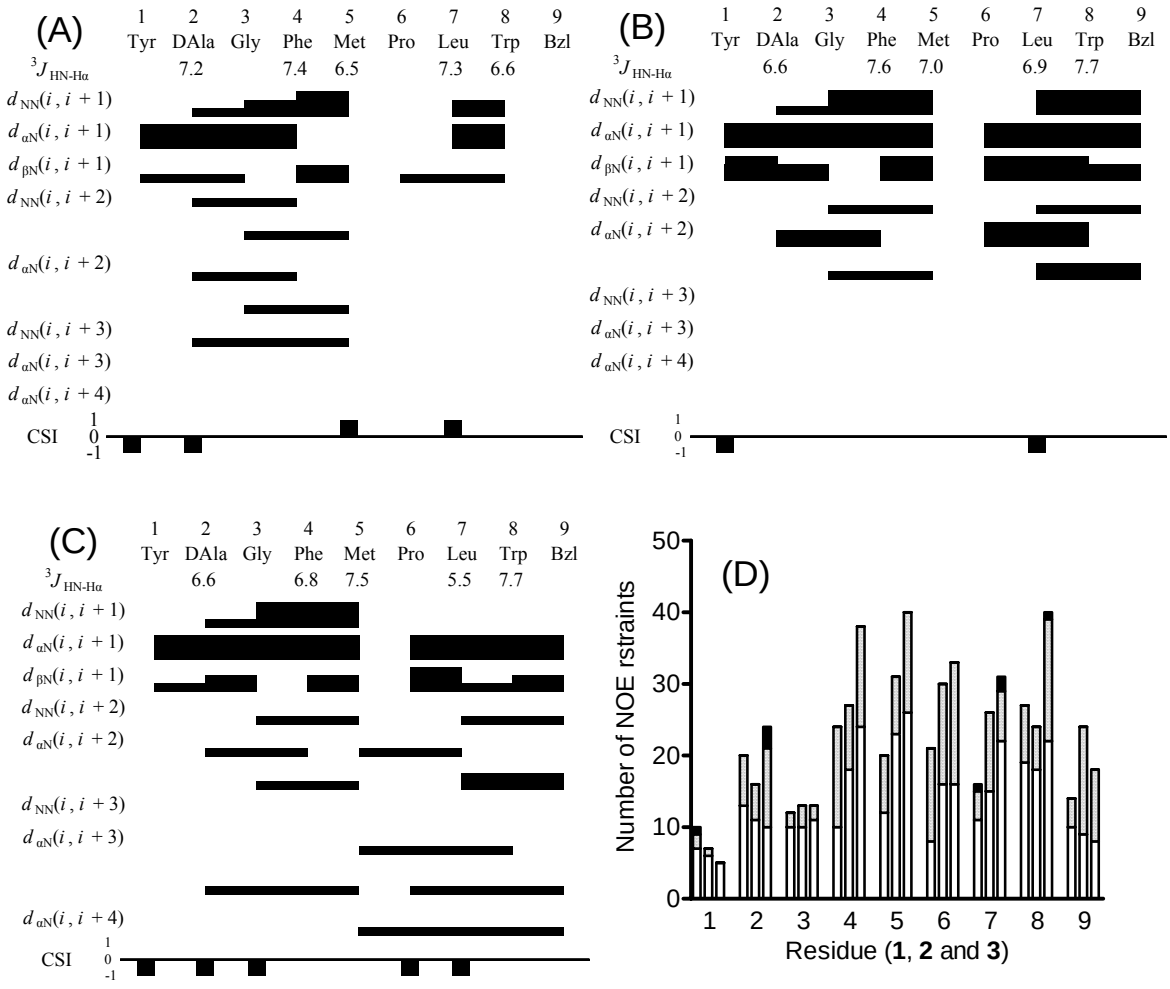

Figure 3.2.4. Diagram of H^N-H^α coupling constants, NOE connectivities, and H^α chemical shift index (CSI) for (A) **TY005**, (B) **TY027** and (C) **TY025**. The H^α CSI was calculated using the random-coil values reported by Andersen et al. Reference [180, 181]. The residual interresidue NOE distance restraints of **TY005** (left), **TY027** (middle) and **TY025** (right) (D). Each column shows the sequential (*i*, *i* + 1; open), medium-range (*i*, *i* + 2-4; hatched) and long-range restraints (*i*, *i* + >4; filled), respectively. The residue Bzl or 9 stands for the respective *C*-terminal moieties.

3.2.2.2. Structural Calculations.

The 20 structures with the lowest total energies after rMD refinement were used to represent the structure of the peptide derivatives in DPC micelles. Since the experimental NOEs and $^{3}J_{\text{HN-H}\alpha}$ were the averaged values in the NMR experiment time course, the obtained low-energy structures did not correspond to a single conformation under these experimental conditions. However, the ensemble of an appropriate number of obtained structures provides sufficient structural figures based on the "averaged" or "dynamic" view of the conformations. Thus, statistics for the 20 best structures were performed as shown in Table 3.2.1. The average restraint violation energies were low (2.48, 2.95 and 1.13 kcal mol^{-1} for **TY005**, **TY027** and **TY025** respectively), with average maximum NOE distance violations of 0.17, 0.11 and 0.11 Å with no dihedral angle violations. The 19 structures were aligned with the most stable structure using all backbone atoms (Figure 3.2.5a), only the backbone atoms of residues 1-4 (Figure 3.2.5b) or 5-8 (Figure 3.2.5c). The backbone rmsd's of the 19 structures with respect to the most stable structure were 1.80, 1.14 and 0.19 Å for **TY005**, **TY027** and **TY025**, respectively, for all residues. The rmsd values are significantly decreased if alignment is carried out only on the backbone atoms of residues 5-8 (**TY005**: 0.75; **TY027**: 0.45; **TY025**: 0.04), indicating that the *C*-terminal half is much better defined by the NMR restraints than the *N*-terminal half (residues 1-4). This may be due to greater flexibility in the *N*-terminal portion. The decrease in rmsd going from a flexible ester (**TY005**) to a more rigid amide (**TY027**) linkage at the *C*-terminus was expected, but the much larger decrease resulting from removal of two trifluoromethyl groups of **TY027** (**TY025**) was surprising.

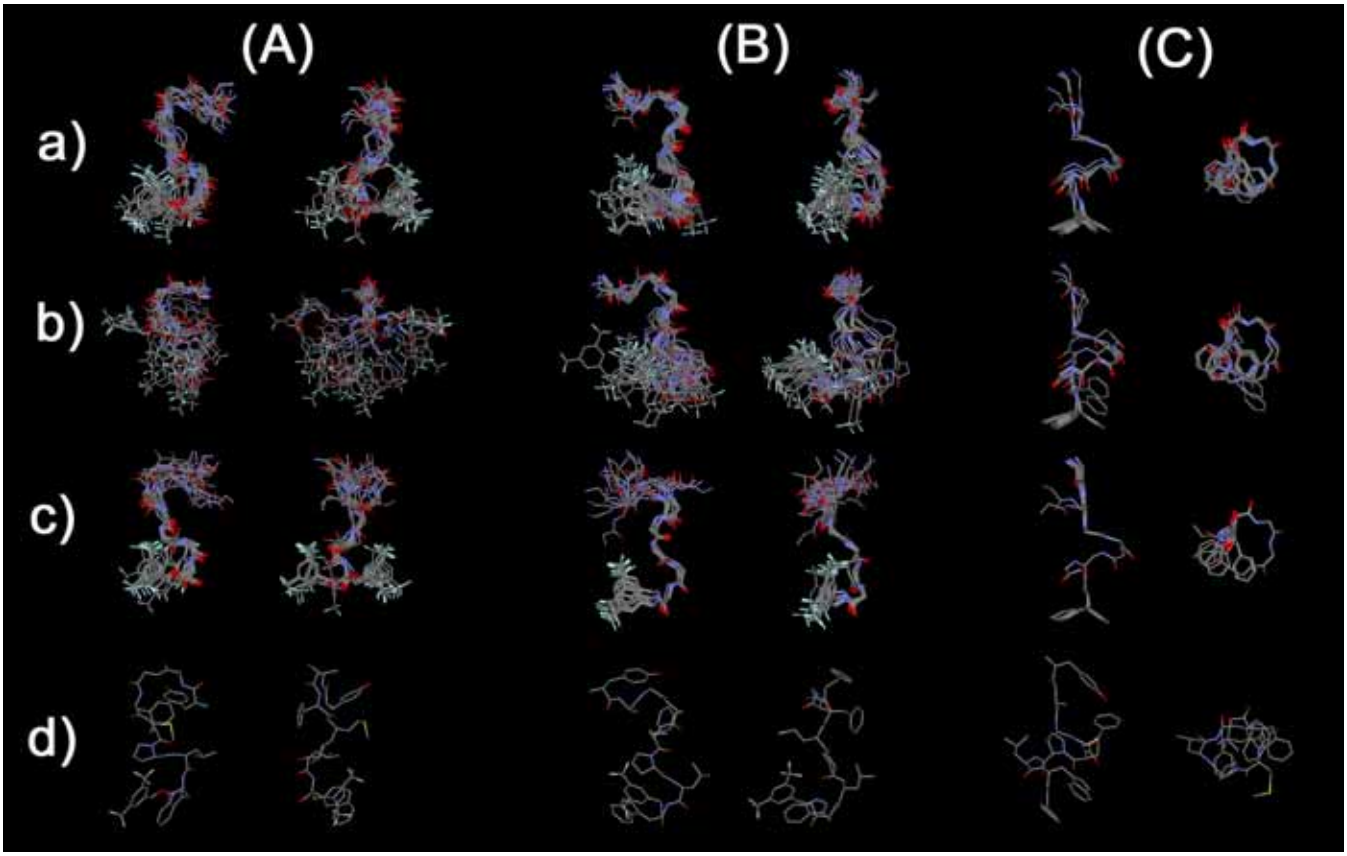

Figure 3.2.5. Ensembles of the best 20 calculated structures in 40-fold DPC micelle / pH 4.5 buffer for (A) **TY005**, (B) **TY027** and (C) **TY025** with the lowest restraint energy, aligned on backbone atoms of residues (a) 1-8 ,(b) 1-4 and (c) 5-8, from *N*-terminal (up in the left image) to *C*-terminal (down). Only backbone atoms with the *C*-terminal benzyl moiety were illustrated in (a), (b) and (c) for easier comparison, and the most stable conformers (d) are shown with all non-hydrogen atoms.

In Met-Enkephalin (Tyr^1-Gly^2-Gly^3-Phe^4-Met^5-OH) and Leu-Enkephalin (Tyr^1-Gly^2-Gly^3-Phe^4-Leu^5-OH), which form the basis for the design of the *N*-terminal portion of peptide sequence of **TY005**, **TY027** and **TY025**, a *β*-turn structure was often found between Tyr^1 and Phe^4 by several methods including X-ray crystallography and NMR spectroscopy in the environments which mimic the membrane bilayer.[182, 183] In the cases of peptide derivatives **TY005** and **TY027**, a distance of less than 7 Å between the C_α of D-Ala^2 and the C_α of Met^5 was observed in 15 of the best 20 structures for **TY005**, and in all 20 structures for **TY027**, whereas the *β*-turn between Tyr^1 and Phe^4 was found only 5

and 3 structures in the best 20 structures of **TY005** and **TY027**, respectively (Table 3.2.2).[184] This result implied the existence of an alternative *β*-turn in the residues 2 to 5 for both **TY005** and **TY027**, and all of them were classified as Type IV ("distorted") *β*-turn by their backbone dihedral angles. A second *β*-turn structure was found from Pro^6 to the *C*-terminal benzyl moiety (residue 9) in which the distance between the $C_\alpha(Pro^6)$ and the benzylic carbon (CH_2) of the *C*-terminus was less than 7 Å in 17 and 19 of the best 20 structures for **TY005** and **TY027**, respectively (Table 3.2.2). For peptide derivative **TY027**, 6 of 19 turns found in **TY027** were classified as Type I *β*-turns, and a hydrogen bond between the H^N of residue 9 and the carbonyl oxygen atom in Pro^6 was observed in 9 of the 19 (Table 3.2.3), The *C*-terminal ester (**TY005**) showed only distorted *β*-turns in this region, with no hydrogen bonds, consistent with the larger backbone rmsd observed for *C*-terminal half (0.75 Å vs 0.45 Å for **TY027**). These implied that the secondary structure elements were consistent with the observed NOE connectivities (Figure 3.2.4).

Table 3.2.1. Structural statistics

Compound	**TY005**		**TY027**		**TY025**	
	final 20 structures	most stable structure	final 20 structures	most stable structure	final 20 structures	most stable structure
rmsd from NOE dist restraints (Å)[a]	0.025 ± 0.004	0.028	0.027 ± 0.004	0.016	0.016 ± 0.001	0.016
rmsd from backbone φ angle restraints (deg)[b]	-[c]	-[c]	-[c]	-[c]	0.0 ± 0.0	0.0
NOE dist restraints violations						
> 0.01 Å	13.9 ± 2.5	11	14.6 ± 1.5	14	14.2 ± 1.1	15
> 0.1 Å	2.5 ± 1.4	3	3.9 ± 1.2	3	1.0 ± 0.0	1
max dist violations (Å)	0.17 ± 0.04	0.22	0.16 ± 0.02	0.13	0.11 ± 0.00	0.12
dihedral backbone angle violations						
> 0.1°	-[c]	-[c]	-[c]	-[c]	0 ± 0	0
> 1°	-[c]	-[c]	-[c]	-[c]	0 ± 0	0
max dihdral violations (deg)	-[c]	-[c]	-[c]	-[c]	0 ± 0	0
rms deviation from ideal geometry[d]						
bond length (Å)[e]	0.0061 ± 0.0004	0.0063	0.0052 ±0.0002	0.0052	0.0035 ± 0.00004	0.0035
bond valence angles (deg)[f]	2.14 ± 0.11	2.16	1.78 ± 0.05	1.72	1.25 ± 0.003	1.25
out-of-plane angles (deg)[g]	3.57 ± 0.63	3.25	2.73 ± 0.40	2.90	1.54 ± 0.09	1.45
AMBER energies (kcal mol^{-1})			9.08			
restraint[h]	2.48 ± 0.67	2.78	2.95 ± 0.58	2.41	1.13 ± 0.07	1.20
bond stretching	2.07 ± 0.22	2.20	1.42 ± 0.08	1.40	1.68 ± 0.02	1.70
bond angles	19.28 ± 1.84	19.49	12.8 ± 0.8	11.89	14.28 ± 0.22	14.00
dihedral angles	12.24 ± 1.9	9.54	9.57 ± 1.61	7.99	14.52 ± 0.38	14.53
planarity	1.63 ± 1.11	1.15	0.74 ± 0.33	0.61	0.19 ± 0.03	0.17
van der Waals[i]	–11.65 ± 3.1	–12.61	–12.23 ± 1.4	–13.80	–17.4 ± 0.75	–18.41
electrostatic[j]	–9.6 ± 0.91	–9.93	–11.5 ± 0.68	–11.84	–9.59 ± 0.41	–9.82
Total	13.25 ± 2.12	9.08	–0.01 ± 2.25	–4.44	3.14 ± 0.78	1.61

Table 3.2.1. Structural statistics (continued)

atomic rmsd (Å): final 19 structures v.s. most stable structure	**TY005**		**TY027**		**TY025**	
	backbone atoms (N, C^{α}, C')	all non-hydrogen atoms	backbone atoms (N, C^{α}, C')	all non-hydrogen atoms	backbone atoms (N, C^{α}, C')	all non-hydrogen atoms
Calculated on whole molecule	1.80 ± 0.47	2.72 ± 0.92	1.14 ± 0.43	2.09 ± 0.64	0.19 ± 0.20	0.84 ± 0.28
Calculated only on 1-4 res.	1.11 ± 0.54	2.49 ± 1.12	1.05 ± 0.63	2.16 ± 0.98	0.14 ± 0.30	0.32 ± 0.66
Calculated only on 5-8 res. and *C*-terminus	0.75 ± 0.26	1.82 ± 0.90	0.45 ± 0.38	1.02 ± 0.25	0.04 ± 0.01	0.76 ± 0.42

[a] The total number of NOE restraints were 136 for **TY005**, 155 for **TY027** and 184 for **TY025**, respectively. [b] Two backbone φ angle restraints were applied only on **3**. [c] no restraints used. [d] Derived from the rMD calculations using the AMBER force field in DISCOVER. [e] The number of bond length were 160 for **TY005**, 161 for **TY027** and 155 for **TY025**, respectively. [f] The number of bond valence angles were 285 for **TY005**, 287 for **TY027** and 275 for TY025, respectively. [g] The number of out-of-plane angles were 36 for **TY005**, 36 for **TY027** and 37 for **TY025**, respectively. [h] Calculated with force constants of 25 kcal mol^{-1} $Å^{-2}$ and 100 kcal mol^{-1} rad^{-2} for the NOE distance and dihedral angle restraints, respectively. [i] Calculated with the Lennard-Jones potential using the AMBER force field and a 12 Å cutoff. [j] Calculated with a distance-dependent dielectric constant ($\epsilon = 4r$).

Table 3.2.2. Number of structures with less than 7 Å distance between alpha carbons of *i* th and (*i* + 3) th residues.[a]

Residues	Tyr[1]-Phe[4]	DAla[2]-Met[5]	Gly[3]-Pro[6]	Met[5]-Trp[8]	Pro[6]-Bzl[9]
TY005	5	15	0	0	17
TY027	3	20	0	0	19
TY025[b]	0	2	20	20	18

[a] Out of the best 20 calculated structures. Bzl stands for the cross-peaks derived from the corresponding aromatic protons of benzyl moiety (residue 9). [b] Helical structure was found, in which no *β*-turn structures should not be defined according to the original definition. Ref. 184.

Table 3.2.3. Observed hydrogen bonds[a]

Molecule	No.[b]	Donor	Acceptor	Distance (Å)[c]	Angle (deg)[d]
TY005	14	Leu[7] H^N	Met[5] O	1.91 ± 0.07	141.1 ± 6.0
	9	Bzl[9] H^{Ne}	Pro[6] O	2.16 ± 0.11	158.5 ± 1.9
TY027	7	Gly[3] H^N	Tyr[1] O	2.05 ± 0.11	137.8 ± 8.1
	5	Trp[8] H^N	Met[5] O	2.04 ± 0.02	132.3 ± 1.1
TY025	No hydrogen bond observed				

[a] The hydrogen bonds which were observed in more than five structures were listed. [b] The number of structures of the final 20 for which the listed hydrogen bond is observed. [c] The distance is the mean proton-oxygen distance (± SD) in the structures for which a hydrogen bond is observed. [d] The angle is the mean N-H- - -O angle (± SD) in the structures for which a hydrogen bond is observed. [e] Amide proton of *C*-terminal benzyl moiety.

Comparing the tandem *β*-turn structures of **TY005** and **TY027**, the peptide with no trifluoromethyl groups in the *C*-terminus (**TY025**) showed significantly different structural properties. First, the backbone of **TY025** had a well-defined helical structure, consistent with the NOE connectivities and CSI values (Figure 3.2.5). It is noteworthy that not only the *C*-terminal half of **TY025**, but also its *N*-

terminus was found to be quite structured (Table 3.2.1). Thus, removal of two trifluoromethyl groups from the *C*-terminus led to a drastical conformational change for the whole molecules from tandem *β*-turn structures to a helical structure (Figure 3.2.5).

This well-defined structure of **TY025** was also confirmed by the Ramachandran plot and angular order parameters (Figure 3.2.6).[185] In the Ramachandran plot of **TY025**, only seven clear spots, corresponding to the respective residues 2-8, were found. Among them, only Gly^3 has positive *φ* angles in all of its 20 best structures. On the other hand, the corresponding Ramachandran plots for **TY005** and **TY027** showed more scattered views together with the positive *φ* angles for Gly^3 (10 structures in **TY005** and 3 structures in **TY027**), Phe^4 (3 structures in **TY005**), Met^5 (13 structures in **TY005** and 20 structures in **TY027**) and Leu^7 (1 structures in **TY005** and 6 structures in **TY027**) in the seven *L*-amino acids and some of *D*-Ala^2 (3 structures in **TY005** and 3 structures in **TY027**) have negative *φ* angles. It is interesting that Met^5 of **TY005** and **TY027,** located between two *β*-turns, had frequent positive *φ* angles. As for the angular order parameters, both the parameters for *φ* and *ψ* angles in **TY025** were close to 1 in all the residues, whereas **TY005** and **TY027** had smaller values in some residues, implying a better-defined structure for **TY025** than for **TY005** and **TY027**, especially in the *N*-terminus where no structural modification was made.

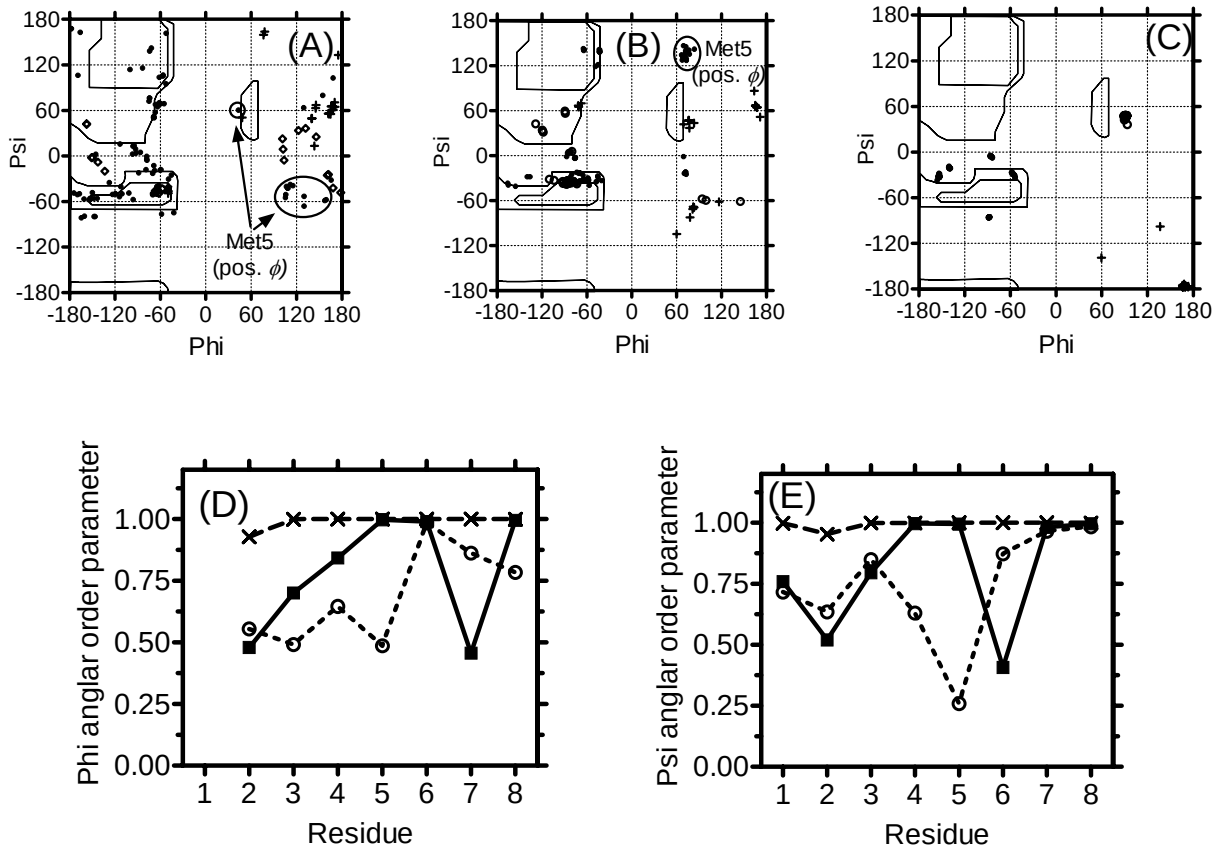

Figure 3.2.6. The *D*-Ala[2] (crosses), Gly[3] (open circle) and Met[5] with positive φ angles (circled) were indicated in the Ramachandran φ,ψ plots for (A) **TY005**, (B) **TY027** and (C) **TY025** for residues 2-7 of 20 final structures. Angular order parameters for φ (D) and ψ (E) angles calculated from the 20 final structures for **TY005** (open circles), **TY027** (filled squares) and **TY025** (crosses). For calculating the ψ angles of Trp[8], Non-carbonyl oxygen atoms of the *C*-terminal ester (**TY005**) and nitrogen atoms of *C*-terminal amide (**TY027** and **TY025**) were used instead of N (i + 3), respectively.

Based on the NMR structural analysis, it is clear that the limited modifications at the *C*-terminal moiety gave rise to several changes in the conformations of the peptide derivatives **TY005**, **TY027** and **TY025** in the presence of membrane-like DPC micelles. The change of ester (**TY005**) into amide (**TY027**) resulted in a better-defined conformation especially in the *C*-terminal portion of the peptide, and a more rigid β-turn structural element with intramolecular hydrogen bonds was found for residues

6-9 of **TY027**. The removal of the trifluoromethyl groups from the *C*-terminus of **TY027** (**TY025**) induced much larger changes in the three-dimensional structures which changed from a tandem β-turn (**TY005** and **TY027**) to a structured helical conformation, implying a large influence of trifluoromethyl groups on the conformations of the entire molecules in the lipid environment. Since the structural modifications were limited only to the *C*-terminus, it is not clear how simple electrostatic or steric changes of these modifications affects the conformations of the entire molecule. Because the molar ratios of **TY005**, **TY27** and **TY025** were low compared to DPC, they presumably form complexes with lipid molecules and thus induce perturbations in the interaction between the compound and micelles due to their unique *C*-terminus. It might be suggested that the highly lipophilic and electronegative trifluoromethyl groups induced such a perturbation, if these trifluoromethyl groups interact with the core of micelles which mostly consists of lipophilic and electrostatically neutral hydrocarbon chains. The ester-to-amide substitution, in which the oxygen atom (hydrogen-bond acceptor) was replaced to the nitrogen with a proton to be a hydrogen-bond donor, also can introduce some changes in the interactive mode between these compounds and membrane-like micelles. Therefore, the interaction of compound with DPC micelles might be compound-specific which is consistent with the different three-dimensional molecular structures of each compound. In order to confirm these implications, further NMR experiments using paramagnetic agents as well as fluorescence experiments were performed to estimate such differences in the membrane-compound interactions.

3.2.2.3. Fluorescence Study

It is well known that the intrinsic fluorescence spectrum of the indole ring in tryptophan shifts to shorter wavelength ("blue shifted") as the polarity of the solvent surrounding the tryptophan residue decreases, and this blue shift is a good index to monitor the lipophilicity of the environment close to the tryptophan.[186, 187] The fluorescence of Trp^8 in **TY005**, **TY27** and **TY025** was measured in the presence

and absence of DPC micelles, in order to examine the interaction between the peptides and membrane-like micelles. The fluorescence spectra in DPC micelles were compared to the spectra in the EtOH-buffer solution (EtOH : pH 7.4 HEPES buffer = 1 : 1), which was chosen as the standard since the solubilities of the peptide derivatives **TY005**, **TY27** and **TY025** in aqueous media were too low to run the experiment (Table 3.2.4).[188] The emission spectra were obtained by excitation at 290 nm to avoid excitement of the tyrosine residue.

Obvious blue shifts of fluorescence spectra from the standard solution were observed in all three peptide derivatives (6 nm, **TY005**; 10 nm, **TY027**; 10 nm, **TY025**, respectively, Figure 3.2.7), implying that the indole ring in Trp^8 at the *C*-terminal of all peptides was buried inside the micelles, and that the peptides have strong interactions with the lipophilic core of the micelles, at least in the *C*-terminus.

Because poorly water-soluble peptides **TY005**, **TY27** and **TY025** were easily dissolved at millimolar concentration in the presence of micelles, strong interactions between the peptide derivatives **TY005**, **TY27** and **TY025** and micelles were also suggested (Table 3.2.4). Among compounds **TY005**, **TY27** and **TY025**, **TY005** showed a smaller blue-shift than **TY027** and **TY025**, suggesting that the surroundings near the indole ring of Trp^8 in *C*-terminal ester (**TY005**) were less lipophilic than was the case for the *C*-terminal amides (**TY027** and **TY025)**, both of which had better-defined structures in DPC micelles than **TY005** (Table 3.2.1). Therfore, the lipophilicity near Trp^8 was mostly influenced by ester-amide substitution rather than the removal of trifluoromethyl groups, and the lipophilic environment at the *C*-terminus might have some responsibility for the structured conformations of the peptide derivatives.

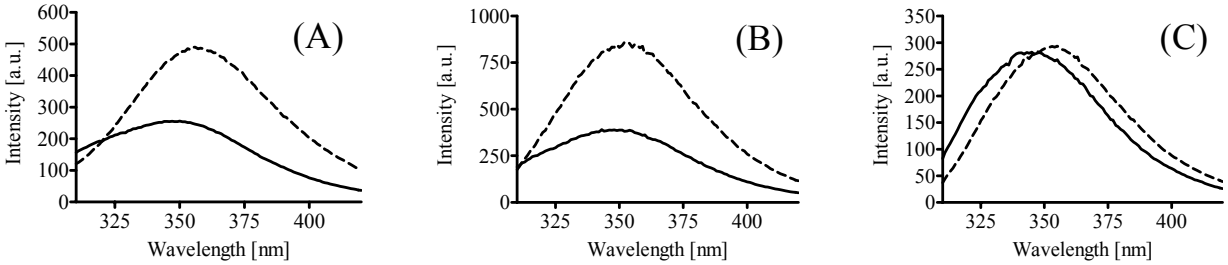

Figure 3.2.7. Fluorescence spectra of (A) **TY005** (B) **TY027** (C) **TY025**: the spectra were recorded at 500 μg/mL at 290 nm excitation in 40-fold DPC micelle / pH 7.4 HEPES buffer (solid line) or EtOH : pH 7.4 HEPES buffer = 1 : 1 solution (broken line).

Table 3.2.4. Solubility and lipophilicity of peptide derivatives

No	lipophilicity		Solubility[c] (μg/ml)
	$logD_{7.4}$[a]	AlogP[b]	
TY005	> 4.0	5.74	< 0.2
TY027	> 4.0	5.45	< 0.2
TY025	3.6	3.97	1.1

[a] Logarithm of octanol/saline distribution coefficient in 0.05 M HEPES buffer in 0.1 M NaCl solution. [b] Calculated with ALOGPS 2.1 software. See references [189, 190]. [c] solubility in 0.05 M HEPES buffer in 0.1 M NaCl solution.

3.2.2.4. Paramagnetic Broadening Studies on ^{1}H NMR.

To obtain further information about the interaction between peptide derivatives **TY005**, **TY27** and **TY025** and DPC micelles, a nitroxyl spin-label, 5-doxylstearic acid (5-DOXYL), and Mn^{2+} ions ($MnCl_2$) were used to induce selective broadening of NMR resonances close to the paramagnetic probes.[49, 191] The cross-peaks of protons exposed to an aqueous exterior are broadened or disappear due to the paramagnetic effect of Mn^{2+}, while cross-peaks of protons located inside the micelles and close to the phosphate groups of DPC are broadened by the free radical on the doxyl group, which is bound

to carbon 5 of the stearic acid.[21] The paramagnetic effects of these agents on the peptide resonances were studied by comparing TOCSY spectra in the presence and absence of the paramagnetic agents, and all peaks were classified into three categories according to their sensitivities to the paramagnetic agents: missed by 5-DOXYL only (in the micelle, but not deeply buried); missed by both Mn^{2+} and 5-DOXYL (the proton is at or near the surface of micelles) and preserved by either agent (deeply buried in the micelle) (Figure 3.2.8). In fact, none of the ^{1}H resonances were missed by Mn^{2+} only, indicating a strong association with the micelle for all three derivatives.

For all three peptide derivatives **TY005**, **TY27**, and **TY025**, nearly all of the H^{N} related cross-peaks were categorized as sensitive to both Mn^{2+} and 5-DOXYL, implying that the peptide backbones are located at or near the surface of micelles. On the other hand, most of the side-chain resonances were missed only by 5-DOXYL or were non-sensitive to either agent. Thus, generally, the backbones of **TY005**, **TY27**, and **TY025** lie close to the surface with their side-chains buried in the micelles. However, there is one notable exception to this general observation: the H^{N} resonances of Met^{5} in **TY005**, **TY27**, and **TY025** were affected only by 5-DOXYL, implying that the protons are not exposed to the surface of the micelles. Moreover, the side-chain cross-peaks of Met^{5} in only **TY005** were missed by either paramagnetic agent, indicating that Met^{5} side-chain of **TY005** was exposed to the surface of micelle, whereas those of **TY027** and **TY025** were sensitive only to 5-DOXYL, indicating a different orientation in the side-chain of Met^{5}.

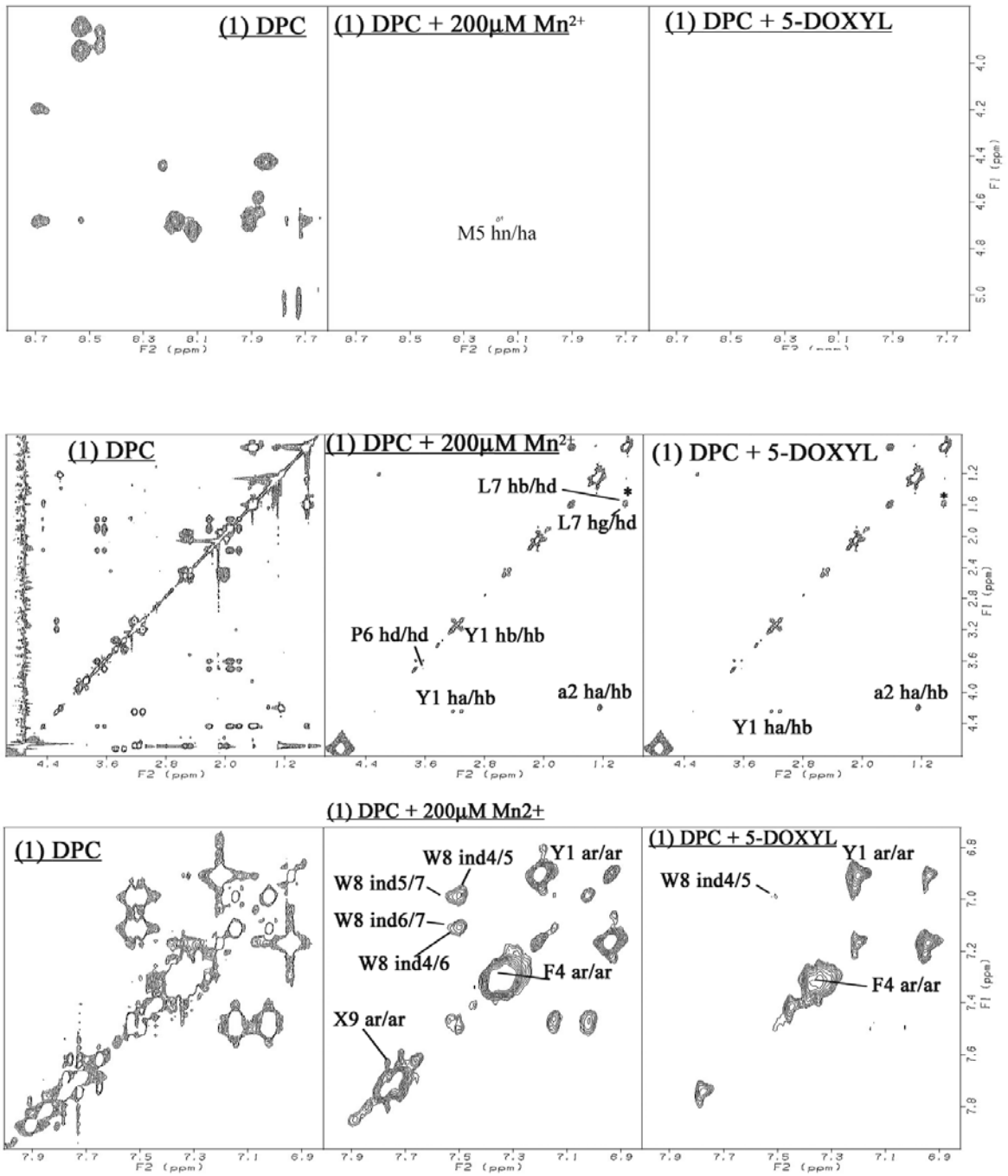

Figure 3.2.8A. Effect of Radicals on TOCSY Spectra. **TY005** with DPC micelles (left column), with 200 µM Mn^{2+} (middle) and 5-DOXYL stearic acid (right). Preserved resonances (labeled) are in a phase not missed by the phase-specific radical probe (Mn^{2+} or DOXYL). X9 represents the cross-peaks derived from the corresponding aromatic protons of benzyl moiety. The resonances with asterisk (*) are DPC or 5-DOXYL derived ones. Spectra were compared from the same noise level.

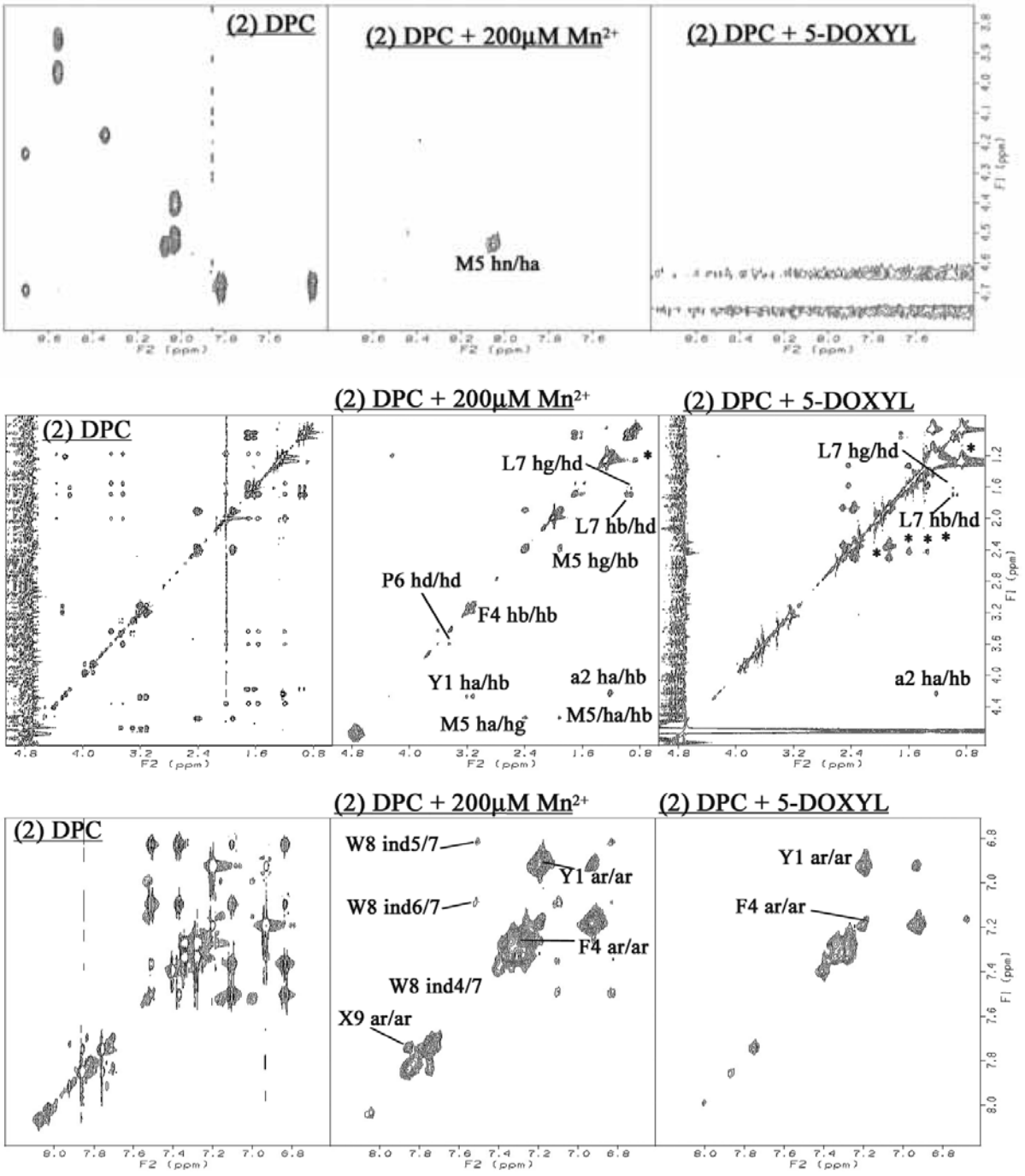

Figure 3.2.8B. Effect of Radicals on TOCSY Spectra. **TY027** with DPC micelles (left column), with 200 μM Mn^{2+} (middle) and 5-DOXYL stearic acid (right). Preserved resonances (labeled) are in a phase not missed by the phase-specific radical probe (Mn^{2+} or DOXYL). X9 represents the cross-peaks derived from the corresponding aromatic protons of benzyl moiety. The resonances with asterisk (*) are DPC or 5-DOXYL derived ones. Spectra were compared from the same noise level.

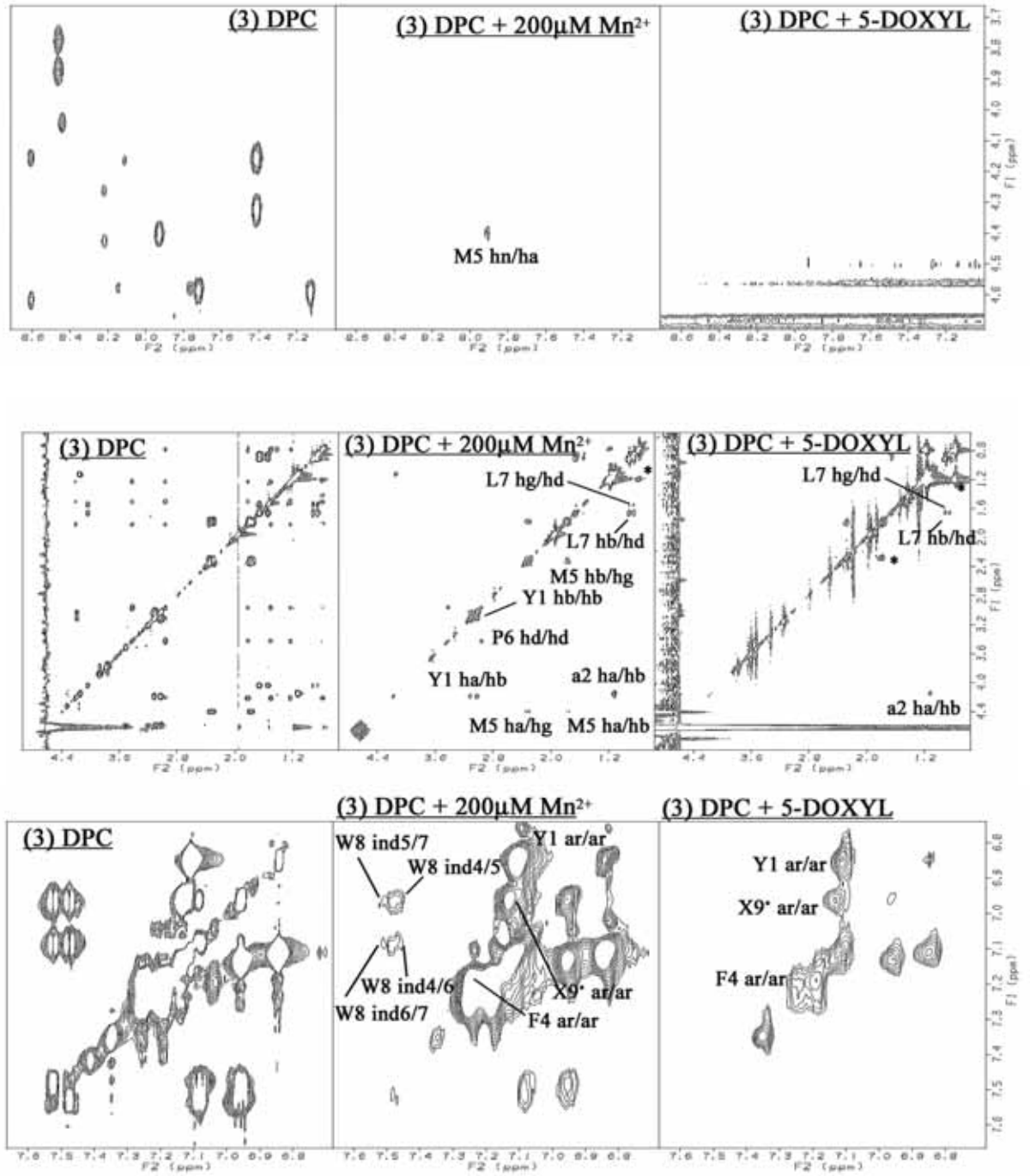

Figure 3.2.8C. Effect of Radicals on TOCSY Spectra. **TY025** with DPC micelles (left column), with 200 μM Mn^{2+} (middle) and 5-DOXYL stearic acid (right). Preserved resonances (labeled) are in a phase not missed by the phase-specific radical probe (Mn^{2+} or DOXYL). X9 represents the cross-peaks derived from the corresponding aromatic protons of benzyl moiety. The resonances with asterisk (*) are DPC or 5-DOXYL derived ones. Spectra were compared from the same noise level.

The sensitivity of side-chain protons to broadening by 5-DOXYL provides insight into their portioning in depth in the micelles. The cross-peaks of two different aromatic protons (*para* and *ortho*) in the *C*-terminal benzyl moiety were eliminated in **TY005** and **TY027** by 5-DOXYL, but the resonance of **TY025** were preserved in spite of the hydrophobic trifluoromethyl group in **TY005** and **TY027**. On the other hand, the cross-peaks of the aromatic protons of Trp^8 were unaffected in **TY005**, but were sensitive to 5-DOXYL for **TY027** and **TY025**. Therefore, the *C*-terminal benzyl moiety (**TY005** and **TY027**) and Trp^8 (**TY027** and **TY025**) appear to be located close to the phosphate moiety of DPC micelles, but the Trp^8 of **TY005** and the *C*-terminus of **TY025** were rather deeply buried into the micelles.

The important implication from these paramagnetic experiments was that all the compounds **TY005, TY27** and **TY025** showed different orientations at each *C*-terminus in DPC micelles. Thus, both of the modifications, the ester-to-amide substitution and the removal of trifluoromethyl groups, was shown to change the interaction between compound and membrane-like micelles, as suggested from the NMR conformations of **TY005, TY027** and **TY025**.

3.2.2.5. The Relationships of Molecular Conformation in DPC Micelles and Biological Activities.

Finally, in order to evaluate the biological influences of three-dimensional molecular structures in the presence of membrane-mimicking micelles and compound-micelles interactions, the relevance of the bioactivities of peptide derivatives to the obtained conformations was examined.

One important change due to the substitution of *C*-terminal ester in **TY005** for an amide (**TY027**) gave rise to increased species difference at the human and rat NK1 receptors (Table 3.1.2). This substitution changed hydrogen-bonding interactions and planarity of the *C*-terminus which might induce a conformational change in the lipidic surroundings as found in the NMR conformations (Figure 3.2.5). The summation of these changes could explain the activity shifts at the NK1 receptors. As found

in the comparison of **TY027** and **TY025**, the existence of two trifluoromethyl groups at the *C*-terminus plays an important role in the affinities for both rNK1 and hNK1 receptors (Table 3.1.2). Since the 3,5-dimethyl-substituted analogue of L-732,138 (L-708,568) was reported to have 16-fold reduced affinity for the human NK1 receptor as compared to L-732,138,[41] one good explanation of the influence by trifluoromethyl introduction was that the electronegative phenyl ring at the *C*-terminus might be preferred by NK1 receptors.[146] Another possibility is that the induced conformational changes to a well-defined helical structure due to the trifluoromethyl groups interfered with the binding of the compound at the NK1 receptor.

For the δ and μ opioid agonist activities, **TY027** showed 24-fold δ selectivity, as expected from the existence of Met[5],[136] with four-fold higher affinity at the hDOR and two times higher affinity at the rMOR than **TY005.** It is interesting that the modification was made only in the *C*-terminus, which is far from the opioid agonist pharmacophore, but large shift in the opioid activities were observed (Table 3.1.2).

It should be noted again that **TY027**, which had the better-defined conformation in DPC micelles than **TY005**, showed increased opioid activities, although the primary sequences for opioid agonist pharmacophore were exactly the same for both of **TY005** and **TY027** (Figure 3.2.2). Moreover, the elimination of two trifluoromethyl groups (**TY027** to **TY025**) led to further increased affinity at both the DOR and the MOR with 4.1-fold δ-selectivity, although this compound also had the same sequence for opioid pharmacophore at the *N*-terminus. As discussed above, **TY025** had a structured helical conformation in DPC micelles, whereas **TY005** and **TY027** showed β-rich conformations. Furthermore, the interactions between the compounds and the membranes were found different for compounds **TY005**, **TY027** and **TY025**.

3.2.3. Summary of the Section

The results in this section show that even small and limited structural modification in the ligand could induce relatively large changes in their three-dimensional molecular structures from a *β*-structure to a helical conformation in membrane-mimicking DPC micelles, together with significantly shifted biological activities. In addition, the reported data suggest that the removal of trifluoromethyl groups from the *C*-terminus induced much larger changes in the three-dimensional conformations than the substitution of the ester to amide, implying a large influence of lipophilic and electronegative trifluoromethyl groups on the three-dimensional molecular structure in a lipid media. The important finding of this section is that the substituent in the *C*-terminus, especially a trifluoromethyl group, played a critical role in determining the three-dimensional molecular structure of the tested peptide derivatives in pseudo-membrane with the direct relevance to their observed bioactivities, suggesting the importance of their membrane-bound states in biological behaviors. These findings provide significant information regarding the nature of peptide drug-membrane interactions as well as the specific driving force to use three-dimensional molecular structures to manipulate bioactivities, both of which could be make an useful guide to new aspects of modern medicinal chemistry.

3.3. Experimental Section

3.3.1. Materials.

All amino acid derivatives, PyBOP and HOBt were purchased from EMD Biosciences (Madison, WI), Bachem (Torrance, CA), and Chem Impex International (Wood Dale, IL). Myo-[2-^{3}H(N)]-inositol; [Tyrosyl-3,5-^{3}H(N)] *D*-Ala^{2}-Mephe^{4}-glyol^{5}-enkephalin (DAMGO); [Tyrosyl-2,6-^{3}H(N)]-(2-*D*-Penicillamine, 5-*D*-Penicillamine) enkephalin (DPDPE); [^{3}H]-substance P; and [^{35}S]-guanosine 5`-(γ-thio) triphosphate (GTPγS) were purchased from Perkin Elmer (Wellesley, MA). Bovine serum albumin (BSA), protease inhibitors, Tris and other buffer reagents were obtained from Sigma (St. Louis, MO). Culture medium (MEM, DMEM and IMDM), Penicillin/ Streptomycin and fetal calf serum (FCS) were purchased from Invitrogen (Carlsbad, CA). Perdeuterated DPC was purchased from C/D/N Isotopes (Quebec, Canada). ACS grade organic solvents were purchased from VWR Scientific (West Chester, PA), and other reagents were obtained from Sigma-Aldrich (St. Louis, MO) and used as obtained.

3.3.2. Procedure for the Preparation of Peptide Derivatives Using Solution Phase Chemistry: TY001, 003, 004, 005, 006, 007, 018, 019, and 023.

H-Pro-Leu-Trp-O-3,5-Bzl(CF_3)$_2$·HCl. Boc-Pro-Leu-OH (2.05 g, 6.41 mmol) and H-Trp-O-3,5-Bzl(CF_3)$_2$·HCl (2.76 g, 6.41 mmol)[144, 145] were dissolved in DMF (20 mL). HOBt (865 mg, 7.69 mmol), PyBOP (3.33 g, 7.69 mmol) and NMM (1.42 g, 14.1 mmol) were added to the solution at 0°C. After stirring overnight at room temperature, saturated aqueous sodium bicarbonate was added to the solution and most of the organic solvent was removed under reduced pressure. The residue was extracted with ethyl acetate three times followed by washing with saturated aqueous sodium chloride. The solution was dried over anhydrous sodium sulfate. The solvent was evaporated and the crude

peptide was precipitated in cold petroleum ether, centrifuged and dried under reduced pressure. The obtained solid was dissolved in 4 M HCl in 1,4-dioxane (5 mL) at 0°C. After stirring for 1h at r.t., the solution was concentrated under vacuum. Saturated aqueous sodium bicarbonate was added to the residue and extracted with ethyl acetate three times followed by washing the combined solution with saturated aqueous sodium chloride. The solution was dried over anhydrous sodium sulfate and concentrated under reduced pressure. The obtained residue was purified chromatography by silica gel (DCM : MeOH = 100 : 2 to 100 : 10). The residue was dissolved in dichloromethane (10 mL) and 4 M HCl in 1,4-dioxane (3 mL) was added at 0°C. The precipitate was centrifuged, dried under reduced pressure to obtain the title compound (2.40 g, 55.4%).

^{1}H-NMR (DMSO-d_6) δ: 0.78(3H, d, *J*=5.5 Hz), 0.81(3H, d, *J*=5.5 Hz), 1.33-1.42(2H, m), 1.50-1.60(1H, m), 1.65-1.73(1H, m), 1.74-1.89(2H, m), 2.16-2.27(1H, m), 3.10-3.26(4H, m), 4.10-4.20(1H, m), 4.40(1H, dd, *J*=7.5, 15.5 Hz), 4.58(1H, dd, *J*=7.0, 14.5 Hz), 5.16(1H, d, *J*=13.5 Hz), 5.24(1H, *d*, J=13.5 Hz), 6.96(1H, dd, *J*=7.5, 7.5 Hz), 7.05(1H, dd, *J*=7.5, 7.5 Hz), 7.20(1H, s), 7.33(1H, d, *J*=8.5 Hz), 7.47(1H, d, *J*=8.0 Hz), 7.96(2H, s), 8.07(1H, s), 8.46(1H, bs), 8.60-8.68(2H, m), 9.98(1H, bs), 10.93(1H, s).: MS (ESI) 641 $(MH)^+$

H-Tyr-*D*-Ala-Gly-Phe-Xxx-Pro-Leu-Trp-O-3,5-Bzl(CF_3)$_2$·TFA (Xxx = Phe, D-Phe, Gly, Leu, Met, Met(O), Nle, N-Me-Nle or a covalent bond). H-Pro-Leu-Trp-O-3,5-Bzl(CF_3)$_2$·HCl was coupled stepwise with 1.1 eq of Boc-Xxx-OH, Boc-Phe-OH, and Boc-Tyr-*D*-Ala-Gly-OH using the standard PyBOP/HOBt procedure to afford crude H-Tyr-*D*-Ala-Gly-Phe-Xxx-Pro-Leu-Trp-O-3,5-Bzl(CF_3)$_2$·TFA. In every coupling, PyBOP (1.2 eq), HOBt (1.2 eq), and NMM (2.2 eq) were used in DMF. After the coupling was completed, saturated aqueous sodium bicarbonate was added to the solution and most of the organic solvent was removed under reduced pressure. The residue was extracted with ethyl acetate three times followed by washing with saturated aqueous sodium chloride. The solution was dried over sodium sulfate. The solvent was evaporated and the crude peptide was

precipitated in cold ether or cold petroleum ether, centrifuged and dried under reduced pressure. The obtained N^{α}-Boc-protected peptide was treated with 4 M HCl in 1,4-dioxane (for Boc-Xxx-OH and Boc-Phe-OH) or TFA (for Boc-Tyr-*D*-Ala-Gly-OH). After the deprotection was completed, the solution was concentrated and the crude peptide was precipitated in cold ether, centrifuged and dried under reduced pressure. The yields of obtained crude peptides through these couplings were as follows: H-Tyr-*D*-Ala-Gly-Phe-Pro-Leu-Trp-O-3,5-Bzl$(CF_3)_2$·TFA (TY001), 61%; H-Tyr-*D*-Ala-Gly-Phe-Phe-Pro-Leu-Trp-O-3,5-Bzl$(CF_3)_2$·TFA (TY003), 96%; H-Tyr-*D*-Ala-Gly-Phe-Leu-Pro-Leu-Trp-O-3,5-Bzl$(CF_3)_2$·TFA (TY004), 63%; H-Tyr-*D*-Ala-Gly-Phe-Met-Pro-Leu-Trp-O-3,5-Bzl$(CF_3)_2$·TFA (TY005), 61%; H-Tyr-*D*-Ala-Gly-Phe-Gly-Pro-Leu-Trp-O-3,5-Bzl$(CF_3)_2$·TFA (TY006), 66%; H-Tyr-*D*-Ala-Gly-Phe-*D*-Phe-Pro-Leu-Trp-O-3,5-Bzl$(CF_3)_2$·TFA (TY007), 60%; H-Tyr-*D*-Ala-Gly-Phe-Nle-Pro-Leu-Trp-O-3,5-Bzl$(CF_3)_2$·TFA (TY018), 55%; H-Tyr-*D*-Ala-Gly-Phe-*N*-Me-Nle-Pro-Leu-Trp-O-3,5-Bzl$(CF_3)_2$·TFA (TY019), 49%; H-Tyr-*D*-Ala-Gly-Phe-Met(O)-Pro-Leu-Trp-O-3,5-Bzl$(CF_3)_2$·TFA (TY023), 67%. Pure peptides were obtained following RP-HPLC purification, then lyophilized.

3.3.3. Procedure for the Preparation of Peptide Derivatives Using Solid Phase Chemistry on 2-Chlorotrityl Resin: TY001, 005, 008, 010, 011, 012, 013, and 018.

H-Tyr-*D*-Ala-Gly-Phe-Xxx-Pro-Leu-Trp-Y-3,5-Bzl$(R)_2$·TFA (Xxx = Met, Nle or a covalent bond; Y = O, NH or NMe; R = H or CF_3).

Boc-Tyr(tBu)-*D*-Ala-Gly-Phe-Pro-Leu-Trp(Boc)-OH. The peptide was synthesized manually by the N^{α}-Fmoc solid-phase methodology using HCTU as the coupling reagents. 2-Chlorotrityl resin (2.0 g, 1.56 mmol/g) was placed into a 50 mL polypropylene syringe with the frit on the bottom and swollen in DMF (20 mL) for 1 h. The resin was washed with DMF (3 x 15 mL) and then with DCM (3 x 15 mL). Fmoc-Trp(Boc)-OH (1.2 equiv) was dissolved in 30 mL of DCM, and then DIEA (5 equiv)

was added. The reaction mixture was transferred into the syringe with the resin, then shaken for 2 h. The resin was washed three times with DMF (15 mL) and three times with DCM (15 mL), and then with DMF (3 x 15 mL). The Fmoc protecting group was removed by 20% piperidine in DMF (1 x 2 min and 1 x 20 min). The deprotected resin was washed with DMF (3 x 15 mL), DCM (3 x 15 mL) and then with DMF (3 x 15 mL). Fmoc-Leu-OH (3 equiv) and HCTU (2.9 equiv) were dissolved in 30 mL of DMF, then DIEA (6 equiv) was added. The coupling mixture was transferred into the syringe with the resin, and then shaken for 2 h. All the other amino acids, Pro, Phe, Gly, *D*-Ala and Tyr were consecutively coupled using the procedure described above, using the TNBS test (all the amino acids except for Phe) or chloranil test (only for Phe) to check the extent of coupling. In case of a positive test result, the coupling was repeated until a negative test result was obtained. The resulting batch of the resin-bound protected Boc-Tyr(tBu)-*D*-Ala-Gly-Phe-Pro-Leu-Trp(Boc) was carefully washed with DMF (3 x 15 mL), DCM (3 x 15 mL), DMF (3 x 15 mL), and DCM (3 x 15 mL), and dried under vacuum. The dry resin was placed in 10 mL fritted polypropylene syringes and swollen with DCM for 1 h. The peptide was cleaved off the solid support with 1% v/v TFA in DCM (30 mL) for 30 min, and most of the organic solvent was removed under vacuum. The obtained crude peptide was precipitated out by the addition of chilled petroleum ether (45 mL) to give a white precipitate. The suspension was centrifuged for 20 min at 7000 rpm, and then the liquid was decanted off. The crude peptide was washed with petroleum ether (2 x 50 mL), and after the final centrifugation, the intermediate peptide was dried under vacuum (2 h) to obtain the title compound (1.99 g, 57.0%). The purity of the final products (99.8%) was checked by analytical RP-HPLC using a Hewlett Packard 1090m system (230 nm) on a reverse phase column (Vydac 218TP104 C-18 4.6 × 250 mm, 5 μm). The peptide was eluted with a linear gradient of aqueous CH_3CN/0.1% CF_3CO_2H (30-100% in 40 minutes) at a flow rate of 1.0 mL/min. The crude peptide was used for next reactions without further purification. MS (ESI) 1109 $(MH)^+$. The NMR data are found as a table at the end of this chapter.

Boc-Tyr(tBu)-*D*-Ala-Gly-Phe-Met-Pro-Leu-Trp(Boc)-OH. The title peptide was prepared using the same method as described for Boc-Tyr(tBu)-D-Ala-Gly-Phe-Pro-Leu-Trp(Boc)-OH. The yield of obtained crude peptide was 75% and the purity of the final crude products was 87% (RP-HPLC, 230 nm, Vydac 218TP104 C-18 4.6 × 250 mm, 5 μm). ^{1}H-NMR (one isomer was found in DMSO-d_6): 0.79(3H, d, *J*=6.6 Hz), 0.84(3H, d, *J*=6.6 Hz), 1.10(3H, d, *J*=6.6 Hz), 1.24(9H, s), 1.26(9H, s), 1.38-1.41(2H, m), 1.61(10H, s), 1.70-1.77(3H, m), 1.80-1.94(3H, m), 2.01(3H, s), 2.42-2.47(2H, m), 2.67(1H, d-d, *J*=3.6, 13.2 Hz), 2.75(1H, d-d, *J*=9.6, 13.8 Hz), 2.87(1H, d-d, *J*=4.2, 13.2 Hz), 2.94(1H, d-d, 2.4, 13.2 Hz), 3.04(1H, d-d, 8.4, 15.0 Hz), 3.14(1H, d-d, 4.8, 15.0 Hz), 3.48-3.53(1H, m), 3.54-3.63(2H, m), 3.68(1H, d-d, *J*=5.4, 16.8 Hz), 4.15(1H, d-d, *J*=6.0, 12.0 Hz), 4.20-4.30(2H, m), 4.32(1H, d-d, 3.6, 7.8 Hz), 4.48-4.55(2H, m), 4.58(1H, *J*=7.2, 14.4 Hz), 6.83(2H, d, *J*=7.8 Hz), 6.92(1H, d, *J*=8.4 Hz), 7.12(2H, d, *J*=7.8 Hz), 7.14-7.24(7H, m), 7.30(1H, t, *J*=7.8 Hz), 7.47(1H, s), 7.87-7.92(2H, m), 7.98-8.08(4H, m), 8.30(1H, d, *J*=7.2 Hz). MS (ESI): 1262 $(M+Na)^+$.

H-Tyr-*D*-Ala-Gly-Phe-Pro-Leu-Trp-O-3,5-Bzl(CF_3)$_2$·TFA (TY001). Boc-Tyr(tBu)-*D*-Ala-Gly-Phe-Pro-Leu-Trp(Boc)-OH (150 mg, 0.135 mmol) and 3,5-bis(trifluoromethyl)benzyl bromide (104 mg, 0.338 mmol) were dissolved in DMF (2 mL). Cesium carbonate (220 mg, 0.676mmol) was added to the solution at 0 ºC. After stirring for 2 h at r.t., saturated aqueous sodium bicarbonate (50 mL) was added to the solution, and extracted with ethyl acetate (30 mL) three times. The combined organic phases were washed with 5% aqueous citrate and saturated aqueous sodium chloride (50 mL each), and dried over sodium sulfate. The solvent was evaporated and the protected peptide was precipitated in cold petroleum ether (PE, 45 mL). The PE suspension was centrifuged for 20 min at 7000 rpm, and then the liquid was decanted off. The crude peptide was washed with petroleum ether (2 x 50 mL), and after the final centrifugation, the intermediate peptide was dried under vacuum. The obtained protected peptide was treated with 83% v/v TFA, 5% water, 5% thioanisole, 2.5% 1,2-ethanedithiol and 5% phenol (1.5 mL, 1 h). The crude peptide was precipitated out by the addition of chilled diethyl ether (45 mL) to give white precipitates. The suspension was centrifuged for 20 min at 7000 rpm, and then

the liquid was decanted. The crude peptides were washed with diethyl ether (2 x 45 mL), and after the final centrifugation, the peptides were dried under vacuum (2 h). The resulting white residues (116 mg, quantitative) were dissolved in 3: 1 mixture of acetonitrile and distilled water (5 mL), and the insoluble impurities were removed by passing the solutions through syringe filters (Gelman Laboratory, Ann Arbor, MI, Acrodisc 13 mm syringe filter with 0.45 μM PTFE membrane). Final purification was accomplished by preparative RP-HPLC, then lyophilized.

H-Tyr-*D*-Ala-Gly-Phe-Met-Pro-Leu-Trp-O-Bzl·TFA (TY005). The title peptide was prepared using the same method as described for H-Tyr-*D*-Ala-Gly-Phe-Pro-Leu-Trp-O-3,5-Bzl(CF_3)$_2$·TFA (TY001). The yield of obtained crude peptide was 95%.

H-Tyr-*D*-Ala-Gly-Phe-Pro-Leu-Trp-O-Bzl·TFA (TY011). The title peptide was prepared using the same method as described for H-Tyr-*D*-Ala-Gly-Phe-Pro-Leu-Trp-O-3,5-Bzl(CF_3)$_2$·TFA (TY001). The yield of obtained crude peptide was 98%.

H-Tyr-*D*-Ala-Gly-Phe-Nle-Pro-Leu-Trp-O-Bzl·TFA (TY018). The title peptide was prepared using the same method as described for H-Tyr-*D*-Ala-Gly-Phe-Pro-Leu-Trp-O-3,5-Bzl(CF_3)$_2$·TFA (TY001). The yield of obtained crude peptide was 98%.

H-Tyr-*D*-Ala-Gly-Phe-Pro-Leu-Trp-NH-Bzl·TFA (TY008). Boc-Tyr(tBu)-*D*-Ala-Gly-Phe-Pro-Leu-Trp(Boc)-OH (50 mg, 0.045 mmol) and Cl-HOBt (8.7 mg, 0.054 mmol) were dissolved in DMF (1 mL). Benzylamine (5.8 mg, 0.090 mmol) and EDC (10.4mg, 0.054 mmol) were added to the solution at room temperature and stirred until the starting material disappeared in TLC; then saturated aqueous sodium bicarbonate (50 mL) was added. The reaction mixture was extracted with ethyl acetate (30 mL) three times. The combined organic phases were washed with 5% aqueous citrate and saturated aqueous sodium chloride (50 mL each), then dried over sodium sulfate. The solvent was evaporated and the crude peptide was precipitated in cold petroleum ether (45 mL). The product was twice dispersed in cold petroleum ether, centrifuged and decanted, then dried under reduced pressure.

The obtained protected peptide was treated with 82.5% v/v TFA, 5% water, 5% thioanisole, 2.5% 1,2-ethanedithiol, and 5% phenol (1.5 mL, 1 h). The crude peptide was precipitated out by the addition of chilled diethyl ether (45 mL) to give a white precipitate. The resulting peptide suspensions were centrifuged for 20 min at 7000 rpm, and the liquid was decanted. The crude peptides were washed with diethyl ether (2 x 45 mL), and after a final centrifugation, the peptides were dried under vacuum (2 h). The resulting white residues (53 mg, quantitative) were dissolved in a 3 : 1 mixture of acetonitrile and distilled water (1 mL), and the insoluble impurities were removed by passing the solutions through syringe filters (Gelman Laboratory, Acrodisc 13 mm syringe filter with 0.45 μM PTFE membrane). Final purification was accomplished by preparative RP-HPLC. The pure title compound was obtained after lyophilization.

H-Tyr-*D*-Ala-Gly-Phe-Pro-Leu-Trp-NMe-Bzl·TFA (TY010). The title peptide was prepared using the same method as described for H-Tyr-*D*-Ala-Gly-Phe-Pro-Leu-Trp-NH-3,5-Bzl·TFA (TY008). The crude peptide was obtained quantitatively.

H-Tyr-*D*-Ala-Gly-Phe-Pro-Leu-Trp-NH-3,5-Bzl(CF_3)$_2$·TFA (TY012). The title peptide was prepared using the same method as described for H-Tyr-*D*-Ala-Gly-Phe-Pro-Leu-Trp-NH-3,5-Bzl·TFA (TY008). The yield of obtained crude peptides was 98%.

H-Tyr-*D*-Ala-Gly-Phe-Pro-Leu-Trp-NMe-3,5-Bzl(CF_3)$_2$·TFA (TY012). The title peptide was prepared using the same method as described for H-Tyr-*D*-Ala-Gly-Phe-Pro-Leu-Trp-NH-3,5-Bzl·TFA (TY008). The crude peptide was obtained quantitatively.

H-Tyr-*D*-Ala-Gly-Phe-Met-Pro-Leu-Trp-NH-3,5-Bzl(CF_3)$_2$·TFA (TY027). The title peptide was prepared using the same method as described for H-Tyr-*D*-Ala-Gly-Phe-Pro-Leu-Trp-NH-3,5-Bzl·TFA (TY008). The crude peptide was obtained quantitatively.

H-Tyr-*D*-Ala-Gly-Phe-Met-Pro-Leu-Trp-NH-Bzl·TFA (TY025). The title peptide was prepared using the same method as described for H-Tyr-*D*-Ala-Gly-Phe-Pro-Leu-Trp-NH-3,5-Bzl·TFA (TY008).

The crude peptide was obtained quantitatively.

3.3.4. Characterization of Peptides.

Coupling and deprotection reactions were monitored by TLC. Preparative RP-HPLC was performed on Waters Delta Prep 4000 with Vydac 218TP C-18 column (22 x 250mm, 10-15 μm, 42-57% of acetonitrile) or Waters XTerra C-18 column (19 x 250 mm, 10 μm, 40-60% of acetonitrile). The purified peptides were characterized by HRMS, TLC, analytical HPLC and ^{1}H-1D-NMR. Sequential assignment of proton resonances was achieved by 2D-TOCSY NMR experiments.[192] High-resolution mass spectra were taken in the positive ion mode using ESI methods at the University of Arizona Mass Spectrometry Facility. TLC was performed on aluminum sheets coated with a 0.2 mm layer of silica gel 60 F_{254} Merck using the following solvent systems: (1) $CHCl_3$: MeOH : AcOH = 90 : 10 : 3; (2) EtOAc : *n*-BuOH : water : AcOH = 5 : 3 : 1 : 1; and (3) *n*-BuOH : water : AcOH = 4 : 1 : 1. TLC chromatograms were visualized by UV light and by ninhydrin spray followed by heating (hot plate). Analytical HPLC was performed on a Hewlett Packard 1100 with Waters NOVA-Pak C-18 column (3.9 x 150 mm, 5 μm). ^{1}H-1D-NMR spectra were recorded on a Bruker DRX-500 spectrometer. 2D-TOCSY NMR spectra were performed on a Bruker DRX-600 spectrometer equipped with a 5mm Nalorac triple-resonance single-axis gradient probe. The NMR experiments were conducted in DMSO-d_6 solution at 298 K. Spectra were referenced to residual solvent protons as 2.49 ppm. The processing of NMR data was performed with the XwinNmr software (Bruker BioSpin, Fremont, CA) and the Felix 2000 package (Accelrys Inc., San Diego, CA). In TOCSY experiments, the TPPI mode[193] with MLEV-17 Mixing Sequence[194] were used with a mixing time of 62.2 ms, at a spin-lock field of 8.33 kHz. TOCSY spectra were acquired with 2k complex pairs in t_2 and 750 FIDs using a 90°-shifted sine-squared window function in both dimensions.

3.3.5. Cell Lines.

For opioid receptors, the cDNA for the human δ opioid receptor (DOR) was a gift from Dr. Brigitte Kieffer (IGBMC, Illkirch, France). The cDNA for the rat μ opioid receptor (MOR) was a gift from Dr. Huda Akil (University of Michigan, MI). Stable expression of the rat MOR (pCDNA3) and the human DOR (pCDNA3) in the neuroblastoma cell line, HN9.10 were achieved with the respective cDNAs by calcium phosphate precipitation followed by clonal selection in neomycin. Expression of the respective receptors was initially verified and the level of expression periodically monitored by radioligand saturation analysis (see below). All cells were maintained at 37˚C, with a 95% air/ 5% CO_2 humidified atmosphere in a Forma Scientific incubator in Dulbecco's modified Eagle's medium (DMEM) with 10% bovine serum albumin (BSA) and 100 U mL penicillin/100 μg mL streptomycin. *For the NK1 receptor,* the hNK1 and rNK1/CHO cell line were obtained from Dr. James Krause (University of Washington Medical School, St. Louis, MI). Expression of the receptor was verified as previously described by Krause.[195] All cells were maintained at a 37° C, 95% air and 5% CO_2, humidified atmosphere, in a Forma Scientific incubator in Ham'S F12 with 2.5 mM HEPES, 10% fetal bovine serum and 100 U mL penicillin/100 μg mL streptomycin/ 500 μg mL Geneticin.

3.3.6. Radioligand Labeled Binding Assays.

For opioid receptors, crude membranes were prepared as previously described[196] from the transfected cells that express the rat MOR (rMOR) or the human DOR (hDOR). The protein concentration of the membrane preparations was determined by the Lowry method and the membranes were stored at -80˚C until use. Membranes were resuspended in assay buffer (50 mM Tris, pH 7.4, containing 50 μg/mL bacitracin, 30 μM bestatin, 10 μM captopril, 100 μM phenylmethylsulfonylfluoride (PMSF), 1 mg/mL BSA). The dissociation constant (K_d) of tritiated [*D*-Ala^2, NMePhe^4, Gly^5-ol]-enkephalin ([^{3}H]DAMGO) at the rMOR and that of tritiated c[*D*-Pen^2, *D*-

Pen^5]-enkephalin ([^{3}H]DPDPE) at the hDOR were as previously described.[147] For competition analysis, ten concentrations of a test compound were each incubated, in duplicates, with 50 μg of membranes from rMOR or hDOR expressing cells and the Kd concentration of [^{3}H]DAMGO (1.0 nM, 50 Ci/mmol), or of [^{3}H]DPDPE (1.0 nM, 44 Ci/mmol), respectively. Naloxone (10 μM) was used to define the non-specific binding of the radioligands in all assays. . The samples were incubated in a shaking water bath at 25˚C for 3 hours, followed by rapid filtration through Whatman Grade GF/B filter paper (Gaithersburg, MD) pre-soaked in 1% polyethyleneimine, washed 4 times each with 2 mL of cold saline. *For the NK1 receptor,* competition binding assays for the NK1 receptor were carried out on crude membranes prepared from transfected CHO cells expressing the rat NK1 receptor. Ten concentrations of a test compound were each incubated, in duplicates, with 50-100 μg of membrane homogenate and 0.3 - 0.4 nM [^{3}H] substance P (135 Ci/mmol, Perkin Elmer) in 1 mL final volume of assay buffer (50 mM Tris, pH 7.4, containing 5 mM $MgCl_2$, 50 μg/mL bacitracin, 30 μM bestatin, 10 μM captopril, 100 μM phenylmethylsulfonyl fluoride (PMSF) at 25 °C for 20 min. Substance P at 10 μM was used to define the non-specific binding. Membrane concentrations used in the assay were within the tissue linearity range. The [^{3}H] substance P concentration was selected based on the saturation binding experiments which showed a high affinity binding with K_d = 0.16 ± 0.03 nM. The incubation times correspond to the binding equilibrium as determined from the kinetics experiments. The reaction was terminated by rapid filtration and washed as described above. The filter-bound radioactivity was measured by liquid scintillation counting (Beckman LS 6000SC). Log IC_{50} value for each test compound was determined from non-linear regression analysis of data collected from two independent experiments performed in duplicates (40 independent experimental values) using GraphPad Prizm 4 software (GraphPad, San Diego, CA). The inhibition constant, K_i, was calculated from the antilogarithmic IC_{50} value by the Cheng and Prusoff equation.

3.3.7. [^{35}S]GTPγS Binding Assay.

The method was carried out as previously described.[196] Membrane from transfected rMOR or hDOR cells (10 μg) in a final volume of 1 mL of reaction mix (50 mM Hepes, pH 7.4, 1 mM EDTA, 5 mM $MgCl_2$, 30 μM GDP, 1 mM dithiothreitol, 100 mM NaCl, 0.1 mM PMSF, 0.1% BSA, 0.1 nM [^{35}S]GTPγS) was incubated with various concentrations of the test drug for 90 min at 30 °C in a shaking water bath. Reactions were terminated by rapid filtration through Whatman GF/B filters (pre-soaked in water), followed by 4 washes with 4 mL of ice-cold wash buffer (50 mM Tris, 5 mM $MgCl_2$, 100 mM NaCl, pH 7.4). The radioactivity was determined by liquid scintillation counting as above. Basal level of [^{35}S]GTPγS binding was defined as the amount bound in the absence of any test drug. Non-specific binding was determined in the presence of 10 μM unlabeled GTPγS. Total binding was defined as the amount of radioactivity bound in the presence of test drug. The effect of the drug at each concentration on [^{35}S]GTPγS binding was calculated as a percentage by the following equation: [Total bound- Basal]/ [Basal - Non-specific]×100. Data were analyzed by non-linear least-squares regression analysis using GraphPad Prism4 using data collected from 2 independent experiments. The EC_{50} for a test drug is converted from the logarithmic EC_{50} value derived from the best fit curve, and the maximum stimulatory effect is expressed as E_{max} ± standard error

For both radioligand and [^{35}S]GTPγS binding, two independent experiments were adopted as the standard procedure for the initial evaluation of all compounds using cell lines, each compound typically on multiple receptor types, to determine both affinity and biological activity. These initial analyses were designed to identify trends of structure-activity relationship as rapidly as possible and were not intended for determining geometric mean values of K_i or EC_{50}. The data pooled from 2 independent experiments indicated that the data are reproducible.

3.3.8. Guinea Pig Isolated Ileum Assay.

The *in vitro* tissue bioassays were performed as described previously.[147, 148] Male Hartley guinea pigs under ether anesthesia were sacrificed by decapitation and a non-terminal portion of the ileum removed and the longitudinal muscle with myenteric plexus (LMMP) was carefully separated from the circular muscle as described previously.[197] These tissues were tied to gold chains with suture silk and mounted between platinum wire electrodes in 20 mL organ baths at a tension of 1 g and bathed in oxygenated (95:5 O_2:CO_2) Kreb's bicarbonate buffer at 37 °C and stimulated electrically (0.1 Hz, 0.4 msec duration) at supramaximal voltage. Following an equilibration period, compounds were added cumulatively to the bath in volumes of 14-60 μL until maximum inhibition was reached. A baseline PL-017 was constructed to determine tissue integrity and allow calculation of antagonist activity before opioid analogue testing began. If no agonist activity was observed at 1 μM, a repeat PL-017 dose-response curve was constructed to test for antagonist qualities.

All testings for substance P antagonist activities were performed in the presence of 1 μM naloxone to block opioid effects on the tissue. Two minutes after naloxone was added to the bath, the test peptide was added. Four minutes after naloxone was added, the test dose of substance P was added to the bath, the peak height was noted and the tissues were washed. Possible agonist activity of the analogue also was observed during this period. Testing was stopped at 1 mM concentrations of the test compound.

3.3.9. Mouse Isolated Vas Deferens (MVD) Assay.

The *in vitro* tissue bioassay was performed as described previously.[147, 148] Male ICR mice under ether anesthesia were sacrificed by cervical dislocation and the vasa deferentia was removed. Tissues were tied to gold chains with suture silk and mounted between platinum wire electrodes in 20 mL organ baths at a tension of 0.5 g and bathed in oxygenated (95:5 O_2:CO_2) magnesium free Kreb's

buffer at 37 °C and stimulated electrically (0.1 Hz, single pulses, 2.0 msec duration) at supramaximal voltage as previously described.[198] Following an equilibration period, compounds were added to the bath cumulatively in volumes of 14-60 μL until maximum inhibition was reached. Response to an IC_{50} dose of DPDPE (10 nM) was measured to determine tissue integrity before test compound testing.

3.3.10. Analysis of the GPI and MVD Assays.

For opioid data analysis, percentage inhibition was calculated using the average tissue contraction height for 1 min preceding the addition of the agonist divided by the contraction height 3 min after exposure to the dose of agonist. IC_{50} values represent the mean of not less than 4 tissues. IC_{50} and E_{max} estimates were determined by computerized nonlinear least-squares analysis (the pharmacological statistics package FlashCalc: Dr. Michael Ossipov, University of Arizona, Tucson, AZ). *For substance P data analysis*, the height of the maximum peak produced during the control substance P dose-response curve was used as a 100 % response and other values calculated as a percentage. *Ke* values represent the mean of not less than 4 tissues and determined by computerized nonlinear least-squares analysis (FlashCalc).

3.3.11. Experimental Procedure: *In Vivo* Determination of Antinociceptive Activities of Bifunctional Peptide TY005 (H-Tyr-*D*-Ala-Gly-Phe-Met-Pro-Leu-Trp-O-3,5-Bzl(CF_3)$_2$).

Male Sprague Dawley rats (200-225 g) were obtained and cared for under the University of Arizona IACUC standards. Food and water was available ad libitum. All preparations and testing were performed in accordance with the policies and recommendations of the International Association for the Study of Pain, National Institute of Health and Animal Care at the University of Arizona. *Intrathecal catheter implantation*: Rats were anesthetized using ketamine/xylazine 100 mg/kg i.p. and placed in a steriotaxic head holder. The cisternum magnum was exposed and an 8 mm catheter was

implanted, as described,[199] terminating in the lumbar region of the spinal chord. Animals were allowed to recover for 5 days. *Compound administration*: 5μL of each treatment was given followed 1 μL air bubble/ 9μL saline push. *Infrared thermal testing (IR, behavioral)*: Rats were allowed to acclimate within Plexiglas holders for baseline testing (pre- and post- nerve ligation/ exposure) for 20 minutes. A mobile radiant heat source was used to direct heat to the left hind paw. Paw withdrawal latencies were measured in seconds, with an automatic shutoff of the heat source at 33.8 seconds. On test days, animals were administered a treatment and tested with radiant heat, every 15 minutes after said administration. Paw withdrawal latencies were calculated and expressed as the Mean Withdrawal Latency ± SEM in Prism (by Graph Pad Prism4).

3.3.12. NMR Spectroscopy in DPC Amphipathic Media.[51, 52]

All NMR spectra were recorded on a Bruker DRX600 600 MHz spectrometer with 5 mm Nalorac triple-resonance single-axis gradient probe. The peptide concentration for the NMR experiments varied from 3.5 to 4 mM. The samples were prepared by dissolving the peptide in 0.5 mL of 45 mM sodium acetate-d_3 buffer (pH 4.5) containing 40 equivalents of dodecylphosphocholine-d_{38} and 1 mM sodium azide (90% H_2O/10% D_2O) followed by sonication for 5 min. Two-dimensional double quantum filtered correlation (DQF-COSY), nuclear Overhauser enhancement spectroscopy[200] (NOESY), and total correlation spectra[192] (TOCSY) were acquired using standard pulse sequences and processed using XwinNmr and Felix 2000 (Accelrys Inc, San Diego, CA). The mixing time for NOESY spectra was 450 ms. All 2D spectra were acquired in the TPPI mode with 2k or 1k complex data points in t_2 and 750 real data points in t_1, and the spectral processing used 90º-shifted sine bell window functions in both dimensions. For suppressing the H_2O signal, the 3-9-19 WATERGATE pulse sequence was used.[201] Experiments were conducted at 310 K, and referenced to the H_2O shift (4.631 ppm). Coupling constants ($^3J_{NH\text{-}H\alpha}$) were measured from 2D DQF-COSY spectra by analysis of the fingerprint region. The matrix rows of each of the upper and lower halves of a cross-peak were summed to give an

antiphase 1D spectrum, which was fitted using a 5-parameter Levenberg-Marquardt nonlinear least-squares protocol[202] to a general antiphase doublet. The analysis yielded two independent determinations of the J coupling and line width for each cross-peak, one from the upper half and one from the lower half, and the one with better fitted curve was used for structure calculations. Cross-peak volumes for determination of distance restraints were measured using the Felix 2000 software. In the radical experiment using Mn^{2+}, a stock solution of 5 mM $MnCl_2$ was prepared and added to the sample to achieve a total concentration of 200 μM in Mn^{2+}. The DPC micelles with 5-DOXYL stearic acid were prepared as the same procedure with about 1 mg mL^{-1} of 5-DOXYL stearic acid but sonicating for 30 min.

3.3.13. Conformational Structure Determination.

The methods used for structure calculations have been described previously.[51, 52] The volumes of the assigned cross-peaks in the 2D NOESY spectrum were converted into upper distance bounds of 3.0, 3.8, 4.8, or 5.8 Å. For overlapping cross-peaks, the distance categories was increased by one or two levels, depending on the qualitative estimate of the extent of overlap. Pseudoatoms were created for nonstereospecifically assigned methylene protons with a correction of 1.0 Å applied to their upper bound distances.[28] In addition to the distance constraints, φ dihedral angle constraints derived from $^3J_{HN\text{-}H\alpha}$ coupling constants were set to between −90 and 40° for $^3J_{HN\text{-}H\alpha} < 6$ Hz and to between −150 and −90° for $^3J_{HN\text{-}H\alpha} > 8$ Hz. Dihedral angle constraints of 180° ± 5° for peptide bonds (ω) were also used to maintain the planarity of these bonds.

Simulated annealing molecular dynamics analysis was done for all the peptides to obtain an ensemble of NMR structures using the NOE-derived distance constraints and dihedral angle (φ) constraints using the DGII[203] program within the software package Insight II 2000 (Accelrys Inc., San Diego, CA). Solvent was not explicitly included in the calculations. All the embedded structures

successfully passed the simulated annealing step and were minimized using the consistent valency force field (CVFF) (Accelrys Inc.). The 50 structures with the lowest penalty function were further refined by two rounds of restrained molecular dynamics (rMD) using the all-atom AMBER force field with additional parameters for fluorine atom,[204-207] using the standalone DISCOVER ver. 2.98 program (Accelrys Inc.). A 12.0 Å cutoff for nonbonded interactions and a distance-dependent dielectric constant (4*r*) were used. All amide bonds were constrained to *trans* conformation by a 100 kcal mol^{-1} rad^{-2} energy penalty. The distance constraints and dihedral angles (φ) constraints were applied with a force constant of 25 kcal mol^{-1} $Å^{-2}$ and 100 kcal mol^{-1} rad^{-2} were applied, respectively. After 100 steps of steepest descents minimization and 1000 steps of conjugate gradient minimization on the initial structures, an rMD equilibration at 500 K was performed for 1.5 ps, during which a scale factor of 0.1 was applied to the experimental restraint force constants. During the next 2 ps, full values of the experimental restraint force constants were applied. A further 1 ps rMD simulation was run at 500 K, and the system was then cooled to 0 K over 3 ps. After another 1 ps at 0 K, 100 cycles of steepest descents and 2000 steps of conjugate gradient minimization were performed. The final 20 structures with the lowest energies were used for the analysis. All calculations were performed on a Silicon Graphics Octane computer.

3.3.14. Fluorescence Emission Spectra.

The Fluorescence spectra were recorded on a Cary Eclipse fluorescence spectrometer (Varian, Darmstadt, Germany). Emission spectra were obtained by excitation at 290 nm and recorded in the wavelength range of 310-420 nm with continuous stirring at 25°C. A scan step was 1 nm and scan speed was 120 nm min^{-1}. Excitation and emission bandwidths were set at 5 and 10 nm, respectively. The peptide concentration was 500μM in HEPES buffer (10 mM HEPES, 150 mM NaCl, 1 mM NaN_3,

0.1 mM EDTA, pH = 7.40) with 40-fold DPC or standard solution (EtOH : HEPES buffer = 1 : 1).[188] At least two scans were accumulated and averaged for each spectrum.

3.3.15. Octanol/saline Distribution (logD7.4).[136]

HEPES buffer (0.05 M HEPES buffer in 0.1 M NaCl, pH 7.4, 500 μL) was added to 2 mg of peptide and mixed with 500 μL of 1-octanol. The sample was shaken at r.t. for 12 h to allow equilibrating. The sample was centrifuged at 6500 rpm in a VanGuard V6500 (GlaxoSmithKline, Research Triangle Park, NC) for 15 min. The layers were separated and each layer was centrifuged once again. The peptide concentrations in the obtained layers were analyzed by HPLC (30-70% of acetonitrile containing 0.1% TFA within 20 min and up to 95% within additional 5 min, 1 mL/min, 230 nm, Vydac 218TP104 C-18 column). The logarithm of 1-octanol / saline distribution ($logD_{7.4}$) was calculated as the ratio of peptide concentration in the 1-octanol and saline phases.

3.3.16. Solubility.

HEPES buffer (0.05 M HEPES buffer in 0.1 M NaCl, pH 7.4, 500 μL) was added to 1 mg of peptide. The sample was vortexed for 30 sec, sonicated for 5 min, shaken at r.t. for 2 h, and then allowed to be stayed overnight to equilibration. The sample was filtrated with an Acrodisc Syringe Filter (13 mm, 0.45 μm pore, PTFE membrane, Pall Life Sciences, East Hills, NY). The peptide concentration of the obtained filtrate was analyzed by HPLC (30-70% of acetonitrile containing 0.1% TFA within 20 min and up to 95% within additional 5 min, 1 mL/min, 230 nm, Vydac 218TP104 C-18 column).

Table 3.3.1. ^{1}H Resonance Assignments of bifunctional peptides in DMSO at 298K.

H-Tyr-*D*-Ala-Gly-Phe-Pro-Leu-Trp-O-3,5-Bzl(CF_3)$_2$·TFA (**TY001**); 2 amide bond rotamers at the Pro^6 N, ca. 7:1 ratio; ^{1}H-NMR (DMSO-d_6) δ:				
AA	NH	α	β	misc.
Tyr^1	8.06/8.10(3H, bs)	3.93-4.05(1H, m)	2.84(1H, dd, *J*=7.0, 11.5 Hz), 2.90(1H, dd, *J*=6.5, 11.5 Hz)	6.70(2H, d, *J*=8.0 Hz: PhH), 7.02(2H, d, *J*=8.5 Hz: PhH), 9.33(1H, bs: PhOH)
D-Ala^2	8.50/8.60(1H, d, *J*=6.5 Hz)	4.28-4.33(1H, m)	1.05/1.10(3H, d, *J*=7.0 Hz)	-
Gly^3	8.14/8.25(1H, t, *J*=5.5 Hz)	3.59/3.55(1H, dd, *J*=6.0, 17.0 Hz), 3.70/3.73(1H, dd, *J*=5.5, 16.5 Hz)	-	-
Phe^4	8.23(1H, d, *J*=8.0 Hz)	4.63-4.70(1H, m)	2.73(1H, dd, *J*=9.5, 14.0 Hz), 2.98(1H, dd, *J*=3.5, 14.0 Hz)	7.12-7.30(5H, m: PhH)
Pro^5	-	4.31-4.35/4.14-4.17(1H, m)	1.69-1.77/1.69-1.73(1H, m), 1.89-1.96/1.69-1.73 (1H, m)	1.77-1.91/1.57-1.62(2H, m: γCH_2), 3.45-3.52/3.33-3.38(1H, m: δCH_2), 3.56-3.64/3.22-3.26(1H, m: δCH_2)
Leu^6	7.84(1H, d, *J*=8.5 Hz)	4.30-4.38/4.25-4.28(1H, m)	1.37(2H, dd, *J*=7.5, 7.5 Hz)	1.53-1.65(1H, m: γCH_2), 0.78/0.72(3H, d, *J*=6.5 Hz: δCH_2), 0.80(3H, d, *J*=6.5 Hz: δCH_2)
Trp^7	8.41(1H, d, *J*=6.5H¥z)	4.56(1H, dd, *J*=7.0, 14.0 Hz)	3.15(1H, dd, *J*=6.5, 15.0 Hz), 3.21(1H, dd, *J*=6.5, 15.0 Hz)	6.95(1H, dd, *J*=7.5, 7.5 Hz: Ind5), 7.05(1H, dd, *J*=7.0, 7.0 Hz: Ind6), 7.15(1H, s: Ind2), 7.32(1H, d, *J*=8.0 Hz: Ind4), 7.46(1H, d, *J*=7.5 Hz: Ind7), 10.88(1H, bs, IndNH)
3,5-Bn(CF_3)$_2$	-	-	-	5.12(1H, d, *J*=13.0 Hz: CH_2Ph), 5.22(1H, d, *J*=13.5 Hz: CH_2Ph), 7.93(2H, s: PhH), 8.06(1H, s: PhH)

H-Tyr-*D*-Ala-Gly-Phe-Pro-Leu-Trp-O-Bzl·TFA (**TY011**); 2 amide bond rotamers at the Pro[6] N, ca. 7:1 ratio; ^{1}H-NMR (DMSO-d_6) δ:				
AA	NH	α	β	misc.
Tyr[1]	8.06 (3H, bs)	3.93-4.03(1H, m)	2.84(1H, dd, *J*=7.0, 13.5 Hz), 2.90(1H, dd, *J*=6.5, 13.5 Hz)	6.70(2H, d, *J*=8.5 Hz: PhH), 7.02(2H, d, *J*=8.5 Hz: PhH), 9.33(1H, bs: PhOH)
D-Ala[2]	8.51/8.60(1H, d, *J*=6.5 Hz)	4.27-4.32(1H, m)	1.05/1.10(3H, d, *J*=7.0 Hz)	-
Gly[3]	8.16/8.23(1H, t, *J*=5.5 Hz)	3.59(1H, dd, *J*=6.0, 16.5 Hz), 3.70/3.74(1H, dd, *J*=6.0, 17.0 Hz)	-	-
Phe[4]	8.23/8.25(1H, d, *J*=7.5 Hz)	4.61-4.71(1H, m)	2.74(1H, dd, *J*=9.0, 13.5 Hz), 2.99(1H, dd, *J*=4.5, 14.0 Hz)	7.10-7.33(5H, m: PhH)
Pro[5]	-	4.31-4.36/4.13-4.16(1H, m)	1.71-1.77/1.70-1.76(1H, m), 1,91-1.96/1.70-1.76(1H, m)	1.78-1.90/1.59-1.61(2H, m: γCH_2), 3.47-3.52(1H, m: δCH_2), 3.56-3.63(1H, m: δCH_2)
Leu[6]	7.86/8.21(1H, d, *J*=8.0 Hz)	4.33-4.40/4.25-4.29(1H, m)	1.36-1.48(2H, m)	1.55-1.68(1H, m: γCH_2), 0.83/0.76(3H, d, *J*=6.5 Hz: δCH_2), 0.86(3H, d, *J*=6.5 Hz)
Trp[7]	8.33(1H, d, *J*=7.0 Hz)	4.56(1H, dd, *J*=6.5, 14.0 Hz)	3.12(1H, dd, *J*=7.5, 14.5 Hz), 3.19(1H, dd, *J*=6.5, 14.5 Hz)	6.99(1H, dd, *J*=7.5, 7.5 Hz: Ind5), 7.08(1H, dd, *J*=7.5, 7.5 Hz: Ind6), 7.16(1H, s: Ind2), 7.34(1H, d, *J*=8.5 Hz: Ind4), 7.48(1H, d, *J*=7.5 Hz: Ind7), 10.86(1H, bs, IndNH)
Bzl	-	4.97(1H, d, *J*=13.0 Hz), 5.02(1H, d, *J*=12.5 Hz)	-	7.10-7.33(5H, m: PhH)

H-Tyr-*D*-Ala-Gly-Phe-Pro-Leu-Trp-NH-Bzl·TFA (**TY008**); 2 amide bond rotamers at the Pro^6 N, ca. 5:1 ratio; ^{1}H-NMR (DMSO-d_6) δ:				
AA	NH	α	β	misc.
Tyr^1	8.05/8.09(3H, bs)	3.94-4.04(1H, m)	2.84(1H, dd, *J*=7.5, 14.0 Hz), 2.90(1H, dd, *J*=7.0, 13.5 Hz)	6.70(2H, d, *J*=8.0 Hz: PhH), 7.02(2H, d, *J*=8.0 Hz: PhH), 9.33(1H, bs: PhOH)
D-Ala^2	8.52/8.60(1H, d, *J*=6.5 Hz)	4.28-4.33(1H, m)	1.05/1.10(3H, d, *J*=7.0 Hz)	-
Gly^3	8.16/8.23(1H, t, *J*=5.5 Hz)	3.59 (1H, dd, *J*=6.0, 16.0 Hz), 3.70/3.73(1H, dd, *J*=5.5, 16.5 Hz)	-	-
Phe^4	8.23/8.25(1H, d, *J*=8.0 Hz)	4.63-4.70/4.48-4.53(1H, m)	2.74/2.95(1H, dd, *J*=9.5, 14.0 Hz), 2.98/3.27(1H, dd, *J*=4.0, 14.0 Hz)	7.05-7.30(5H, m: PhH)
Pro^5	-	4.29-4.34/4.10-4.14(1H, m)	1.69-1.76/1.67-1.75(1H, m), 1.90-1.98/1.67-1.75 (1H, m)	1.76-1.90/1.55-1.58(2H, m: γCH_2), 3.45-3.51/3.17-3.25(1H, m: δCH_2), 3.56-3.63/3.32-3.35(1H, m: δCH_2)
Leu^6	7.96/8.27(1H, d, *J*=6.5 Hz)	4.23-4.33/4.15-4.18(1H, m)	1.40(2H, dd, *J*=7.5, 7.5 Hz)	1.55-1.65(1H, m: γCH_2), 0.83/0.77(3H, d, *J*=6.5 Hz: δCH_2), 0.88/0.86(3H, d, *J*=6.5 Hz: δCH_2)
Trp^7	7.84/7.82(1H, d, *J*=8.0 Hz)	4.57(1H, dd, *J*=7.5, 14.0 Hz)	3.03/3.01(1H, dd, *J*=7.5, 14.5 Hz), 3.15/3.10(1H, dd, *J*=6.0, 14.5 Hz)	6.96(1H, dd, *J*=7.5, 7.5 Hz: Ind5), 7.06(1H, dd, *J*=8.0, 8.0 Hz: Ind6), 7.09(1H, s: Ind2), 7.33(1H, d, *J*=8.0 Hz: Ind4), 7.56(1H, d, *J*=7.5 Hz: Ind7), 10.88(1H, bs, IndNH)
Bzl	8.36/8.43(1H, t, *J*=5.5 Hz)	-	-	4.15-4.25/4.25-4.32(2H, m), 7.05-7.30(5H, m: PhH)

H-Tyr-*D*-Ala-Gly-Phe-Pro-Leu-Trp-NMe-Bzl·TFA (**TY010**); 2 amide bond rotamers at the Pro^6 N, ca. 7:1 ratio (read from NH-DAla), 2 amide bond rotamers at the BzlN, ca. 2:1 ratio (read from IndNH-Trp); ^{1}H-NMR (DMSO-d_6) δ:				
AA	NH	α	β	misc.
Tyr[1]	8.06(3H, bs)	3.96(1H, m)	2.83(1H, dd, *J*=7.8, 13.8 Hz), 2.88(1H, dd, *J*=6.6, 13.8 Hz)	6.69/6.70(2H, d, *J*=7.8 Hz: PhH), 7.00(2H, d, *J*=8.4 Hz: PhH), 9.33(1H, bs: PhOH)
D-Ala[2]	8.50/8.59(1H, d, *J*=7.2 Hz)	4.26-4.33(1H, m)	1.03/1.09(3H, d, *J*=6.6 Hz)	-
Gly[3]	8.15/8.24(1H, t, *J*=5.4 Hz)	3.56-3.63 (1H, m), 3.69/3.74(1H, dd, *J*=6.0, 16.8 Hz)	-	-
Phe[4]	8.22/8.20/7.68(1H, d, *J*=7.8 Hz)	4.63-4.70/4.22-4.25/4.50-4.56(1H, m)	2.75/2.90/2.83(1H, dd, *J*=9.6, 13.8 Hz), 2.92-3.08/3.12-3.16/2.78-2.90(1H, m)	6.90-7.30(5H, m: PhH)
Pro[5]	-	4.34-4.39/4.13-4.17(1H, m)	1.77-1.88/1.62-1.65(1H, m), 1.95-2.03/1.73-1.78 (1H, m)	1.88-1.95/1.80-1.86(2H, m: γCH_2), 3.50-3.57(1H, m: δCH_2), 3.58-3.67(1H, m: δCH_2)
Leu[6]	7.91/7.87/8.25(1H, d, *J*=8.4 Hz)	4.32-4.41/4.31-4.37/4.25-4.28(1H, m)	1.44/1.41/1.45(2H, dd, *J*=7.2, 7.2 Hz)	1.60-1.65/1.60-1.62/1.42-1.45(1H, m: γCH_2), 0.81-0.90/0.76-0.79(6H, m: δCH_2)
Trp[7]	8.22/8.20/8.18/8.16(1H, d, *J*=7.8 Hz)	5.07/4.98(1H, dd, *J*=7.8, 14.4 Hz)	2.90-3.05(1H, m), 3.11-3.25 (1H, m)	6.96/6.88(1H, dd, *J*=7.2, 7.2 Hz: Ind5), 7.05/7.03(1H, dd, *J*=7.2, 7.2 Hz: Ind6), 7.12/7.12/7.07/7.07(1H, s: Ind2), 7.33/7.32(1H, d, *J*=8.4 Hz: Ind4), 7.55/7.35/7.54(1H, d, *J*=8.4 Hz: Ind7), 10.86/10/82(1H, bs, IndNH)
Bzl	-	-	-	2.68/2.66(3H, s, NCH_3), 6.90-7.30(5H, m: PhH)

H-Tyr-*D*-Ala-Gly-Phe-Pro-Leu-Trp-NH-3,5-Bzl(CF_3)$_2$·TFA (**TY012**); 2 amide bond rotamers at the Pro^6 N, ca. 6:1 ratio (read from H_β-DAla); ^{1}H-NMR (DMSO-d_6) δ:				
AA	NH	α	β	misc.
Tyr[1]	8.05/8.10(3H, bs)	3.92-4.00(1H, m)	2.83(1H, dd, *J*=7.2, 13.8 Hz), 2.88(1H, dd, *J*=6.6, 13.8 Hz)	6.69(2H, d, *J*=8.4 Hz: PhH), 7.00(2H, d, *J*=8.4 Hz: PhH), 9.32(1H, bs: PhOH)
D-Ala[2]	8.49/8.58(1H, d, *J*=7.8 Hz)	4.28-4.33(1H, m)	1.03/1.08(3H, d, *J*=6.6 Hz)	-
Gly[3]	8.14/8.24(1H, t, *J*=5.4 Hz)	3.52-3.63(1H, m), 3.68/3.70(1H, dd, *J*=5.4, 16.8 Hz)	-	-
Phe[4]	8.22(1H, d, *J*=7.8 Hz)	4.62-4.67(1H, m)	2.71(1H, dd, *J*=9.0, 13.8 Hz), 2.95(1H, dd, *J*=3.6, 13.8 Hz)	7.12-7.28(5H, m: PhH)
Pro[5]	-	4.30-4.34/4.14-4.17(1H, m)	1.65-1.74/1.68-1.74(1H, m), 1.87-1.96/1.68-1.74 (1H, m)	1.75-1.86/1.53-1.58(2H, m: γCH_2), 3.44-3.52/3.21-3.25(1H, m: δCH_2), 3.56-3.64/3.31-3.36(1H, m: δCH_2)
Leu[6]	7.91/8.20(1H, m)	4.24-4.28/4.18-4.22(1H, m)	1.40/1.43(2H, dd, *J*=7.2, 7.2 Hz)	1.51-1.64/1.38-1.41(1H, m: γCH_2), 0.79/0.73(3H, d, *J*=6.6 Hz: δCH_2), 0.83(3H, d, *J*=6.6 Hz: δCH_2)
Trp[7]	7.95(1H, m)	4.52(1H, dd, *J*=7.2, 13.8 Hz)	3.02(1H, dd, *J*=7.2, 14.4 Hz), 3.14(1H, dd, *J*=5.4, 14.4 Hz)	6.93(1H, dd, *J*=7.2, 7.2 Hz: Ind5), 7.03(1H, dd, *J*=7.2, 7.2 Hz: Ind6), 7.09(1H, s: Ind2), 7.30(1H, d, *J*=7.8 Hz: Ind4), 7.52(1H, d, *J*=7.8 Hz: Ind7), 10.80(1H, bs, IndNH)
3,5-Bn(CF_3)$_2$	8.59(1H, t, *J*=6.0 Hz)	-	-	4.35(1H, dd, *J*=5.4, 9.6 Hz: CH_2Ph), 4.45(1H, dd, *J*=5.4, 10.2 Hz: CH_2Ph), 7.89(2H, s: PhH), 7.94(1H, s: PhH)

H-Tyr-*D*-Ala-Gly-Phe-Pro-Leu-Trp-NMe-3,5-Bzl(CF_3)$_2$·TFA (**TY013**); 2 amide bond rotamers at the Pro^6 N, ca. 9:1 ratio (read from NH-DAla), 2 amide bond rotamers at the BzlN, ca. 3:1 ratio (read from IndNH-Trp); ^{1}H-NMR (DMSO-d_6) δ:				
AA	NH	α	β	misc.
Tyr[1]	8.06(3H, bs)	3.98(1H, m)	2.84(1H, dd, *J*=8.5, 14.5 Hz), 2.90(1H, dd, *J*=7.0, 14.5 Hz)	6.70(2H, d, *J*=8.5 Hz: PhH), 7.02(2H, d, *J*=8.5 Hz: PhH), 9.32(1H, bs: PhOH)
D-Ala[2]	8.49/8.58(1H, d, *J*=7.5 Hz)	4.27-4.33(1H, m)	1.05/1.10(3H, d, *J*=6.5 Hz)	-
Gly[3]	8.16/8.25(1H, t, *J*=5.0 Hz)	3.55-3.62 (1H, m), 3.70/3.75(1H, dd, *J*=6.0, 16.5 Hz)	-	-
Phe[4]	8.25/8.23/7.66(1H, d, *J*=7.5 Hz)	4.63-4.70/4.48-4.52(1H, m)	2.68-2.75/2.78-2.85(1H, m), 2.94-3.04/2.78-2.85/3.04-3.08(1H, m)	7.15-7.30(5H, m: PhH)
Pro[5]	-	4.33-4.37/4.16-4.19(1H, m)	1.75-1.83/1.74-1.79(2H, m)	1.86-1.92/1.60-1.64(1H, m: γCH_2), 1.94-2.00/1.60-1.64(1H, m: γCH_2), 3.49-3.57(1H, m: δCH_2), 3.60-3.67(1H, m: δCH_2)
Leu[6]	7.83/7.85/8.16(1H, d, *J*=7.5 Hz)	4.32-4.40/4.25-4.30(1H, m)	1.38-1.44/1.40-1.45/1.33-1.38(2H, m)	1.56-1.67/1.40-1.45(1H, m: γCH_2), 0.84/0.77(3H, d, *J*=7.5 Hz: δCH_2), 0.87/0.82(3H, d, *J*=7.5 Hz: δCH_2)
Trp[7]	8.35/8.32/8.30/8.17(1H, d, *J*=8.0 Hz)	4.90-5.00 (1H, m)	2.95-3.03(1H, m), 3.11-3.23 (1H, m)	6.97/6.88(1H, dd, *J*=7.5, 7.5 Hz: Ind5), 7.07/7.02(1H, dd, *J*=7.5, 7.5 Hz: Ind6), 7.13/7.12(1H, s: Ind2), 7.34/7.30(1H, d, *J*=8.0 Hz: Ind4), 7.54/7.53(1H, d, *J*=8.0 Hz: Ind7), 10.83/10/80(1H, bs, IndNH)
3,5-Bn(CF_3)$_2$	-	-	-	2.77/2.79(3H, s, NCH_3), 7.85(2H, s: PhH), 7.98(1H, s: PhH)

H-Tyr-*D*-Ala-Gly-Phe-Phe-Pro-Leu-Trp-O-3,5-Bzl(CF_3)$_2$·TFA (**TY003**); Only one isomer was found; ^{1}H-NMR (DMSO-d_6) δ:				
AA	NH	α	β	misc.
Tyr[1]	8.05(3H, bs)	3.93-4.20(1H, m)	2.78(1H, dd, *J*=8.5, 14.0 Hz), 2.89(1H, dd, *J*=8.5, 14.0 Hz)	6.70(2H, d, *J*=8.5 Hz: PhH), 7.02(2H, d, *J*=8.0 Hz: PhH), 9.33(1H, bs: PhOH)
D-Ala[2]	8.53(1H, d, *J*=7.5 Hz)	4.31-4.40(1H, m)	1.06(3H, d, *J*=7.0 Hz)	-
Gly[3]	8.17(1H, t, *J*=6.0 Hz)	3.59(1H, dd, *J*=5.5, 16.5 Hz), 3.69(1H, dd, *J*=5.5, 17.0 Hz)	-	-
Phe[4]	7.89(1H, d, *J*=9.0 Hz)	4.50-4.59(1H, m)	2.69(1H, dd, *J*=9.5, 14.0 Hz), 2.89-2.96(1H, m)	7.12-7.29(5H, m: PhH)
Phe[5]	8.45(1H, d, *J*=8.0 Hz)	4.65(1H, dd, *J*=6.5, 12.5 Hz)	2.90-2.95(1H, m), 2.96-3.06(1H, m)	7.12-7.29(5H, m: PhH)
Pro[6]	-	4.28-4.39(1H, m)	1.80-1.88(1H, m), 1.89-1.97(1H, m)	1.69-1.80(2H, m: γCH_2), 3.40-3.51(2H, m: δCH_2)
Leu[7]	7.87(1H, d, *J*=8.5 Hz)	4.31-4.40(1H, m)	1.34-1.42(2H, m)	1.53-1.64(1H, m: γCH_2), 0.74(3H, d, *J*=6.5 Hz: δCH_2), 0.79(3H, d, *J*=6.0 Hz: δCH_2)
Trp[8]	8.40(1H, d, *J*=7.0 Hz)	4.51-4.60(1H, m)	3.15(1H, dd, *J*=6.5, 15.0 Hz), 3.21(1H, dd, *J*=6.5, 14.0 Hz)	6.95(1H, dd, *J*=7.5, 7.5 Hz: Ind5), 7.05(1H, dd, *J*=7.5, 7.5 Hz: Ind6), 7.17(1H, s: Ind2), 7.32(1H, d, *J*=8.0 Hz: Ind4), 7.46(1H, d, *J*=8.0 Hz: Ind7), 10.88(1H, bs, IndNH)
3,5-Bn(CF_3)$_2$	-	-	-	5.12(1H, d, *J*=13.5 Hz: CH_2Ph), 5.21(1H, d, *J*=13.0 Hz: CH_2Ph), 7.90(2H, s: PhH), 8.05(1H, s: PhH)

H-Tyr-*D*-Ala-Gly-Phe-*D*-Phe-Pro-Leu-Trp-O-3,5-Bzl(CF_3)$_2$·TFA (**TY007**), 2 amide bond rotamers at the Pro^6 N, ca. 1:1 ratio; ^{1}H-NMR (DMSO-d_6) δ:				
AA	NH	α	β	misc.
Tyr^1	8.03/8.07(3H, bs)	3.93-4.03(1H, m)	2.78-2.92(2H, m)	6.70(2H, d, *J*=8.5 Hz: PhH), 7.02(2H, d, *J*=8.0 Hz: PhH), 9.33(1H, bs: PhOH)
D-Ala^2	8.50/8.56(1H, d, *J*=7.5 Hz)	4.31(1H, qua, *J*=6.5 Hz)	1.03/1.05(3H, d, *J*=7.0 Hz)	-
Gly^3	8.13-8.21(1H, m)	3.50-3.71(2H, m)	-	-
Phe^4	7.79/7.88(1H, d, *J*=7.5 Hz)	4.44-4.50/4.58-4.64(1H, m)	2.26-2.34/2.50-2.58(1H, m), 2.48-2.53/2.72-2.80(1H, m)	7.07-7.30(5H, m: PhH)
D-Phe^5	8.66/8.68(1H, d, *J*=8.0 Hz)	4.36-4.44/4.71(1H, m/dd, *J*=6.5, 13.0 Hz)	2.71-2.76/2.75-2.81(1H, m), 2.90-2.89(1H, m)	6.88-6.92, 7.07-7.30(5H, m: PhH)
Pro^6	-	4.22-4.28/4.84-4.88(1H, m)	1.65-1.70/1.94-1.99(1H, m), 1.77-1.82/2.12-2.18(1H, m)	1.62-1,65/1.63-1.69(1H, m: γCH_2), 1.70-1.77/1.70-1.75(1H, m: γCH_2),3.48-3.55/3.45-3.49(1H, m: δCH_2), 3.12-3.15/3.35-3.40(1H, m: δCH_2)
Leu^7	7.82/8.27(1H, d, *J*=7.5 Hz)	4.20-4.27/4.42-4.48(1H, m)	1.35-1.46(2H, m)	1.52-1.62(1H, m: γCH_2), 0.75/0.77(3H, d, *J*=6.5 Hz: δCH_2), 0.80/0.81(3H, d, *J*=6.5 Hz: δCH_2)
Trp^8	8.29/8.63(1H, d, *J*=9.0 Hz)	4.50-4.58(1H, m)	3.09-3.22(2H, m)	6.94(1H, dd, *J*=7.5, 7.5 Hz: Ind5), 7.05(1H, dd, *J*=8.0, 8.0 Hz: Ind6), 7.17(1H, s: Ind2), 7.31(1H, d, *J*=7.5 Hz: Ind4), 7.41/7.46(1H, d, *J*=7.5 Hz: Ind7), 10.86/10.88(1H, bs, IndNH)
3,5-Bn(CF_3)$_2$	-	-	-	5.08/5.10(1H, d, *J*=13.0 Hz: CH_2Ph), 5.17/5.19(1H, d, *J*=13.0 Hz: CH_2Ph), 7.90/7.91(2H, s: PhH), 8.05(1H, s: PhH)

H-Tyr-*D*-Ala-Gly-Phe-Gly-Pro-Leu-Trp-O-3,5-Bzl(CF_3)$_2$·TFA (**TY006**), 2 amide bond rotamers at the Pro^6 N, ca. 2:1 ratio; ^{1}H-NMR (DMSO-d_6) δ:				
AA	NH	α	β	misc.
Tyr^1	8.05(3H, bs)	3.92-4.03(1H, m)	2.84(1H, dd, *J*=7.0, 13.5 Hz), 2.90 (1H, dd, *J*=6.5, 13.5 Hz)	6.70(2H, d, *J*=8.0 Hz: PhH), 7.02(2H, d, *J*=8.5 Hz: PhH), 9.33(1H, bs: PhOH)
D-Ala^2	8.52(1H, d, *J*=7.0 Hz)	4.28-4.33(1H, m)	1.06(3H, d, *J*=7.0 Hz)	-
Gly^3	8.13-8.20(1H, m)	3.57-3.65(1H, m), 3.67-3.75(1H, m)	-	-
Phe^4	8.01-8.06(1H, m)	4.53-4.65 (1H, m)	2.25(1H, dd, *J*=10.0, 13.5 Hz), 2.97-3.07(1H, m)	7.12-7.24(5H, m: PhH)
Gly^5	8.27/8.11(1H, t, *J*=5.5 Hz)	3.83-3.94/3.29-3.38(1H, m), 3.90-4.00(1H, m)	-	-
Pro^6	-	4.30-4.35/4.43-4.45(1H, m)	1.78-1.87/1.69-1.75(2H, m)	1.67-1.73/1.76-1.84(1H, m: γCH_2), 1.91-1.99/2.10-2.18(1H, m: γCH_2), 3.40-3.53/3.35-3.44(2H, m: δCH_2)
Leu^7	7.91/8.25(1H, d, *J*=8.5 Hz)	4.28-4.33/4.37-4.44(1H, m)	1.32-1.43(2H, m)	0.75/0.76(3H, d, *J*=6.0/5.0 Hz: δCH_2), 0.79(3H, d, *J*=6.5 Hz: δCH_2), 1.50-1.60(1H, m: γCH_2)
Trp^8	8.29/8.51(1H, d, *J*=7.0 Hz)	4.52-4.60(1H, m)	3.14(1H, dd, *J*=6.5, 14.0 Hz), 3.21(1H, dd, *J*=6.5, 14.0 Hz)	6.96(1H, dd, *J*=7.5, 7.5 Hz: Ind5), 7.05(1H, dd, *J*=7.0, 7.0 Hz: Ind6), 7.17(1H, s: Ind2), 7.32(1H, d, *J*=8.0 Hz: Ind4), 7.45/7.47(1H, d, *J*=7.5/5.5 Hz: Ind7), 10.86/10.88(1H, bs, IndNH)
3,5-Bn(CF_3)$_2$	-	-	-	5.11/5.14(1H, d, *J*=13.5 Hz: CH_2Ph), 5.20/5.22(1H, d, *J*=13.0 Hz: CH_2Ph), 7.92/7.94(2H, s: PhH), 8.05(1H, s: PhH)

H-Tyr-*D*-Ala-Gly-Phe-Leu-Pro-Leu-Trp-O-3,5-Bzl(CF_3)$_2$·TFA (**TY004**); Only one isomer was found; ^{1}H-NMR (DMSO-d_6) δ:				
AA	NH	α	β	misc.
Tyr[1]	8.12(3H, bs)	4.00(1H, bs)	2.84-2.93(2H, m)	6.71(2H, d, *J*=7.5 Hz: PhH), 7.03(2H, d, *J*=8.0 Hz: PhH), 9.49(1H, bs: PhOH)
D-Ala[2]	8.57(1H, d, *J*=7.0 Hz)	4.28-4.38(1H, m)	1.06(3H, d, *J*=6.5 Hz)	-
Gly[3]	8.20(1H, m)	3.61(1H, dd, *J*=5.0 16.5 Hz), 3.72(1H, dd, *J*=5.0, 17.0 Hz)	-	-
Phe[4]	7.91(1H, m)	4.48-4.59(1H, m)	2.68-2.78(1H, m), 2.90-3.00(1H, m)	7.12-7.27(5H, m: PhH)
Leu[5]	8.39(1H, d, *J*=6.5 Hz)	4.50-4.61(1H, m)	1.41-1.49(2H, m)	0.86(3H, d, *J*=7.5 Hz: δCH_2), 0.88(3H, d, *J*=7.0 Hz: δCH_2), 1.57-1.67(1H, m: γCH_2)
Pro[6]	-	4.27-4.40(1H, m)	1.71-1.85(2H, m)	1.81-1.96(1H, m: γCH_2), 3.10-3.25(2H, m: δCH_2)
Leu[7]	7.85(1H, d, *J*=7.5 Hz)	4.30-4.44(1H, m)	1.30-1.38(2H, m)	0.76(3H, d, *J*=6.0 Hz: δCH_2), 0.79(3H, d, *J*=6.0 Hz: δCH_2), 1.51-1.60(1H, m: γCH_2)
Trp[8]	8.33(1H, d, *J*=7.5 Hz)	4.50-4.59(1H, m)	3.18(2H, s)	6.96(1H, dd, *J*=7.0, 7.0 Hz: Ind5), 7.05(1H, dd, *J*=7.5, 7.5 Hz: Ind6), 7.17(1H, s: Ind2), 7.33(1H, d, *J*=8.0 Hz: Ind4), 7.46(1H, d, *J*=8.0 Hz: Ind7), 10.87(1H, bs, IndNH)
3,5-Bn(CF_3)$_2$	-	-	-	5.12(1H, d, *J*=13.0 Hz: CH_2Ph), 5.21(1H, d, *J*=13.5 Hz: CH_2Ph), 7.93(2H, s: PhH), 8.04(1H, s: PhH)

H-Tyr-*D*-Ala-Gly-Phe-Met-Pro-Leu-Trp-O-3,5-Bzl(CF_3)$_2$·TFA (**TY005**); Only one isomer was found; ^{1}H-NMR (DMSO-d_6) δ:				
AA	NH	α	β	misc.
Tyr[1]	8.05(3H, bs)	3.93-4.13(1H, m)	2.86(1H, dd, *J*=6.5, 9.5 Hz), 2.89(1H, dd, *J*=6.5, 9.5 Hz)	6.69(2H, d, *J*=8.0 Hz: PhH), 7.03(2H, d, *J*=8.0 Hz: PhH), 9.33(1H, bs: PhOH)
D-Ala[2]	8.55(1H, d, *J*=8.0 Hz)	4.28-4.39(1H, m)	1.06(3H, d, *J*=7.0 Hz)	-
Gly[3]	8.19(1H, t, *J*=5.0 Hz)	3.63(1H, dd, *J*=6.5 16.0 Hz), 3.71(1H, dd, *J*=6.5, 16.0 Hz)	-	-
Phe[4]	7.97(1H, d, *J*=8.0 Hz)	4.50-4.59(1H, m)	2.74(1H, dd, *J*=9.5, 13.0 Hz), 2.90-2.99(1H, m)	7.17-7.25(5H, m: PhH)
Met[5]	8.41(1H, d, *J*=9.5 Hz)	4.59-4.66(1H, m)	1.75-1.81(1H, m), 1.89-1.95(1H, m)	2.45-2.51(2H, m: γCH_2), 2.03(3H, s: SCH_3)
Pro[6]	-	4.28-4.39(1H, m)	1.68-1.74(1H, m), 1.92-1.98(1H, m)	1.75-1.81(1H, m: γCH_2), 1.85-1.92(1H, m: γCH_2), 3.52-3.61(2H, m: δCH_2)
Leu[7]	7.88(1H, d, *J*=8.0 Hz)	4.27-4.38(1H, m)	1.31-1.37(2H, m)	1.52-1.61(1H, m: γCH_2), 0.76(3H, d, *J*=6.5 Hz: δCH_2), 0.79(3H, d, *J*=6.5 Hz: δCH_2)
Trp[8]	8.39(1H, d, *J*=7.5 Hz)	4.50-4.59(1H, m)	3.14(1H, dd, *J*=6.5, 9.5 Hz), 3.20(1H, dd, *J*=6.5, 9.5 Hz)	6.96(1H, dd, *J*=7.5, 7.5 Hz: Ind5), 7.07(1H, dd, *J*=7.0, 7.0 Hz: Ind6), 7.17(1H, s: Ind2), 7.32(1H, d, *J*=8.0 Hz: Ind4), 7.47(1H, d, *J*=7.5 Hz: Ind7), 10.86(1H, bs, IndNH)
3,5-Bn(CF_3)$_2$	-	-	-	5.11(1H, d, *J*=13.0 Hz: CH_2Ph), 5.21(1H, d, *J*=13.5 Hz: CH_2Ph), 7.92(2H, s: PhH), 8.05(1H, s: PhH)

H-Tyr-*D*-Ala-Gly-Phe-Met(O)-Pro-Leu-Trp-O-3,5-Bzl(CF_3)$_2$·TFA (**TY023**), 2 amide bond rotamers at the Pro^6 N, ca. 10:1 ratio; ^{1}H-NMR (DMSO-d_6) δ:				
AA	NH	α	β	misc.
Tyr^1	8.08/8.11(3H, bs)	3.98(1H, bs)	2.83-2.94(2H, m)	6.70(2H, d, *J*=8.0 Hz: PhH), 7.02(2H, d, *J*=8.5 Hz: PhH), 9.38(1H, bs: PhOH)
D-Ala^2	8.54(1H, d, *J*=7.0 Hz)	4.29-4.36(1H, m)	1.07(3H, d, *J*=7.0 Hz)	-
Gly^3	8.26-8.35(1H, m)	3.57-3.65(1H, m), 3.65-3.78(1H, m)	-	-
Phe^4	8.01(1H, d, *J*=8.0 Hz)	4.52-4.57(1H, m)	2.74-2.80(1H, m), 2.93-3.00(1H, m)	7.13-7.28(5H, m: PhH)
Met(O)^5	8.44-8.49/8.48-8.51(1H, m)	4.61-4.73(1H, m)	1.85-1.93(1H, m), 2.02-2.10(1H, m)	2.66-2.74(1H, m: γCH_2), 2.77-2.84(1H, m: γCH_2), 2.50(3H, s: SCH_3)
Pro^6	-	4.29-4.33(1H, m)	1.65-1.72(1H, m), 1.93-2.01(1H, m)	1.71-1.79(1H, m: γCH_2), 1.78-1.87(1H, m: γCH_2), 3.51-3.57/3.46-3.51(H, m: δCH_2), 3.51-3.57/3.55-3.60(H, m: δCH_2)
Leu^7	7.91/8.25(1H, d, *J*=8.5 Hz)	4.29-4.36(1H, m)	1.30-1.40(2H, m)	0.76(3H, d, *J*=5.0 Hz: δCH_2), 0.79(3H, d, *J*=6.5 Hz: δCH_2), 1.50-1.62(1H, m: γCH_2)
Trp^8	8.38/8.21(1H, d, *J*=6.5 Hz)	4.51-4.57/4.47-4.52(1H, m)	3.15(1H, dd, *J*=7.5, 14.5 Hz), 3.21 (1H, dd, *J*=6.5, 15.0 Hz)	6.96(1H, dd, *J*=7.5, 7.5 Hz: Ind5), 7.05(1H, dd, *J*=7.5, 7.5 Hz: Ind6), 7.17(1H, s: Ind2), 7.32(1H, d, *J*=8.0 Hz: Ind4), 7.46(1H, d, *J*=8.0 Hz: Ind7), 10.88(1H, bs, IndNH)
3,5-Bn(CF_3)$_2$	-	-	-	5.12/5.21(1H, d, *J*=13.5 Hz: CH_2Ph), 5.21/5.29(1H, d, *J*=13.5 Hz: CH_2Ph), 7.92/7.99(2H, s: PhH), 8.05(1H, s: PhH)

H-Tyr-*D*-Ala-Gly-Phe-Nle-Pro-Leu-Trp-O-3,5-Bzl(CF_3)$_2$·TFA (**TY018**); Only one isomer was found; ^{1}H-NMR (DMSO-d_6) δ:				
AA	NH	α	β	misc.
Tyr[1]	8.05(3H, bs)	3.98(1H, bs)	2.84(1H, dd, *J*=7.5, 13.5 Hz), 2.91(1H, dd, *J*=7.0, 13.5 Hz))	6.71(2H, d, *J*=7.5 Hz: PhH), 7.03(2H, d, *J*=8.5 Hz: PhH), 9.33(1H, bs: PhOH)
D-Ala[2]	8.53(1H, d, *J*=7.0 Hz)	4.29-4.36(1H, m)	1.07(3H, d, *J*=7.0 Hz)	-
Gly[3]	8.19(1H, t, *J*=6.0 Hz)	3.62(1H, dd, *J*=5.5, 15.0 Hz), 3.71(1H, dd, *J*=5.5, 15.0 Hz)	-	-
Phe[4]	7.92(1H, d, *J*=8.0 Hz)	4.53-4.59(1H, m)	2.73(1H, dd, *J*=10.5, 15.0 Hz), 2.90-3.00(1H, m)	7.13-7.28(5H, m: PhH)
Nle[5]	8.32(1H, d, *J*=7.5 Hz)	4.45(1H, dd, *J*=7.0, 13.0 Hz)	1.46-1.52(1H, m), 1.60-1.68(1H, m)	0.80-0.88(3H, m: εCH_3), 1.16-1.30(4H, m: γCH_2, δCH_2)
Pro[6]	-	4.33-4.38(1H, m)	1.80-1.93(2H, m)	1.69-1.80(2H, m: γCH_2), 3.42-3.51(1H, m: δCH_2), 3.51-3.60(1H, m: δCH_2)
Leu[7]	7.83(1H, d, *J*=8.5 Hz)	4.26-4.39(1H, m)	1.31-1.38(2H, m)	0.76(3H, d, *J*=6.5 Hz: δCH_2), 0.79(3H, d, *J*=5.5 Hz: δCH_2), 1.52-1.60(1H, m: γCH_2)
Trp[8]	8.38(1H, d, *J*=7.0 Hz)	4.52-4.55(1H, m)	3.14(1H, dd, *J*=7.0, 14.0 Hz), 3.20(1H, dd, *J*=7.0, 15.0 Hz)	6.96(1H, dd, *J*=7.5, 7.5 Hz: Ind5), 7.05(1H, dd, *J*=7.5, 7.5 Hz: Ind6), 7.17(1H, s: Ind2), 7.32(1H, d, *J*=8.0 Hz: Ind4), 7.46(1H, d, *J*=8.5 Hz: Ind7), 10.86(1H, bs, IndNH)
3,5-Bn(CF_3)$_2$	-	-	-	5.11(1H, d, *J*=13.5 Hz: CH_2Ph), 5.21(1H, d, *J*=13.5 Hz: CH_2Ph), 7.93(2H, s: PhH), 8.04(1H, s: PhH)

H-Tyr-*D*-Ala-Gly-Phe-*N*-Me-Nle-Pro-Leu-Trp-O-3,5-Bzl(CF_3)$_2$·TFA (**TY019**), 2 amide bond rotamers at the Pro^6 N, ca. 10:1 ratio; ^{1}H-NMR (DMSO-d_6) δ:				
AA	NH	α	β	misc.
Tyr^1	8.05/8.09(3H, bs)	3.97(1H, bs)	2.81-2.93(2H, m)	6.71(2H, d, *J*=8.5 Hz: PhH), 7.03(2H, d, *J*=8.5 Hz: PhH), 9.32(1H, bs: PhOH)
D-Ala^2	8.54/8.60(1H, d, *J*=7.0 Hz)	4.30-4.38(1H, m)	1.03-1.10(3H, m)	-
Gly^3	8.23/8.24-27(1H, t/m, *J*=5.5 Hz)	3.69(2H, d, *J*=5.5 Hz)	-	-
Phe^4	8.35(1H, d, *J*=8.5 Hz)	4.95/4.97-5.01(1H, dd/m, *J*=8.0, 16.0 Hz)	2.74-2.81(1H, m), 2.96-3.03(1H, m)	7.13-7.28(5H, m: PhH)
Nle^5	-	5.09-5.13(1H, m)	1.40-1.48(1H, m), 1.60-1.68(1H, m)	0.80-0.88(3H, m: εCH$_3$), 1.13-1.35(4H, m: γCH$_2$, δCH$_2$)
Pro^6	-	4.17-4.22/4.24-4.28(1H, dd/m, *J*=2.5, 8.0 Hz)	1.66-1.72/1.67-1.82(1H, m), 1.83-1.92/1.85-1.93(1H, m)	1.60-1.68/1.75-1.80(1H, m: γCH$_2$), 1.72-1.78/1.79-1.85(1H, m: γCH$_2$), 2.86-2.97/3.23-3.28(1H, m: δCH$_2$), 3.31-3.39/3.43-3.48(1H, m: δCH$_2$)
Leu^7	7.82(1H, d, *J*=8.0 Hz)	4.26-4.32(1H, m)	1.32-1.42(2H, m)	0.73-0.76(3H, m), 0.77-0.81(3H, m), 1.52-1.56(1H, m: γCH$_2$)
Trp^8	8.22/8.31-8.33(1H, d/m, *J*=6.5 Hz)	4.52(1H, dd, *J*=7.0, 14 Hz)	3.14(1H, dd, *J*=7.5, 15.0 Hz), 3.21(1H, dd, *J*=6.5, 15.0 Hz)	6.96(1H, dd, *J*=7.5, 7.5 Hz: Ind5), 7.06(1H, dd, *J*=7.0, 7.0 Hz: Ind6), 7.15(1H, s: Ind2), 7.32(1H, d, *J*=8.0 Hz: Ind4), 7.45(1H, d, *J*=7.5 Hz: Ind7), 10.87(1H, bs, IndNH)
3,5-Bn(CF_3)$_2$	-	-	-	5.11(1H, d, *J*=13.0 Hz: CH$_2$Ph), 5.20(1H, d, *J*=13.5 Hz: CH$_2$Ph), 7.90(2H, s: PhH), 8.03(1H, s: PhH)

H-Tyr-*D*-Ala-Gly-Phe-Pro-Met-Leu-Trp-NH-3,5-Bzl(CF_3)$_2$·TFA (**TY027**); Only one isomer was found; ^{1}H-NMR (DMSO-d_6) δ:				
AA	NH	α	β	misc.
Tyr[1]	8.04(3H, bs)	3.93-4.00(1H, m)	2.80-2.92(2H, m)	6.69(2H, d, *J*=7.2 Hz: PhH), 7.01(2H, d, *J*=7.2 Hz: PhH), 9.31(1H, bs: PhOH)
D-Ala[2]	8.50(1H, d, *J*=7.8 Hz)	4.28-4.33(1H, m)	1.04(3H, d, *J*=6.6 Hz)	-
Gly[3]	8.17(1H, t, *J*=6.0 Hz)	3.60(1H, dd, *J*=5.4, 16.8 Hz), 3.69 (1H, dd, *J*=5.4, 16.2 Hz)	-	-
Phe[4]	7.93-8.00(1H, m)	4.50-4.55(1H, m)	2.72(1H, dd, *J*=9.6, 13.8 Hz), 2.89-2.95(1H, m)	7.13-7.28(5H, m: PhH)
Met[5]	8.38(1H, d, *J*=7.2 Hz)	4.59(1H, dd, *J*=7.8, 14.4 Hz)	1.70-1.80(1H, m), 1.86-1.94(1H, m)	2.42-2.47 (2H, m: γCH_2), 2.02(3H, s: δCH_3)
Pro[5]	-	4.28-4.33(1H, m)	1.63-1.68(1H, m), 1.85-1.92(1H, m)	1.66-1.84(2H, m: γCH_2), 3.50-3.60(2H, m: δCH_2)
Leu[6]	7.95-8.02(1H, m)	4.21(1H, dd, *J*=8.0, 15.0 Hz)	1.38(2H, dd, *J*=7.2, 7.2 Hz)	1.53-1.61(1H, m: γCH_2), 0.76(3H, d, *J*=6.6 Hz: δCH_2), 0.82(3H, d, *J*=6.6 Hz: δCH_2)
Trp[7]	7.92(1H, d, *J*=7.8 Hz)	4.50-4.55(1H, m)	3.01(1H, dd, *J*=7.8, 14.4 Hz), 3.13(1H, dd, *J*=5.4, 14.4 Hz)	6.94(1H, dd, *J*=7.8, 7.8 Hz: Ind5), 7.04(1H, dd, *J*=8.4, 8.4 Hz: Ind6), 7.08(1H, s: Ind2), 7.30(1H, d, *J*=8.4 Hz: Ind4), 7.51(1H, d, *J*=7.8 Hz: Ind7), 10.88(1H, bs, IndNH)
3,5-Bzl(CF_3)$_2$	8.57(1H, t, *J*=6.0 Hz)	4.32(1H, dd, *J*=5.4, 16.2 Hz), 4.44(1H, d, *J*=6.6, 15.6 Hz)	-	7.88(2H, s: PhH), 7.94(1H, s: PhH)

H-Tyr-*D*-Ala-Gly-Phe-Pro-Met-Leu-Trp-NH-Bzl·TFA (**TY025**); Only one isomer was found; ^{1}H-NMR (DMSO-d_6) δ:				
AA	NH	α	β	misc.
Tyr[1]	8.03(3H, bs)	3.93-4.02(1H, m)	2.85(1H, dd, *J*=7.5, 14.0 Hz), 2.89(1H, dd, *J*=7.0, 14.0 Hz)	6.70(2H, d, *J*=7.0 Hz: PhH), 7.02(2H, d, *J*=8.5 Hz: PhH), 9.31(1H, bs: PhOH)
D-Ala[2]	8.55(1H, d, *J*=7.5 Hz)	4.33(1H, dd, *J*=6.5, 6.5 Hz)	1.06(3H, d, *J*=6.0 Hz)	-
Gly[3]	8.19(1H, t, *J*=6.0 Hz)	3.62(1H, dd, *J*=6.0, 17.0 Hz), 3.70(1H, dd, *J*=6.0, 16.5 Hz)	-	-
Phe[4]	7.97(1H, dd, *J*=7.5 Hz)	4.56(1H, dd, *J*=7.0, 14.0 Hz)	2.74(1H, dd, *J*=9.5, 13.5 Hz), 2.95(1H, dd, *J*=5.5, 15.0 Hz)	7.05-7.28(5H, m)
Met[5]	8.41(1H, d, *J*=7.5 Hz)	4.61(1H, dd, *J*=7.0, 14.5 Hz)	1.75-1.82(1H, m), 1.89-1.97(1H, m)	2.45-2.52(2H, m: γCH_2), 2.02(3H, s: δCH_3)
Pro[5]	-	4.33(1H, dd, *J*=6.5, 6.5 Hz)	1.70-1.80(2H, m)	1.82-1.88(1H, m: γCH_2), 1.90-1.99(1H, m: γCH_2), 3.49-3.55(1H, m: δCH_2), 3.55-3.62(1H, m: δCH_2)
Leu[6]	8.01(1H, d, *J*=7.5 Hz)	4.19-4.25(1H, m)	1.41(2H, dd, *J*=7.0, 7.0 Hz)	1.55-1.64(1H, m: γCH_2), 0.80(3H, d, *J*=6.5 Hz: δCH_2), 0.86(3H, d, *J*=6.5 Hz: δCH_2)
Trp[7]	7.83(1H, dd, *J*=8.0 Hz)	4.56(1H, dd, *J*=7.0, 14.0 Hz)	3.02(1H, dd, *J*=7.5, 15.0 Hz), 3.15(1H, dd, *J*=6.0, 14.5 Hz)	6.97(1H, dd, *J*=7.5, 7.5 Hz: Ind5), 7.03-7.08(1H, m: Ind6), 7.09(1H, s: Ind2), 7.34(1H, d, *J*=8.0 Hz: Ind4), 7.55(1H, d, *J*=8.0 Hz: Ind7), 10.88(1H, bs, IndNH)
Bzl	8.33(1H, t, *J*=6.0 Hz)	4.18-4.30(2H, m)	-	7.05-7.28(5H, m)

Boc-Tyr(t-Bu)-*D*-Ala-Gly-Phe-Pro-Leu-Trp(Boc)-OH; 2 amide bond rotamers at the Pro[6] N, ca. 7:1 ratio (read from NH-Phe), 2 amide bond rotamers at the –CO-IndN, ca. 5:1 ratio (read from Ind2 Trp); ^{1}H-NMR (DMSO-d_6) δ:				
AA	NH	α	β	misc.
Tyr[1]	6.93/6.91(1H, d, *J*=8.4 Hz)	4.08-4.15(1H, m)	2.60-2.72(1H, m), 2.85(1H, dd, *J*=5.4, 13.8 Hz)	6.82(2H, d, *J*=7.8 Hz: PhH), 7.11(2H, d, *J*=7.8 Hz: PhH), 1.60(9H, s: $(CH3)_3COPh$), 1.23(9H, s: $(CH3)_3CO(CO)N$)
D-Ala[2]	7.98-8.02/7.96-7.98/8.01-8.04(1H, m)	4.22-4.30(1H, m)	1.05-1.12(3H, m)	-
Gly[3]	7.96-8.02/8.04-8.07/8.10-8.14(1H, m)	3.50-3.60/3.59-3.63(1H, m), 3.67/3.70(1H, dd, *J*=6.0, 17.4 Hz)	-	-
Phe[4]	8.17/7.71 (1H, d, *J*=7.8 Hz)	4.60-4.68/4.48-4.50(1H, m)	2.63-2.74/2.80-2.83(1H, m), 2.93/2.84(1H, dd, *J*=4.2, 13.2 Hz)	7.12-7.25(5H, m: PhH)
Pro[5]	-	4.32-4.36/4.03-4.07(1H, m)	1.70-1.86/1.53-1.60(2H, m)	1.89-1.96/1.69-1.72(2H, m: γCH_2), 3.40-3.47/3.21-3.25(1H, m: δCH_2), 3.55-3.63/3.32-3.36(1H, m: δCH_2)
Leu[6]	7.85/8.14(1H, d, *J*=7.8 Hz)	4.25-4.33/4.19-4.22(1H, m)	1.41/1.45 (2H, dd, *J*=7.2, 7.2 Hz)	1.60-1.64/1.39-1.42(1H, m: γCH_2), 0.81/0.74(3H, d, *J*=6.6 Hz: δCH_2), 0.85/0.83(3H, d, *J*=6.6 Hz: δCH_2)
Trp[7]	8.01-8.07(1H, m)	4.50-4.60 (1H, m)	3.05(1H, dd, *J*=8.4, 15.0 Hz), 3.15(1H, dd, *J*=4.8, 15.0 Hz)	7.20-7.25(1H, m: Ind5), 7.30(1H, dd, *J*=7.2, 7.2 Hz: Ind6), 7.48/7.47(1H, s: Ind2), 7.59(1H, d, *J*=7.8 Hz: Ind4), 7.98-8.03(1H, m: Ind7), 1.26/1.27(9H, s: $(CH3)_3CO(CO)N$)

Table 3.3.2. ^{1}H Resonance Assignments for Micelle-Bound Bifunctional Peptides with 40-fold DPC in 90% H_2O/10% D_2O, 45mM CD_3CO_2Na, 1mM NaN_3 at 310 K

H-Tyr-*D*-Ala-Gly-Phe-Met-Pro-Leu-Trp-O-3,5-Bzl$(CF_3)_2$·TFA (**TY005**), 3.8 mM, only for the major isomer, δ:				
AA	NH	α	β	misc.
Tyr[1]		4.26	3.09, 3.20	2,6H: 7.18, 3,5H: 6.93
D-Ala[2]	8.69	4.20	1.22	
Gly[3]	8.52	3.86, 3.96		
Phe[4]	7.89	4.70	3.15, 3.20	2,6H: 7.32, 3,5H: 7.35, 4H[a]
Met[5]	8.17	4.69	1.96, 2.05	γ: 2.45, 2.51, CH_3: 2.08
Pro[6]		4.45	1.59, 2.20	γ: 1.78, 1.90, δ: 3.61, 3.71
Leu[7]	7.84	4.44	1.59	γ: 1.59, δ: 0.86
Trp[8]	8.11	4.73	3.34, 3.47	Ind2: 7.42, Ind4: 7.52, Ind5: 7.13, Ind6: 7.00, Ind7: 7.48
3,5-Bn$(CF_3)_2$		5.02, 5.08		2.6H: 7.70, 4H: 7.76

-Tyr-*D*-Ala-Gly-Phe-Met-Pro-Leu-Trp-NH-3,5-Bzl$(CF_3)_2$·TFA (**TY027**), 3.5 mM, only for the major isomer, δ:				
AA	NH	α	β	misc.
Tyr[1]		4.28	3.11, 3.22	2,6H: 7.20, 3,5H: 6.93
D-Ala[2]	8.71	4.24	1.22	
Gly[3]	8.56	3.86, 3.96		
Phe[4]	7.82	4.68	3.13, 3.19	2,6H: 7.27, 3,5H: 7.34, 4H[a]
Met[5]	8.07	4.55	1.91	γ: 2.40, CH_3: 2.01
Pro[6]		4.36	1.18, 2.01	γ: 1.56, 1.69, δ: 3.44, 3.60
Leu[7]	8.35	4.18	1.71	γ: 1.61, δ: 0.92, 0.98
Trp[8]	7.40	4.67	3.31, 3.47	Ind2: 7.40, Ind4: 7.37, Ind5: 6.83, Ind6: 7.10, Ind7: 7.51
3,5-Bn$(CF_3)_2$	8.03	4.41, 4.52		2.6H: 7.85, 4H: 7.75

H-Tyr-*D*-Ala-Gly-Phe-Met-Pro-Leu-Trp-NH-Bzl·TFA (**TY025**), 4.0 mM, only for the major isomer, δ:				
AA	NH	α	β	misc.
Tyr[1]		4.20	3.04, 3.13	2,6H: 7.11, 3,5H: 6.85
D-Ala[2]	8.62	4.17	1.14	
Gly[3]	8.47	3.78, 3.88		
Phe[4]	7.73	4.60	3.04, 3.11	2,6H: 7.19, 3,5H: 7.26, 4H[a]
Met[5]	7.94	4.41	1.79	γ: 2.31, 2.37, CH_3: 2.04
Pro[6]		4.23	0.78, 1.83	γ: 1.23, 1.50, δ: 2.97, 3.43
Leu[7]	8.46	4.05	1.67	γ: 1.55, δ: 0.85, 0.93
Trp[8]	7.14	4.61	3.23, 3.54	Ind2: 7.36, Ind4: 7.53, Ind5: 6.96, Ind6: 7.10, Ind7: 7.48
Bzl	7.42	4.17, 4.33		2.6H: 7.14, 3,5H: 7.09, 4H[a]

[a]: not observed. Ind# represents the corresponding resonances in indole ring of Trp.

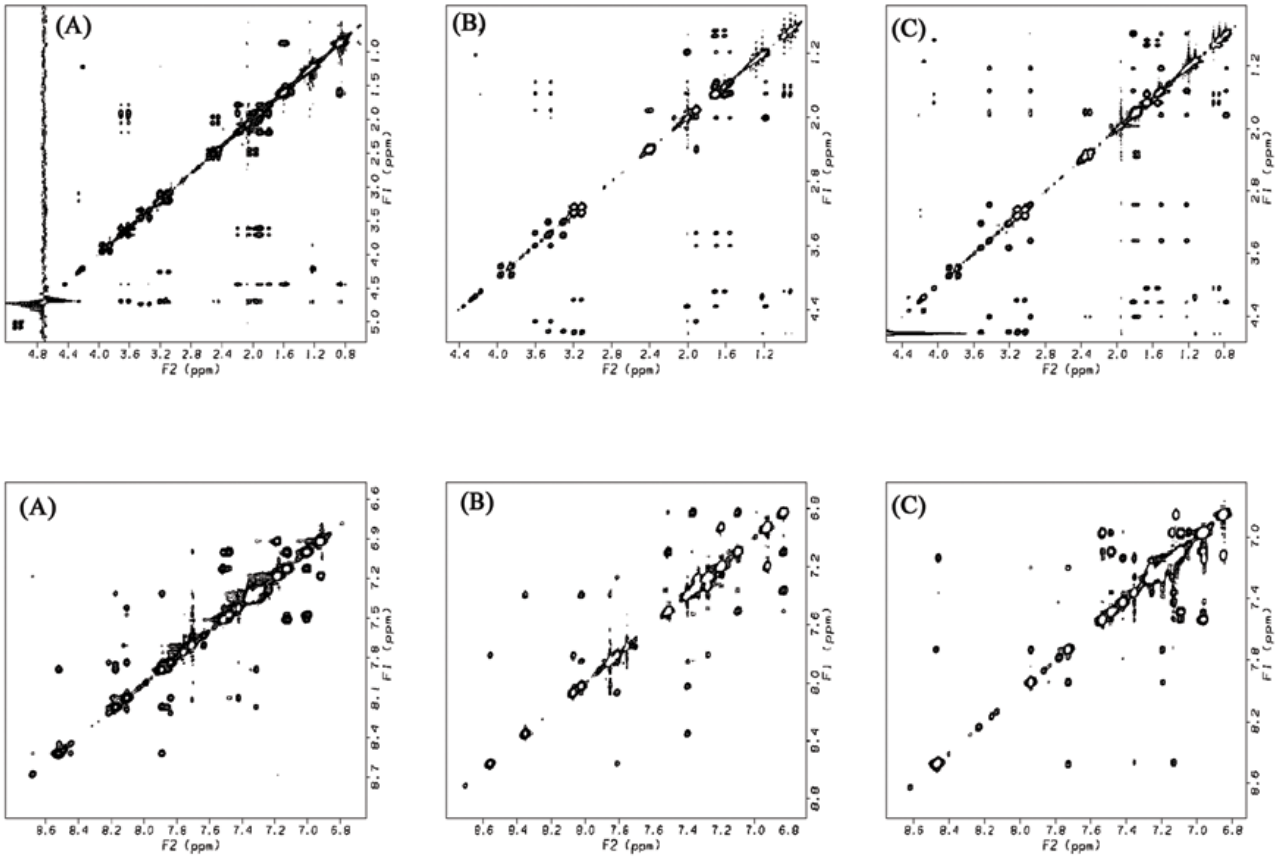

Figure 3.3.1. Side-chain region (upper row) and H^N-H^N reagion (bottom) of the NOESY spectrum of (A) **TY005**, (B) **TY027** and (C) **TY025** in DPC micelles.

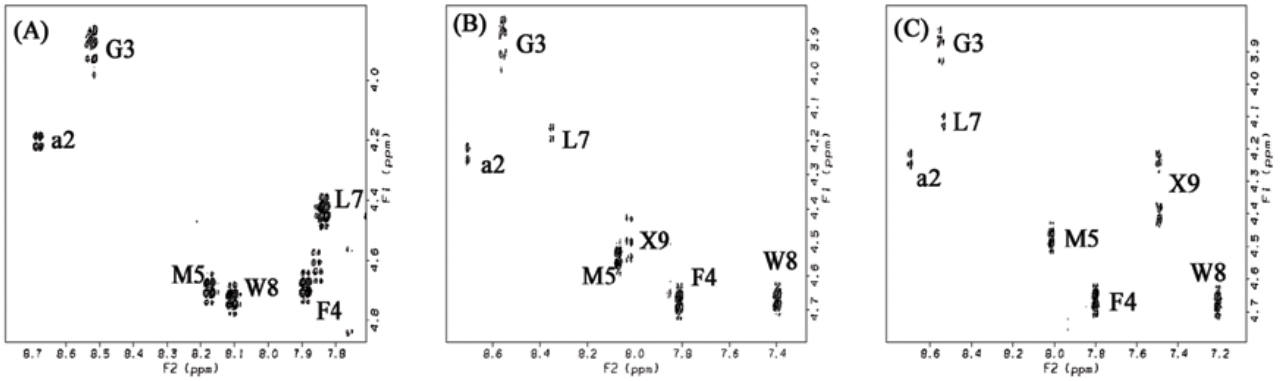

Figure 3.3.2. Fingerprint (H^N-H^α) region of the DQF-COSY spectrum of (A) **TY005**, (B) **TY027** and (C) **TY025** in DPC micelles. Intraresidue H^N-H^α cross-peaks are labeled with residue number. X9 represents the cross-peaks derived from the corresponding *C*-terminal H^N and benzyl protons.

Chapter 4

Conclusions

4.1. Conclusions.

The molecular structure determines various properties and characters of a molecule or a group of molecules, including the binding properties of a bioactive ligand on the targeted receptor. In this thesis, the discussions were made on the determining factors of a molecular structure from the various standpoints (the theoretical chemistry with the orbital-orbital interaction and the structural biochemistry with the NMR experiments). In the first half of this thesis, the importance of electron delocalization, especially the lone pair delocalization of heteroatoms, was suggested in understanding molecular structures and electronic states of 1,2-dihaloethenes and 1,2-dihalodiazenes. This quantum-chemical concept regarding the orbital-orbital interactions could be a guide to new aspect of modern organic chemistry to understand diverse molecular phenomena. Moreover, such a discussion of the thermodynamically stable configuration of these simple molecules can provide important information on the proper molecular structure of bioactive ligand, since *cis*-*trans* configuration has a significant effect on the biological behaviors in many bioactive ligands.[26-28, 30] The latter half of this thesis has shown that only a small and local substitution of a functional group on a peptide ligand, such as the introduction of trifluoromethyl groups at the *C*-terminus, determines the entire conformation of bioactive ligand. It was also suggested that this change in the three-dimensional molecular structure of ligand had the important relevance to the ligand-receptor binding to yield the bioactivities at the opioid and NK1 receptors.

Through these discussions, this thesis could provide important insights and basic information of the factors determining a molecular structure to understand wide-range of chemical phenomena at the molecular level to control their properties and characters, especially for understanding the ligand's binding at the targeted receptor. The decreasing number of approved new drugs in this few years has become a large problem not only for the pharmaceutical market, but for suffering patients who really need new and effective drugs. The information provided in this thesis could be applied for the efficient and rational design of a novel ligand to be a next generation drug candidate.

Chapter 5

References

5.1. References

1. Wermuth, C. G. *The Practice of Medicinal Chemistry*. Academic Press: New York 1996.
2. Corey, F. A. *Organic Chemistry*. McGraw hill: New York, 2000.
3. McMarry, J. E. *Organic Chemistry*. Brooks/Cole, Tomson Learning: New York, 1999.
4. Tomoda, S. *Basic Quantum Chemistry; The Paradigm of Orbital Concepts (written in Japanese)*. Univ. of Tokyo Press: Tokyo, Japan, 2007.
5. March, J. *Advanced Organic Chemistry*. John Weily & Sons: New York, 1992.
6. Weinhold, F. Chemistry. A new twist on molecular shape. *Nature* **2001,** 411, 539-541.
7. Bingham, R. C. The stereochemical consequences of electron delocalization in extended .pi. systems. An interpretation of the cis effect exhibited by 1,2-disubstituted ethylenes and related phenomena. *J. Am. Chem. Soc.* **1976,** 98, 535-540.
8. Wiberg, K. B.; Murcko, M. A.; Laidig, K. E.; MacDougall, P. J. Origin of the "gauche effect" in substituted ethanes and ethenes. *J. Phys. Chem.* **1990,** 94, 6956-6959.
9. Wiberg, K. B. Bent Bonds in Organic Compounds. *Acc. Chem. Res.* **1996,** 29, 229-234.
10. Engkvist, O.; Karlstrom, G.; Widmark, P. O. On the origin of the gauche effect. A quantum chemical study of 1,2-difluoroethane. *Chem. Phys. Lett.* **1997,** 265.
11. Yamamoto, T.; Tomoda, S. On the origin of cis-effect in 1,2-difluoroethene. *Chem. Lett.* **1997,** 26, 1069-1070.
12. Yamamoto, T.; Kaneno, D.; Tomoda, S. The importance of lone pair electron delocalization in the cis–trans isomers of 1,2-dibromoethenes. *Chem. Lett.* **2005,** 34, 1190-1091.
13. Novak, I. Chlorofluoroethenes. Thermochemical stability and cis-effect. *J. Org. Chem.* **2000,** 65, 5057-5058.
14. Kanakaraju, R.; Senthilkumar, K.; Kolandaivel, P. Origin of the cis effect—nonbonded intramolecular

interactions: quantum chemical studies on 1,2-dihaloethylene molecules *J. Mol. Struct. (THEOCHEM)* **2002,** 589-590, 95-102.

15. Hehre, W. J.; Radom, L.; Schleyer, R. v. R.; Pople, J. In *A. Ab Initio Molecular Orbital Theory*, John Wiley & Sons: New York, 1986; p 298.
16. Binkley, J. S.; Pople, J. A. Relative Stability of 1,2-Difluoroethylenes. *Chem. Phys Lett.* **1977,** 45, 197-200.
17. Cremer, D. The Role of Correlation in Calculations on 1,2-Difluoroethylenes. The Cis-Trans Energy Difference. *Chem. Phys. Lett.* **1981,** 81, 481-485.
18. Gandhi, S. R.; Benzel, M. A.; Dykstra, C. E.; Fukunaga, T. Role of electron correlation and polarization functions in the energy difference between cis- and trans-1,2-difluoroethylene. *J. Phys. Chem.* **1982,** 86, 3121-3126.
19. Dixon, D. A.; Fukunaga, T.; Smart, B. E. Geometries and energies of the fluoroethylenes *J. Am. Chem. Soc.* **1986,** 108, 1585-1588.
20. Saebø, S.; Sellers, H. Effect of electron correlation on the structures and relative stability of cis- and trans-1,2-difluoroethylene *J. Phys. Chem.* **1988,** 92, 4266-4269.
21. Epiotis, N. D.; Yates, R. L. Overlap repulsion as an important contributor to aromaticity *J. Am. Chem. Soc.* **1976,** 98, 461-469.
22. Bernardi, F.; Bottoni, A.; Epiotis, N. D.; Guerra, M. Quantitative nonempirical estimates of the effects of orbital interactions. Applications to difluoroethylenes *J. Am. Chem. Soc.* **1978,** 100, 6018-6022.
23. Craig, N. C.; Piper, L. G.; Wheeler, V. L. Thermodynamics of cis-trans Isomerizations. II. The 1-Chloro-2-fluoroethylenes, 1, 2-Difluorocyclopropanes, and Related Molecules. *J. Phys. Chem.* **1971,** 75, 1453-1460.
24. Nordhoff, K.; Anders, E. MO Theoretical Investigation of the Cis Effect Observed in Mono- and Dihalodiazenes *J. Org. Chem.* **1999,** 64, 7485-7491.
25. Yamamoto, T.; Kaneno, D.; Tomoda, S. The importance of lone pair delocalizations: theoretical

investigations on the stability of cis and trans isomers in 1,2-halodiazenes. *J. Org. Chem.* **2008**, In press.

26. Alloatti, D.; Giannini, G.; Cabri, W.; Lustrati, I.; Marzi, M.; Ciacci, A.; Gallo, G.; Tinti, M. O.; Marcellini, M.; Riccioni, T.; Guglielmi, M. B.; Carminati, P.; Pisano, C. Synthesis and biological activity of fluorinated combretastatin analogues. *J. Med. Chem.* **2008,** 51, 2708-2721.
27. Knauer, T. E.; Siegfried, C.; Willingham, A. K.; Matschiner, J. T. Metabolism and biological activity of cis- and trans-phylloquinone in the rat. *J. Nutr.* **1975,** 105, 1519-1524.
28. Mollica, A.; Guardiani, G.; Davis, P.; Ma, S. W.; Porreca, F.; Lai, J.; Mannina, L.; Sobolev, A. P.; Hruby, V. J. Synthesis of Stable and Potent delta/mu Opioid Peptides: Analogues of H-Tyr-c[d-Cys-Gly-Phe-d-Cys]-OH by Ring-Closing Metathesis. *J. Med. Chem.* **2007,** 50, 3138-3142.
29. Carceller, E.; Salas, J.; Merlos, M.; Giral, M.; Ferrando, R.; Escamilla, I.; Ramis, J.; Garcia-Rafanell, J.; Forn, J. Novel azo derivatives as prodrugs of 5-aminosalicylic acid and amino derivatives with potent platelet activating factor antagonist activity. *J. Med. Chem.* **2001,** 44, 3001-3013.
30. Dugave, C.; Demange, L. Cis-trans isomerization of organic molecules and biomolecules: implications and applications. *Chem. Rev.* **2003,** 103, 2475-2532.
31. Morris, G. M.; Goodsell, D. S.; Halliday, R. S.; Huey, R.; Hart, W. E.; Belew, R. K. Automated docking using a Lamarckian genetic algorithm and an empirical binding free energy function. *J. Comp. Chem.* **1998,** 19, 1639-1662.
32. Lengauer, T.; Rarey, M. Computational methods for biomolecular docking. *Curr. Opin. Struct. Biol.* **1996,** 6, 402-406.
33. Blundell, T. L.; Sibanda, B. L.; Sternberg, M. J. E.; Thornton, J. M. Knowledge-based prediction of protein structures and the design of novel molecules. *Nature* **1987,** 326, 347-352.
34. Fetrow, J. S.; Bryant, S. H. New programs for protein tertiary structure prediction. *Bio/Technology* **1993,** 11, 479-484.
35. Vakser, I. A.; Kundrotas, P. Predicting 3D structures of protein-protein complexes. *Curr Pharm*

Biotechnol. **2008** 9, 57-66.

36. Wong, C. F. Flexible ligand-flexible protein docking in protein kinase systems. *Biochim Biophys Acta* **2008** 1784, 244-251.

37. Totrov, M.; Abagyan, R. Flexible ligand docking to multiple receptor conformations: a practical alternative. *Curr. Opin. Struct. Biol.* **2008** 18, 178-184.

38. Berthold, M.; Bartfai, T. Modes of peptide binding in G protein-coupled receptors. *Neurochem. Res.* **1997,** 22, 1023-1031.

39. Noeskea, T. G., A.; Parsonsa, C. G.; Weila, T. Allosteric modulation of family 3 GPCRs. *QSAR Comb. Sci.* **2006,** 25, 134-146.

40. Eguchi, M. Recent advances in selective opioid receptor agonists and antagonists. *Med. Res. Rev.* **2004,** 24, 182-212.

41. Cascieri, M. A.; Macleod, A. M.; Underwood, D.; Shiao, L. L.; Ber, E.; Sadowski, S.; Yu, H.; Merchant, K. J.; Swain, C. J.; Strader, C. D.; Fong, T. M. Characterization of the interaction of N-acyl-L-tryptophan benzyl ester neurokinin antagonists with the human neurokinin-1 receptor. *J. Biol. Chem.* **1994,** 269, 6587-6591.

42. D'Alagni, M.; Delfini, M.; Di Nola, A.; Eisenberg, M.; Paci, M.; Roda, L. G.; Veglia, G. Conformational study of [Met5]enkephalin-Arg-Phe in the presence of phosphatidylserine vesicles. *Eur. J. Biochem.* **1996,** 240, 540-549.

43. Deber, C. M.; Behnam, B. A. Role of membrane lipids in peptide hormone function: binding of enkephalins to micelles. *Proc. Natl. Acad. Sci. U. S. A.* **1984,** 81, 61-65.

44. Sargent, D. F.; Schwyzer, R. Membrane lipid phase as catalyst for peptide-receptor interactions. *Proc. Natl. Acad. Sci. U. S. A.* **1986,** 83, 5774-5778.

45. Wienk, H. L.; Wechselberger, R. W.; Czisch, M.; de Kruijff, B. Structure, dynamics, and insertion of a chloroplast targeting peptide in mixed micelles. *Biochemistry* **2000,** 39, 8219-27.

46. Wienk, H. L.; Wechselberger, R. W.; Czisch, M.; de Kruijff, B. Structure, dynamics, and insertion of a

chloroplast targeting peptide in mixed micelles. *Biochemistry* **2000,** 39, 8219-8227.

47. Bryson, E. A.; Rankin, S. E.; Carey, M.; Watts, A.; Pinheiro, T. J. Folding of apocytochrome c in lipid micelles: formation of alpha-helix precedes membrane insertion. *Biochemistry* **1999,** 38, 9758-9767.

48. Saffman, P. G.; Delbruck, M. Brownian motion in biological membranes. *Proc. Natl. Acad. Sci. U. S. A.* **1975,** 72, 3111-3113.

49. Palian, M. M.; Boguslavsky, V. I.; O'Brien, D. F.; Polt, R. Glycopeptide-membrane interactions: glycosyl enkephalin analogues adopt turn conformations by NMR and CD in amphipathic media. *J. Am. Chem. Soc.* **2003,** 125, 5823-5831.

50. Dhanasekaran, M.; Palian, M. M.; Alves, I.; Yeomans, L.; Keyari, C. M.; Davis, P.; Bilsky, E. J.; Egleton, R. D.; Yamamura, H. I.; Jacobsen, N. E.; Tollin, G.; Hruby, V. J.; Porreca, F.; Polt, R. Glycopeptides related to beta-endorphin adopt helical amphipathic conformations in the presence of lipid bilayers. *J. Am. Chem. Soc.* **2005,** 127, 5435-5448.

51. Jacobsen, N. E.; Abadi, N.; Sliwkowski, M. X.; Reilly, D.; Skelton, N. J.; Fairbrother, W. J. High-resolution solution structure of the EGF-like domain of heregulin-alpha. *Biochemistry* **1996,** 35, 3402-3417.

52. Ying, J.; Ahn, J. M.; Jacobsen, N. E.; Brown, M. F.; Hruby, V. J. NMR solution structure of the glucagon antagonist [desHis1, desPhe6, Glu9]glucagon amide in the presence of perdeuterated dodecylphosphocholine micelles. *Biochemistry* **2003,** 42, 2825-2835.

53. Deslongchamps, P. *Stereoelectronic Effects in Organic Chemistry*. Pergamon: Oxford, 1983.

54. Deslongchamps, P. Stereoelectronic Control in the Cleavage of Tetrahedral Intermediates in the Hydrolysis of Esters and Amides. *Tetrahedron* **1975,** 31, 2463-2490.

55. Gillespie, R. J.; Popelier, P. L. A. *Chemical Bonding and Molecular Geometry. From Lewis to Electron Densities*. Oxford University Press: Oxford, 2001.

56. Wiberg, K. B.; Rush, D. J. Methyl rotational barriers in amides and thioamides. *J. Org. Chem.* **2002,** 67, 826-830.

57. Sovers, O. J.; Kern, C. W.; Pitzer, R. M.; Karplus, M. Bond-Function Analysis of Rotational Barriers: Ethane. *J. Chem. Phys.* **1968,** 49, 2592-2599.

58. Christiansen, P. A.; Palke, W. E. A study of the ethane internal rotation barrier. *Chem. Phys. Lett.* **1975,** 31, 462-466.

59. Schreiner, P. R. Teaching the right reasons: lessons from the mistaken origin of the rotational barrier in ethane. *Angew. Chem. Int. Ed. Engl.* **2002,** 41, 3579-3581.

60. Pophristic, V.; Goodman, L. Hyperconjugation not steric repulsion leads to the staggered structure of ethane. *Nature* **2001,** 411, 565-568.

61. Goodman, L.; Pophristic, V.; Weinhold, F. Origin of Methyl Internal Rotation Barriers. *Acc. Chem. Res.* **1999,** 32, 983-993.

62. Reed, A. E.; Weinhold, F. Natural bond orbital analysis of internal rotation barriers and related phenomena. *Isr. J. Chem.* **1991,** 31, 277-285.

63. Lowe, J. P. Simple molecular orbital explanation for the barrier to internal rotation in ethane and other molecules. *J. Am. Chem. Soc.* **1970,** 92, 3799-3800.

64. Alabugin, I. V.; Zeidan, T. A. Stereoelectronic effects and general trends in hyperconjugative acceptor ability of sigma bonds. *J. Am. Chem. Soc.* **2002,** 124, 3175-3185.

65. Pitzer, K. S.; Hollenberg, J. L. cis- and trans-Dichloroethylenes. The Infrared Spectra from 130-400 Cm.-1 and the Thermodynamic Properties. *J. Am. Chem. Soc.* **1954,** 76, 1493-1496.

66. Waldron, J. T.; Snyder, W. H. Thermodynamics of cis-trans isomerizations. Relative stabilities of the 1,2-dimethoxyethylenes. *J. Am. Chem. Soc.* **1973,** 95, 5491-5495.

67. Natural Bond Orbital NBO 5.0 Homepage. http://www.chem.wisc.edu/~nbo5/

68. Glendening, E. D.; Badenhoop, J. K.; Reed, A. E.; Carpenter, J. E.; Bohmann, J. A.; Morales, C. M.; Weinhold, F. *NBO 5.G Program.*, Theoretical Chemistry Institute, University of Wisconsin: Madison 2001.

69. Reed, A. E.; Weinhold, F. Natural bond orbital analysis of near-Hartree–Fock water dimer. *J. Chem.*

Phys. **1983,** 78, 4066-4073.

70. Reed, A. E.; Weinhold, F. Natural localized molecular orbitals. *J. Chem. Phys.* **1985,** 83, 1736-1740.

71. Reed, A. E.; Curtiss, L. A.; Weinhold, F. Intermolecular interactions from a natural bond orbital, donor-acceptor viewpoint. *Chem. Rev.* **1988,** 88, 899-926.

72. Fukui, K.; Inagaki, S. Orbital interaction rationale for the role of catalysts *J. Am. Chem. Soc.* **1975,** 97, 4445-4452.

73. Inagaki, S.; Fujimoto, H.; Fukui, K. Orbital interaction in three systems *J. Am. Chem. Soc.* **1976,** 98, 4693-4701.

74. Inagaki, S.; Kawata, H.; Hirabayashi, Y. Orbital phase theory for acyclic systems. *Bull. Chem. Soc. Jpn.* **1982,** 55, 3724-3732.

75. Inagaki, S.; Iwase, K. Unnecessary parallelism between kinetic and thermodynamic stabilities of cyclic conjugated hydrocarbons: an orbital phase criterion for reactivity. *Nouv. J. Chim.* **1984,** 8, 73-76.

76. Ma, J.; Inagaki, S. Cyclic Delocalization of the Oxygen Lone Pair Electrons in the Unusual Structures of Disilaoxirane and 1,3-Cyclodisiloxane *J. Phys. Chem. A* **2000,** 104, 8989-8994.

77. Ma, J.; Hozaki, A.; Inagaki, S. Pentagon Stability in Cycloarsanes *Phosphorus, Sulfur, Silicon Relat. Elem.* **2002,** 177, 1705-1708.

78. Ma, J.; Hozaki, A.; Inagaki, S. Pentagon Stability: Cyclic Delocalization of Lone Pairs through sigma Conjugation and Design of Polycyclophosphanes *Inorg. Chem.* **2002,** 41, 1876-1882.

79. Ma, J.; Ding, Y.; Hattori, K.; Inagaki, S. Theoretical Designs of Singlet Localized 1,3-Diradicals *J. Org. Chem.* **2004,** 69, 4245-4255.

80. Naruse, Y.; Ma, J.; Inagaki, S. Relaxation of ring strain by introduction of a double bond. *Tetrahedron Lett.* **2001,** 42, 6553-6556.

81. Naruse, Y.; Inagaki, S. Participation of Geminal Bonds in Organic Reactions. *Chem. Lett.* **2007,** 36, 820-825.

82. Frisch, M. J.; Trucks, G. W.; Schlegel, H. B.; Scuseria, G. E.; Robb, M. A.; Cheeseman, J. R.;

Montgomery, J., J. A.; Vreven, T.; Kudin, K. N.; Burant, J. C.; Millam, J. M.; Iyengar, S. S.; Tomasi, J.; Barone, V.; Mennucci, B.; Cossi, M.; Scalmani, G.; Rega, N.; Petersson, G. A.; Nakatsuji, H.; Hada, M.; Ehara, M.; Toyota, K.; Fukuda, R.; Hasegawa, J.; Ishida, M.; Nakajima, T.; Honda, Y.; Kitao, O.; Nakai, H.; Klene, M.; Li, X.; Knox, J. E.; Hratchian, H. P.; Cross, J. B.; Bakken, V.; Adamo, C.; Jaramillo, J.; Gomperts, R.; Stratmann, R. E.; Yazyev, O.; Austin, A. J.; Cammi, R.; Pomelli, C.; Ochterski, J. W.; Ayala, P. Y.; Morokuma, K.; Voth, G. A.; Salvador, P.; Dannenberg, J. J.; Zakrzewski, V. G.; Dapprich, S.; Daniels, A. D.; Strain, M. C.; Farkas, O.; Malick, D. K.; Rabuck, A. D.; Raghavachari, K.; Foresman, J. B.; Ortiz, J. V.; Cui, Q.; Baboul, A. G.; Clifford, S.; Cioslowski, J.; Stefanov, B. B.; Liu, G.; Liashenko, A.; Piskorz, P.; Komaromi, I.; Martin, R. L.; Fox, D. J.; Keith, T.; Al-Laham, M. A.; Peng, C. Y.; Nanayakkara, A.; Challacombe, M.; Gill, P. M. W.; Johnson, B.; Chen, W.; Wong, M. W.; Gonzalez, C.; Pople, J. A. *Gaussian 03*, Revision C.02; Gaussian, Inc.: Wallingford CT, 2004.

83. *SPARTAN*, ver. 4.1.1; Wavefunction, Inc.: Irvine, CA, 1995.

84. Glendening, E. D.; Carpenter, J. E.; Weinhold, F. *Orbplot* ver. 2.0 NBO Orbital Plotter; Theoretical Chemistry Institute, University of Wisconsin: Madison, 1992.

85. Badenhoop, J. K.; Weinhold, F. Natural bond orbital analysis of steric interactions. *J. Chem. Phys.* **1997,** 107, 5406-5421.

86. Badenhoop, J. K.; Weinhold, F. Natural steric analysis: Ab initio van der Waals radii of atoms and ions. *J. Chem. Phys.* **1997,** 107, 5422-5432.

87. Badenhoop, J. K.; Weinhold, F. Natural steric analysis of internal rotation barriers. *Int. J. Quantum. Chem.* **1999,** 72, 269-280.

88. Schleyer, P. v. R.; Kaupp, M.; Hampel, F.; Bremer, M.; Mislow, K. Relationships in the rotational barriers of all Group 14 ethane congeners H3X-YH3 (X, Y = C, Si, Ge, Sn, Pb). Comparisons of ab initio pseudopotential and all-electron results *J. Am. Chem. Soc.* **1992,** 114, 6791-6797.

89. Spelbos, A.; Huisman, P. A. G.; Mijlhoff, F. C.; Renes, G. H. Molecular structure of cis-1,2-

difluoroethene as determined from gas phase electron diffraction and microwave data. *J. Mol. Struct. (THEOCHEM)* **1978,** 44, 159-168.

90. Kuchitsu, K. *Structure data of free polyatomic molecules*. Springer-Verlag: Berlin, 1994.

91. Craig, N. C.; Brandon, D. W.; Stone, S. C.; Lafferty, W. J. Partial structure for trans-1,2-difluoroethylene from high-resolution infrared spectroscopy *J. Phys. Chem.* **1992,** 96, 1598-1605.

92. Schäfer, L.; Ewband, J. D.; Siam, K.; Paul, D. W.; Monts, D. L. The molecular structures of cis- and trans-1,2-dichloroethene: a real-time gas electron diffraction and ab initio study. *J. Mol. Struct. (THEOCHEM)* **1986,** 145, 135-142.

93. Davis, M. I.; Kappler, H. A.; Cowan, D. J. A Gas-Phase Electron Diffraction Study of cis-Dibromoethylene *J. Phys. Chem.* **1964,** 68, 2005-2007.

94. Mitsunobu, O. The Use of Diethyl Azodicarboxylate and Triphenylphosphine in Synthesis and Transformation of Natural Products Synthesis. *Synthesis* **1981**, 1-28.

95. Mitsunobu, O.; Yamada, M. Preparation of esters of carboxylic and phosphoric acid via quaternary phosphonium slats. *Bull. Chem. Soc. Jpn.* **1967,** 40, 2380-2382.

96. Tsunoda, T.; Otsuka, J.; Yamamiya, Y.; Ito, S. N,N,N',N' -tetramethylazodicarboxamide (TMAD), a new versatile reagent for Mitsunobu reaction. Its application to synthesis of secondary amines. *Chem. Lett.* **1994**, 539-542.

97. Tsunoda, T.; Yamamiya, Y.; Ito, S. 1,1'-(Aazodicarbonyl)dipiperidine-tributylphosphine, a new reagent system for Mitsunobu reaction. *Tetrahedron Lett.* **1993,** 34, 1639-1642.

98. Tsunoda, T.; Yamamiya, Y.; Kawamura, Y.; Ito, S. Mitsunobu acylation of sterically congested secondary alcohols by N,N,N',N'-tetramethylazodicarboxamide-tributylphosphine reagents *Tetrahedron Lett.* **1995,** 36, 2529-2530.

99. Milligan, D. E. Infrared Spectroscopic Study of the Photolysis of Chlorine Azide in Solid Argon at 4.2°K *J. Chem. Phys.* **1961,** 35, 372-373.

100. Tschumper, G. S.; Heaven, M. C.; Morokuma, K. An ab initio Excursion on the Lowest 18 Electronic

Surfaces o f the NCl + NCl System: Some Insight into the Long-Range Self-Quenching Pathways of the First Excited State of NCl. *J. Phys. Chem. A* **2002,** 106, 8453-8460.

101. Tschumper, G. S.; Heaven, M. C.; Morokuma, K. Concerning the Stability of Dichlorodiazene. *Chem. Phys. Lett.* **2003,** 370, 418-424.

102. Schneider, S.; Gerken, M.; Haiges, R.; Schroer, T.; Boatz, J. A.; Dixon, D. A.; Grant, D. J.; Christe, K. O. Synthesis and Characterization of Silyldichloramines, Their Reactions with F- Ions, Instability of N2Cl2 and NCl2-, and Formation of NCl3 *Inorg. Chem.* **2007,** 46, 93-102.

103. Armstrong, G. T.; Marantz, S. Heats of Formation of Two Isomers of Difluorodiazine. *J. Chem. Phys.* **1963,** 38, 169-172.

104. Wolfe, S. Gauche effect. Stereochemical consequences of adjacent electron pairs. and polar bonds. *Acc. Chem. Res.* **1972,** 5, 102-111.

105. Wolfe, S.; Rauk, A.; Tel, F. M.; Csizmadia, G. I. A theoretical study of the Edward–Lemieux effect (the anomeric effect). The stereochemical requirements of adjacent electron pairs and polar bonds. *J. Chem. Soc. B* **1971**, 136-144.

106. Wolfe, S.; Tel, L. M.; Liang, J. H.; Csizmadia, I. G. Stereochemical consequences of adjacent electron pairs. Theoretical study of rotation-inversion in ethylene dicarbanion *J. Am. Chem. Soc.* **1972,** 94, 1361-1364.

107. Epiotis, N. D.; Yates, R. L.; Larson, J. R.; Kirmaier, C. R.; Bernardi, F. Directional effects of sigma. conjugation on geometrical isomerism *J. Am. Chem. Soc.* **1977,** 99, 8379-8388.

108. Straume, K.; Skancke, A. The molecular structure of FNNF. A study of the cis effect. *Chem Phys. Lett.* **1980,** 73, 378-380.

109. Rosengren, K.; Pimentel, G. C. Infrared Detection of Diimide, N2H2, and Imidogen, NH, by the Matrix Isolation Method. *J. Chem. Phys.* **1965,** 43, 507-516.

110. Demaison, J.; Hegelund, F.; Bürger, H. Experimental and ab initio equilibrium structure of trans-diazene HNNH. *J. Mol. Struct. (THEOCHEM)* **1997,** 413-414, 447-456.

111. Back, R. A.; Willis, C.; Ramsay, D. A. Near-ultraviolet Absorption Spectrum of Diimide Vapor *Can. J. Chem.* **1974,** 52, 1006-1012.

112. Zheng, W.; Jewitt, D.; Osamura, Y.; Kaiser, R. I. Formation of nitrogen and hydrogen-bearing molecules in solid ammonia and implications for solar system and interstellar ices. *Astrophysical J.* **2008,** 674, 1242-1250.

113. Wiberg, N.; Fischer, G.; Bachhnber, H. cis- and trans-Diazene (Diimine). *Angew. Chem. Int. Ed. Engl.* **1977,** 16, 780-781.

114. Jursic, B. S. Ab initio and density functional theory study of the diazene isomerization. *Chem. Phys. Lett.* **1996,** 261, 13-17.

115. Lee, T. J.; Rice, J. E.; Scuseria, G. E.; Schaefer, I. H. F. Theoretical Investigations of Molecules Composed Only of Fluorine, Oxygen, and Nitrogen: Determination of the Equilibrium Structures of FOOF, $(NO)_2$, and FNNF and the Transition State Structure for FNNF Cis-Trans Isomerization. *Theor. Chem. Acta.* **1989,** 75, 81-98.

116. Jursic, B. S. Density Functional Calculations of Difluorodiazete Structures with Gaussian-Orbital-Type Approach *Int. J. Quantum, Chem.* **1996,** 57, 213-217.

117. Kuczkowski, R.; Wilson, E. B. Microwave Spectrum, Structure, and Dipole Moment of "Cis"-N2F2 *J. Chem. Phys.* **1963,** 39, 1030-1034.

118. Bohn, R. K.; Bauer, S. H. An electron diffraction study of the structures of cis- and trans N_2F_2 *Inorg. Chem.* **1967,** 6, 309-312.

119. Carlotti, M.; Johns, J. W. C.; Trombetti, A. The v5 Fundamental Bands of N_2H_2 and N_2D_2 *Can. J. Phys.* **1974,** 52, 340-344.

120. Janecka, A.; Fichna, J.; Janecki, T. Opioid receptors and their ligands. *Curr. Top. Med. Chem.* **2004,** 4, 1-17.

121. Gentilucci, L.; Tolomelli, A. Recent advances in the investigation of the bioactive conformation of peptides active at the micro-opioid receptor. conformational analysis of endomorphins. *Curr. Top. Med.*

Chem. **2004,** 4, 105-121.

122. Ling, G. S.; Spiegel, K.; Lockhart, S. H.; Pasternak, G. W. Separation of opioid analgesia from respiratory depression: evidence for different receptor mechanisms. *J. Pharmacol. Exp. Ther.* **1985,** 232, 149-155.

123. Paakkari, P.; Paakkari, I.; Vonhof, S.; Feuerstein, G.; Siren, A. L. Dermorphin analog Tyr-D-Arg2-Phe-sarcosine-induced opioid analgesia and respiratory stimulation: the role of mu 1-receptors? *J. Pharmacol. Exp. Ther.* **1993,** 266, 544-550.

124. Ripley, T. L.; Gadd, C. A.; De Felipe, C.; Hunt, S. P.; Stephens, D. N. Lack of self-administration and behavioural sensitisation to morphine, but not cocaine, in mice lacking NK1 receptors. *Neuropharmacology* **2002,** 43, 1258-1268.

125. King, T.; Gardell, L. R.; Wang, R.; Vardanyan, A.; Ossipov, M. H.; Malan, T. P., Jr.; Vanderah, T. W.; Hunt, S. P.; Hruby, V. J.; Lai, J.; Porreca, F. Role of NK-1 neurotransmission in opioid-induced hyperalgesia. *Pain* **2005,** 116, 276-288.

126. Ma, W.; Zheng, W. H.; Kar, S.; Quirion, R. Morphine treatment induced calcitonin gene-related peptide and substance P increases in cultured dorsal root ganglion neurons. *Neuroscience* **2000,** 99, 529-539.

127. Powell, K. J.; Quirion, R.; Jhamandas, K. Inhibition of neurokinin-1-substance P receptor and prostanoid activity prevents and reverses the development of morphine tolerance in vivo and the morphine-induced increase in CGRP expression in cultured dorsal root ganglion neurons. *Eur. J. Neurosci.* **2003,** 18, 1572-1583.

128. Misterek, K.; Maszczynska, I.; Dorociak, A.; Gumulka, S. W.; Carr, D. B.; Szyfelbein, S. K.; Lipkowski, A. W. Spinal co-administration of peptide substance P antagonist increases antinociceptive effect of the opioid peptide biphalin. *Life Sci.* **1994,** 54, 939-944.

129. Gu, G.; Kondo, I.; Hua, X. Y.; Yaksh, T. L. Resting and evoked spinal substance P release during chronic intrathecal morphine infusion: parallels with tolerance and dependence. *J. Pharmacol. Exp.*

Ther. **2005,** 314, 1362-1369.

130. Mantyh, P. W.; Allen, C. J.; Ghilardi, J. R.; Rogers, S. D.; Mantyh, C. R.; Liu, H.; Basbaum, A. I.; Vigna, S. R.; Maggio, J. E. Rapid endocytosis of a G protein-coupled receptor: substance P evoked internalization of its receptor in the rat striatum in vivo. *Proc. Natl. Acad. Sci. U. S. A.* **1995,** 92, 2622-2626.
131. Kalso, E. Improving opioid effectiveness: from ideas to evidence. *Eur. J. Pain.* **2005,** 9, 131-135.
132. King, T.; Ossipov, M. H.; Vanderah, T. W.; Porreca, F.; Lai, J. Is paradoxical pain induced by sustained opioid exposure an underlying mechanism of opioid antinociceptive tolerance? *Neurosignals* **2005,** 14, 194-205.
133. Hokfelt, T.; Kellereth, J. O.; Nilsson, G. Immunohistochemical studies on the localization and distribution of substance P in cat primary sensory neurons. *Brain Res.* **1975,** 100, 235-252.
134. Marchand, J. E.; Kream, R. M. Substance P and Somatostatin levels in rhumatioid arthesis, molecular physiology. In *Substance P and Related Peptides: Cellular and Molecular Physiology*, New York Academy of Science: New York, 1937; pp 437-438.
135. Kondo, I.; Marvizon, J. C.; Song, B.; Salgado, F.; Codeluppi, S.; Hua, X. Y.; Yaksh, T. L. Inhibition by spinal mu- and delta-opioid agonists of afferent-evoked substance P release. *J. Neurosci.* **2005,** 25, 3651-3660.
136. Yamamoto, T.; Nair, P.; Davis, P.; Ma, S. W.; Navratilova, E.; Moye, M.; Tumati, S.; Vanderah, T. W.; Lai, J.; Porreca, F.; Yamamura, H. I.; Hruby, V. J. Design, synthesis and biological evaluation of novel bifunctional C-terminal modified peptides for δ/μ opioid receptor agonists and neurokinin-1 receptor antagonists. *J. Med. Chem.* **2007,** 50, 2779 - 2786.
137. Yamamoto, T.; Nair, P.; Jacobsen, N. E.; Davis, P.; Ma, S. W.; Navratilova, E.; Lai, J.; Yamamura, H. I.; Vanderah, T. W.; Porreca, F.; Hruby, V. J. The importance of micelle-bound states for the bioactivities of bifunctional peptide derivatives for δ/μ opioid receptor agonists and neurokinin 1 receptor antagonists. *J. Med. Chem.* **2008**, in press.

138. Bonney, I. M.; Foran, S. E.; Marchand, J. E.; Lipkowski, A. W.; Carr, D. B. Spinal antinociceptive effects of AA501, a novel chimeric peptide with opioid receptor agonist and tachykinin receptor antagonist moieties. *Eur. J. Pharmacol.* **2004,** 488, 91-99.

139. Sakurada, T.; Yuhki, M.; Inoue, M.; Sakurada, C.; Tan-No, K.; Ohba, M.; Kisara, K.; Sakurada, S. Opioid activity of sendide, a tachykinin NK1 receptor antagonist. *Eur. J. Pharmacol.* **1999,** 369, 261-266.

140. Kosson, P.; Bonney, I.; Carr, D. B.; Lipkowski, A. W. Endomorphins interact with tachykinin receptors. *Peptides* **2005,** 26, 1667-1669.

141. Shimohigashi, Y. Design Principles: Enkephalins With Predictable Mu/Delta Receptor Specificity. . *NIDA Res. Monogr.* **1986,** 69, 65-100.

142. Horan, P. J.; Mattia, A.; Bilsky, E. J.; Weber, S.; Davis, T. P.; Yamamura, H. I.; Malatynska, E.; Appleyard, S. M.; Slaninova, J.; Misicka, A.; Lipowski, A. W.; Hruby, V. J.; Porreca, F. Antinociceptive Profile of Biphalin, a Dimeric Enkephalin Analog. *J. Pharmacol. Exp. Ther.* **1993,** 265, 1446-1454.

143. MacLeod, A. M.; Merchant, K. J.; Cascieri, M. A.; Sadowski, S.; Ber, E.; Swain, C. J.; Baker, R. N-acyl-L-tryptophan benzyl esters: potent substance P receptor antagonists. *J. Med. Chem.* **1993,** 36, 2044-2045.

144. Millet, R.; Goossens, L.; Goossens, J. F.; Chavatte, P.; Bertrand-Caumont, K.; Houssin, R.; Henichart, J. P. Conformation of the tripeptide Cbz-Pro-Leu-Trp-OBzl(CF3)2 deduced from two-dimensional 1H-NMR and conformational energy calculations is related to its affinity for NK1-receptor. *J. Pept. Sci.* **2001,** 7, 323-330.

145. Millet, R.; Goossens, L.; Bertrand-Caumont, K.; Chavatte, P.; Houssin, R.; Henichart, J. P. Synthesis and biological evaluation of tripeptide derivatives of Cbz-Gly-Leu-Trp-OBzl(CF3)2 as NK1/NK2 ligands. *Lett. Pep. Sci.* **1999,** 6, 255–262.

146. Lewis, R. T.; Macleod, A. M.; Merchant, K. J.; Kelleher, F.; Sanderson, I.; Herbert, R. H.; Cascieri, M.

A.; Sadowski, S.; Ball, R. G.; Hoogsteen, K. Tryptophan-derived NK1 antagonists: conformationally constrained heterocyclic bioisosteres of the ester linkage. *J. Med. Chem.* **1995,** 38, 923-933.

147. Agnes, R. S.; Lee, Y. S.; Davis, P.; Ma, S. W.; Badghisi, H.; Porreca, F.; Lai, J.; Hruby, V. J. Structure-activity relationships of bifunctional peptides based on overlapping pharmacophores at opioid and cholecystokinin receptors. *J. Med. Chem.* **2006,** 49, 2868-2875.
148. Lee, Y. S.; Agnes, R. S.; Badghisi, H.; Davis, P.; Ma, S. W.; Lai, J.; Porreca, F.; Hruby, V. J. Design and synthesis of novel hydrazide-linked bifunctional peptides as delta/mu opioid receptor agonists and CCK-1/CCK-2 receptor antagonists. *J. Med. Chem.* **2006,** 49, 1773-1780.
149. Yamamoto, T.; Nair, P.; Vagner, J.; Davis, P.; Ma, S. W.; Navratilova, E.; Moye, M.; Tumati, S.; Vanderah, T. W.; Lai, J.; Porreca, F.; Yamamura, H. I.; Hruby, V. J. A structure activity relationship study and combinatorial synthetic approach of C-terminal modified bifunctional peptides that are δ/μ opioid receptor agonists and neurokinin 1 receptor antagonists. *J. Med. Chem.* **2008,** 51, 1369-1376.
150. Lipkowski, A. W.; Misicka, A.; Davis, P.; Stropova, D.; Janders, J.; Lachwa, M.; Porreca, F.; Yamamura, H. I.; Hruby, V. J. Biological activity of fragments and analogues of the potent dimeric opioid peptide, biphalin. *Bioorg. Med. Chem. Lett.* **1999,** 9, 2763-2766.
151. Akiyama, K.; Gee, K. W.; Mosberg, H. I.; Hruby, V. J.; Yamamura, H. I. Characterization of [3H][2-D-penicillamine, 5-D-penicillamine]-enkephalin binding to delta opiate receptors in the rat brain and neuroblastoma--glioma hybrid cell line. *Proc. Natl. Acad. Sci. U. S. A.* **1985,** 82, 2543-2547.
152. Rapaka, R. S.; Porreca, F. Development of delta opioid peptides as nonaddicting analgesics. *Pharm. Res.* **1991,** 8, 1-8.
153. Lord, J. A.; Waterfield, A. A.; Hughes, J.; Kosterlitz, H. W. Endogenous opioid peptides: multiple agonists and receptors. *Nature* **1977,** 267, 495-499.
154. Kiritsy-Roy, J. A.; Chan, S. K.; Iwamoto, E. T. Methionine oxidation enhances opioid activity of an enkephalin analog. *Life Sci.* **1983,** 32, 889-893.
155. Glavin, G. B.; Pinsky, C.; Hall, A. M. Effects of metkephamid (LY127623), a selective delta opioid

receptor agonist, on gastric function. *Life Sci.* **1990,** 46, 1075-1079.

156. Burkhardt, C.; Frederickson, R. C.; Pasternak, G. W. Metkephamid (Tyr-D-ala-Gly-Phe-N(Me)Met-NH2), a potent opioid peptide: receptor binding and analgesic properties. *Peptides* **1982,** 3, 869-871.

157. Frederickson, R. C.; Smithwick, E. L.; Shuman, R.; Bemis, K. G. Metkephamid, a systemically active analog of methionine enkephalin with potent opioid alpha-receptor activity. *Science* **1981,** 211, 603-605.

158. Rahman, M. A.; Inoue, T.; Kamei, C. Role of substance P in allergic nasal symptoms in rats. *Eur. J. Pharmacol.* **2006,** 532, 155-161.

159. Cahill, C. M.; Coderre, T. J. Attenuation of hyperalgesia in a rat model of neuropathic pain after intrathecal pre- or post-treatment with a neurokinin-1 antagonist. *Pain* **2002,** 95, 277-285.

160. Datar, P.; Srivastava, S.; Coutinho, E.; Govil, G. Substance P: structure, function, and therapeutics. *Curr. Top. Med. Chem.* **2004,** 4, 75-103.

161. Dobson, C. M. Protein folding and misfolding. *Nature* **2003,** 426, 884-890.

162. Stefani, M.; Dobson, C. M. Protein aggregation and aggregate toxicity: new insights into protein folding, misfolding diseases and biological evolution. *J. Mol. Med.* **2003,** 81, 678-699.

163. Selkoe, D. J. Folding proteins in fatal ways. *Nature* **2003,** 426, 900-904.

164. Barrow, C. J.; Zagorski, M. G. Solution structures of beta peptide and its constituent fragments: relation to amyloid deposition. *Science.* **1991,** 253, 179-182.

165. Fraser, P. E.; Nguyen, J. T.; Surewicz, W. K.; Kirschner, D. A. pH-dependent structural transitions of Alzheimer amyloid peptides. *Biophys. J.* **1991,** 60, 1190-1201.

166. Hughes, J.; Smith, T. W.; Kosterlitz, H. W.; Fothergill, L. A.; Morgan, B. A.; Morris, H. R. Identification of two related pentapeptides from the brain with potent opiate agonist activity. *Nature* **1975,** 258, 577-580.

167. Spadaccini, R.; Temussi, P. A. Natural peptide analgesics: the role of solution conformation. *Cell. Mol. Life Sci.* **2001,** 58, 1572-1582.

168. Rudolph-Bohner, S.; Quarzago, D.; Czisch, M.; Ragnarsson, U.; Moroder, L. Conformational preferences of Leu-enkephalin in reverse micelles as membrane-mimicking environment *Biopolymers* **1997,** 41, 591-606.

169. Kallick, D. A.; Tessmer, M. R.; Watts, C. R.; Li, C. Y. The use of dodecylphosphocholine micelles in solution NMR. *J. Magn. Reson. B* **1995,** 109, 60-65.

170. Kameda, T.; Takada, S. Secondary structure provides a template for the folding of nearby polypeptides. *Proc. Natl. Acad. Sci. U. S. A.* **2006,** 103, 17765-17770.

171. Sargent, D. F.; Schwyzer, R. Membrane lipid phase as catalyst for peptide-receptor interactions. *Proc Natl Acad Sci U S A* **1986,** 83, 5774-8.

172. Yamamoto, T.; Nair, P.; Davis, P.; Ma, S. W.; Moye, S.; Largent, T.; Vanderah, T. W.; Lai, J.; Porreca, F.; Yamamura, H. I.; Hruby, V. J. Design, structure-activity relationships and biological evaluation of novel bifunctional C-terminal modified peptides for δ/μ opioid receptor agonists and neurokinin-1 receptor antagonists. In *232nd ACS National Meeting*, San Francisco, CA, United States, 2006, pp MEDI-7.

173. Braun, W.; Wider, G.; Lee, K. H.; Wuthrich, K. Conformation of glucagon in a lipid-water interphase by ^{1}H nuclear magnetic resonance. *J. Mol. Biol.* **1983,** 169, 921-948.

174. Thornton, K.; Gorenstein, D. G. Structure of glucagon-like peptide (7-36) amide in a dodecylphosphocholine micelle as determined by 2D NMR. *Biochemistry* **1994,** 33, 3532-3539.

175. Arora, A.; Abildgaard, F.; Bushweller, J. H.; Tamm, L. K. Structure of outer membrane protein A transmembrane domain by NMR spectroscopy. *Nat. Struct. Biol.* **2001,** 8, 334-338.

176. Karslake, C.; Piotto, M. E.; Pak, Y. K.; Weiner, H.; Gorenstein, D. G. 2D NMR and structural model for a mitochondrial signal peptide bound to a micelle. *Biochemistry* **1990,** 29, 9872-9878.

177. Lazaridis, T.; Mallik, B.; Chen, Y. Implicit solvent simulations of DPC micelle formation. *J. Phys. Chem. B* **2005,** 109, 15098-15106.

178. Smith, L. J.; Bolin, K. A.; Schwalbe, H.; MacArthur, M. W.; Thornton, J. M.; Dobson, C. M. Analysis

of main chain torsion angles in proteins: prediction of NMR coupling constants for native and random coil conformations. *J. Mol. Biol.* **1996,** 255, 494-506.

179. Wagner, G.; Neuhaus, D.; Worgotter, E.; Vasak, M.; Kagi, J. H.; Wuthrich, K. Nuclear magnetic resonance identification of "half-turn" and 3(10)-helix secondary structure in rabbit liver metallothionein-2. *J. Mol. Biol.* **1986,** 187, 131-135.

180. Wishart, D. S.; Sykes, B. D.; Richards, F. M. The chemical shift index: a fast and simple method for the assignment of protein secondary structure through NMR spectroscopy. *Biochemistry* **1992,** 31, 1647-1651.

181. Andersen, N. H.; Neidigh, J. W.; Harris, S. W.; Lee, G. M.; Liu, Z. H.; Tong, H. Extracting information from the temperature gradients of polypeptide NH chemical shifts. 1. The importance of conformational averaging. *J. Am. Chem. Soc.* **1997,** 119, 8547-8561.

182. Smith, D.; Griffin, J. F. Conformation of [Leu5]enkephalin from X-ray diffraction: features important for recognition at opiate receptor. *Science* **1978,** 199, 1214-1216.

183. Graham, W. H.; Carter, E. S., 2nd; Hicks, R. P. Conformational analysis of Met-enkephalin in both aqueous solution and in the presence of sodium dodecyl sulfate micelles using multidimensional NMR and molecular modeling. *Biopolymers* **1992,** 32, 1755-1764.

184. Wilmot, C. M.; Thornton, J. M. Analysis and prediction of the different types of beta-turn in proteins. *J. Mol. Biol.* **1988,** 203, 221-232.

185. Hyberts, S. G.; Goldberg, M. S.; Havel, T. F.; Wagner, G. The solution structure of eglin c based on measurements of many NOEs and coupling constants and its comparison with X-ray structures. *Protein Sci.* **1992,** 1, 736-751.

186. Beechem, J. M.; Brand, L. Time-resolved fluorescence of proteins. *Annu. Rev. Biochem.* **1985,** 54, 43-71.

187. Vivian, J. T.; Callis, P. R. Mechanisms of tryptophan fluorescence shifts in proteins. *Biophys. J.* **2001,** 80, 2093-2109.

188. Raguz, M.; Brnjas-Kraljevic, J. Resolved fluorescence emission spectra of PRODAN in ethanol/buffer solvents. *J. Chem. Inf. Model* **2005,** 45, 1636-1340.

189. Tetko, I. V.; Gasteiger, J.; Todeschini, R.; Mauri, A.; Livingstone, D.; Ertl, P.; Palyulin, V. A.; Radchenko, E. V.; Zefirov, N. S.; Makarenko, A. S.; Tanchuk, V. Y.; Prokopenko, V. V. Virtual computational chemistry laboratory - design and description. *J. Comput. Aid. Mol. Des.* **2005,** 19, 453-63.

190. VCCLAB.

191. Neidigh, J. W.; Fesinmeyer, R. M.; Prickett, K. S.; Andersen, N. H. Exendin-4 and glucagon-like-peptide-1: NMR structural comparisons in the solution and micelle-associated states. *Biochemistry* **2001,** 40, 13188-13200.

192. Davis, D. G.; Bax, A. Assignment of complex proton NMR spectra via two-dimensional homonuclear Hartmann-Hahn spectroscopy *J. Am Chem. Soc.* **1985,** 107, 2820-2821.

193. Marion, D. W., K. Application of phase sensitive two-dimensional correlated spectroscopy (COSY) for measurements of ^{1}H-^{1}H spin-spin coupling constants in proteins. *Biochem. Biophys. Res. Commun.* **1983,** 113, 967-974.

194. Braunschweiler, L.; Ernst, R. R. Coherence Transfer by Isotropic Mixing: Application of Proton Correlation Spectroscopy. *J. Magn. Reson.* **1983,** 53, 521-528.

195. Boyd, N. D.; Kage, R.; Dumas, J. J.; Krause, J. E.; Leeman, S. E. The peptide binding site of the substance P (NK-1) receptor localized by a photoreactive analogue of substance P: presence of a disulfide bond. *Proc. Natl. Acad. Sci. U. S. A.* **1996,** 93, 433-737.

196. Lorenzen, A.; Fuss, M.; Vogt, H.; Schwabe, U. Measurement of guanine nucleotide-binding protein activation by A1 adenosine receptor agonists in bovine brain membranes: stimulation of guanosine-5'-O-(3-[35S]thio)triphosphate binding. *Mol. Pharmacol.* **1993,** 44, 115-123.

197. Porreca, F.; Burks, T. F. Affinity of normorphine for its pharmacologic receptor in the naive and morphine-tolerant guinea-pig isolated ileum. *J. Pharmacol. Exp. Ther.* **1983,** 225, 688-693.

198. Porreca, F.; LoPresti, D.; Ward, S. J. Opioid agonist affinity in the guinea-pig ileum and mouse vas deferens. *Eur. J. Pharmacol.* **1990,** 179, 129-139.

199. Yaksh, T. L.; Rudy, T. A. Chronic catheterization of the spinal subarachnoid space. *Physiol. Behav.* **1976,** 17, 1031-1036.

200. Kumar, A.; Ernst, R. R.; Wüthrich, K. A two-dimensional nuclear Overhauser enhancement (2D NOE) experiment for the elucidation of complete proton-proton cross-relaxation networks in biological macromolecules. *Biochem. Biophys. Res. Commun.* **1980,** 95, 1-6.

201. Piotto, M.; Saudek, V.; Sklenář, V. Gradient-tailored excitation for single-quantum NMR spectroscopy of aqueous solutions. *J. Biomol. NMR.* **1992,** 2, 661-665.

202. Press, W. H.; Vetterling, W. T.; Teukolsky, S. A. Numerical Recipes in C. The Art of Scientific Computing. In Cambridge University Press: New York, 1988.

203. Havel, T. F. An evaluation of computational strategies for use in the determination of protein structure from distance constraints obtained by nuclear magnetic resonance. *Prog. Biophys. Mol. Biol.* **1991,** 56, 43-78.

204. Weiner, S. J.; Kollman, P. A.; Case, D. A.; Singh, U. C.; Ghio, C.; Alagona, G. S.; Profeta, J.; Weiner, P. A new force field for molecular mechanical simulation of nucleic acids and proteins. *J. Am. Chem. Soc.* **1984,** 106, 765-784.

205. Weiner, S. J.; Kollman, P. A.; Case, D. A. An all atom force field for simulations of proteins and nucleic acids. *J. Comput. Chem.* **1986,** 7, 230-252.

206. Gough, C. A.; DeBolt, S. E.; Kollman, P. A. Derivation of fluorine and hydrogen atom parameters using liquid simulations. *J. Comp. Chem.* **1992,** 13, 963-970.

207. http://amber.scripps.edu/Questions/fluorine.html.